Simulation of Spatial and Temporal Variability of Soil Moisture Using the Simultaneous Heat And Water (SHAW) Model: Applications to Passive Microwave Remote Sensing

by

Swapan Kumar Roy

A Thesis
presented to
The University of Guelph

In partial fulfillment of requirements
for the degree of
Master of Science
in
Geography

Guelph, Ontario, Canada

ABSTRACT

SIMULATION OF SPATIAL AND TEMPORAL VARIABILITY OF SOIL MOISTURE USING THE SIMULTANEOUS HEAT AND WATER (SHAW) MODEL: APPLICATIONS TO PASSIVE MICROWAVE REMOTE SENSING

Swapan Kumar Roy
University of Guelph, 2014

Advisor:
Dr. Aaron A. Berg

Agricultural management practices and land surface heterogeneity may impact soil moisture retrieval at the footprint scales of passive microwave remote sensing. To evaluate the potential impact of land heterogeneity, it was necessary to identify a hydrological model that could simulate soil moisture spatial variation due to differences in soil texture, land management and crop type. In this study, the SHAW model was evaluated for its capacity to accurately simulate the impact of land management technique. SHAW simulated soil moisture showed good agreement with the observed temporal variations of soil moisture data. Given this performance, SHAW was coupled to a radiative transfer model and used to assess the impact of sub-pixel heterogeneity (e.g. soil moisture, texture, land cover) on measured brightness temperature. When the spatial variability was accounted for, the error between the simulated brightness temperatures and the SMOS (Soil Moisture and Ocean Salinity) satellite observations and was improved over simulations that do not account for sub-pixel variability. These results have importance for improving the assimilation of soil moisture and downscaling passive microwave estimates of soil moisture to smaller regions.

Dedicated to my father (Late Sannyashi Kumar Roy) and mother (Chandrabati Roy)

ACKNOWLEDGEMENTS

I wish to express my deepest gratitude to my major supervisor, Dr. Aaron Berg for his continued support allowing for me to successfully complete this thesis. I would also like to thank Dr. Gary Parkin for being a member of my committee, and Dr. Catherine Champagne and for serving on my committee and being an examiner. I feel lucky to have had such a great committee. I also appreciate feedback from Dr. John Lindsay provided as the external examiner for my defense.

I would also like to thank Dr. Tracy Rowlandson for insightful advice, Peter von Bertoldi to provide access to the Elora field data, G.N. Flerchinger for assistance in running the SHAW model for this application, Dr. Susantha Jayasundara for providing information regarding the field management at Elora site, Justin Adams for aiding in the access of the Manitoba Geo-database, Adam Bonnycastle for GIS data interpretation, Dr. Vincent Fortin of Environment Canada for providing the necessary CaPA data, Dr. Richard de Jeu of Vrije Universiteit Amsterdam for the MatLab code to run LPRM, and Jason Patton of Iowa State University for providing the SMOS data. I would also like to thank all of my friends and colleagues who have contributed their support directly or indirectly to this work.

I am thankful to the Agri-Environment Services at Agriculture and Agri-Food Canada (AAFC) and the Canadian Space Agency for providing financial support.

And finally, no words can express to my gratitude to my wife (Ulka), sons (Sambaran and Soumyajoti), mother and other family members. Without their moral support and constant blessings this experience would have never been possible, and at the end, thanks to God.

TABLE OF CONTENTS

LIST OF TABLES

PAGE

LIST OF FIGURES

PAGE

Chapter 1

INTRODUCTION

1.1 Introduction

Soil moisture is an important component of the hydrological cycle as it plays an integral role in mass and energy exchange between the land surface and the atmosphere. Soil moisture can be used in forecasting of air temperature and precipitation, for example, Koster *et al.* (2011) demonstrated that the long-lead predictability of air temperature can be improved with the initialization of soil moisture in land-atmospheric coupling model. Knowledge of the soil moisture state is also important for: irrigation scheduling, nutrient/ fertilizer management plan, site-specific management of some plant diseases and insects, crop yield predictions, and plant health (Jayasundara *et al.*, 2007; Moran *et al.*, 2004). It is also evident that an extreme of soil moisture interferes with agricultural practices leading to reduced agricultural income or the need for financial compensation from governmental and insurance organizations. For example, above average precipitation when coupled with delayed snow melt contributed to the 2011 Assiniboine River flood in western Manitoba, one of the most expensive natural disasters in Canadian prairies. The flooding of agricultural fields reduced agricultural production, resulting in 3 million acres remaining unseeded (Manitoba, 2013). At the other extreme, reduced soil moisture during drought conditions also greatly impact agricultural production. In United States, the 2012 severe drought affected 80% of agricultural land, affecting global crop prices particularly for soybeans and corn (USDA, 2012). Therefore, the development of modelling and observations systems useful for the prediction and observation of soil moisture could have numerous potential applications.

An important consideration for soil moisture modelling is the impact of land management practices on soil moisture amount and variability at the scale of agricultural fields. In Canada,

traditional farming practice follows conventional tillage (CT) where tillage machinery is used to break-up soil to increase porosity, incorporate crop residues/ weeds and nutrient for plant growth. However, no till (NT) practice has increased from 7% to 56% from 1991 to 2011 in Canada as research suggests that NT methods improve soil ecology, result in less erosion and save on fuel and labor costs (Statistics Canada, 2011). Typically, NT results in wetter topsoil due to large number of micro-pores and existing crop residues. Several studies in Canada and US found a difference in drainage between CT and NT, and found inconsistence results (Arshad *et al.*, 1999, Patani *et al.*, 1996). A water budget approach presented in McCoy *et al.* (2006) using precipitation, evaporation from eddy covariance, change in water storage from water reflectometer and runoff from ponding method found that soil drainage using CT method was slightly greater than NT. Using similar monthly water budget approach as described by McCoy *et al.* (2006), Jayasundara *et al.* (2007) reported 7-12% higher nitrogen (NO_3-N concentrations) leaching loss for CT compared to NT during 2000-2004 which is important for Ontario farmers for nutrient management plans. Given the large changes occurring land management practice over Canada, it is important to understand how sensitive hydrological simulation models are to land management practices in water budget simulations.

Passive microwave remote sensing techniques are rapidly being developed for determining soil moisture in the upper soil layer at large scales (Entekhabi *et al.*, 2010; Kerr *et al.*, 2012). These techniques have great potential for large scale, all weather monitoring of soil moisture at the surface, and when combined with hydrological models and data assimilation systems, can be used to determine full root zone soil moisture estimates. As methods are developed to improve the estimation of soil moisture using passive microwave remote sensing techniques, it is

important to understand the role of surface heterogeneity, such as those produced by land management practice that may impact the soil moisture retrieval at large footprint (e.g. SMOS observation) scales. Land surface heterogeneity produces errors in soil moisture retrieval over large footprints where numerous factors can affect brightness temperature (which represents surface soil moisture) in non-linear way (Panciera *et al.*, 2011). However, very few studies assessed the impact of agricultural land surface heterogeneity on soil moisture retrievals over highly heterogeneous agricultural land surface conditions. Therefore, it is the goal of this thesis to evaluate a hydrological model for the assessment of agricultural water budgets under different land management techniques and then use this model for assessing the impact of agricultural land management on retrievals of satellite brightness temperature used for the estimation of soil moisture.

1.2 Research Aims and Objectives

This research aims to evaluate the Simultaneous Heat And Water (SHAW) model for different agricultural management practices (CT and NT), and the effect of heterogeneity of land surface on integrated SHAW and with a radiative transfer modeled to simulate passive microwave brightness temperatures. The study has been carried out with the following objectives:

a) to assess the effect of CT and NT on root zone soil moisture and soil temperature regimes using SHAW model for soybean agricultural fields;
b) to assess the ability of SHAW to predict surface soil moisture under fields with different crops and soil texture; and

c) to assess the heterogeneity of land surface due to agricultural practice on simulated brightness temperatures to improve soil moisture retrievals from a radiative transfer model.

Chapter 2

Sensitivity of Simultaneous Heat And Water (SHAW) Model to Till and No-till Agricultural Management

Motivation

Soil moisture data are an important requirement for hydrological and weather forecasting models, as well as in agricultural watersheds. Traditionally, soil moisture is measured with direct or gravimetric soil moisture measurement method with field collected soil samples for oven drying in laboratory. This method is destructive and not suitable for large scale mapping. Therefore, indirect methods using soil sensor based on dielectric properties of soil water is becoming popular due to its reliable, fast and non-destructive nature. The use of soil sensors in a field is affected by rodents and vehicle trafficking during agricultural management operations. Moreover, indirect measurement is not sufficient for large areas where soil moisture is widely varied with precipitation occurrence, soil texture, slope, vegetation, and agricultural management. The literature indicates that agricultural land management practices (tillage) impact soil water budgets, and that no tillage is gaining popularity over conventional tillage in Canada (McCoy *et al.*, 2006; Statistics Canada, 2011). In practice, soil moisture information from surface to deeper soil layers is very important for agricultural producers. Therefore, it is necessary to investigate the effects of different tillage methods on soil water budgets for the whole root zone soil profile using available agricultural hydrological models, like the SHAW (Simultaneous Heat and Water) model.

Abstract

Conventional tillage (CT) practices often result in unacceptable levels of wind erosion due to the burial of crop residues and exposure of fine soil particles. Therefore, no till (NT) systems with minimum disturbance and operational costs are gaining popular widely in Canada. It is well known that changes to soil tillage practices can influence soil moisture and soil temperature regimes. The objective of this study is to investigate the SHAW (Simultaneous Heat and Water) model for simulating management effects of tillage practice on soil temperature and moisture regimes for soybean growing season under conventional and no-tillage managements during 2010. The model was run with supplied weather, site characteristics, plant growth, and initial soil moisture and soil temperature data in paired CT and NT treatments. The NT treatment was observed to retain more surface soil moisture over the extended summer period (July-September) compared to CT due to the interception of soil moisture by existing crop residue. During the early growing season, CT gained more surface soil moisture than NT due to disturbance of the soil or adopted tillage operation. Overall, the SHAW simulated soil moisture at different soil depths followed the general trends of the observed field data. At the overall root zone soil, the average root mean square errors (RMSEs) for conventional tillage and no-tillage for the soybean growing season were found to be 0.042 m^3 m^{-3} and 0.028 m^3 m^{-3}, respectively. The trends between surface simulated soil moisture and observed data for CT and NT were almost similar (r > 0.70**) at all soil depths. The average SHAW over-predicted soil temperatures were 2.6˚C for CT and 1.9 ˚C for NT for 1-m soil profile throughout the growing season. Overall, SHAW proved adequate in simulating soil moisture and temperature over 1 m soil profile, and therefore it may serve as a useful modeling tool for tillage and residue management.

Keywords: hydrological modeling (SHAW), soil moisture, soil temperature, conventional tillage and no tillage

2.1. Introduction

Soil moisture is an important component in the atmospheric moisture cycle having impacts on agriculture, modeling of land/atmosphere interaction, hydrology, forestry and engineering. It links the hydrologic cycle and the energy budget of land surfaces by regulating latent heat fluxes. The soil moisture availability at the root level of vegetation affects plant growth and ultimately moisture availability in the root zone is more important than precipitation occurrence. In agricultural watersheds, soil moisture content information has been used for irrigation scheduling, site-specific management of diseases and insects, improving crop yield prediction, indicator of plant health, mobility of farm management vehicles, etc. (Moran *et al.*, 2004). Furthermore, the knowledge of initial soil wetness state has been shown to improve the forecast of the air temperature and precipitation (Drewitt *et al.*, 2012). Therefore, improvement of soil moisture estimation has broad reaching implications.

Direct measures of soil moisture can be obtained using gravimetric methods, where soil samples are collected from the field and brought back to the laboratory for weighing and drying (Klute, 1986). Unfortunately, this method is destructive, laborious and expensive particularly when repeated over long time intervals. Therefore, *in-situ* measurements of the "dielectric" properties of soils, which when related to the soil moisture (Topp *et al.*, 1980) are useful for reliable, fast and non-destructive measurement. For these techniques, the dielectric constant is strongly dependent on the volumetric moisture content of soil and almost independent of soil density,

texture, temperature and used frequencies in measurement (Jackson, 1990; Topp *et al.*, 1980). Electrical measurements of soil moisture are not without problems, however, as installed sensors on agricultural fields are affected by animals (rodents) and management activities during tillage, planting, fertilizing and harvesting. Furthermore, it is evident that *in-situ* soil moisture varies widely both spatially and temporally at the field scale due to spatio-temporal variations of precipitation, soil texture, slope, vegetation, etc. Therefore, *in-situ* measurements of soil moisture are generally representative of a small area of an agricultural field. Nevertheless, soil moisture estimates at field scale are typically scarce both spatially and temporally for operational uses. As a result, hydrological models remain a very important tool for researchers to provide estimates of spatial and temporal variation in land surface moisture.

At the field scale, the variability of surface soil moisture is not only affected by precipitation, soil texture, slope, etc., but it is also affected by adopted land management practices (Arshad *et al.*, 1999; Fuentes *et al.*, 2004; McCoy *et al.*, 2006). In Canada, traditional farming practice has focused on conventional tillage (CT) practices where conventional tillage machinery is used to break-up the soil thereby increasing porosity and allowing for increased air exchange for plant root growth. It is also an effective way of incorporating crop residues and manure or nutrients evenly, destroying weeds and breaking up sod fields (Reicosky and Saxton, 2006; Statistics Canada, 2011). Despite these potential advantages of CT agriculture, farmers have increasingly substituted conventional tillage with no-till (NT) seeding techniques or conservation tillage in recent decades. No-till is less ecologically disruptive as specialized machinery is used to slice a thin slit into the soil to deposit seeds. This technique is less disruptive of the soil ecology, and typically results in less erosion with potential savings on fuel and labor costs for the producers

(Reicosky and Saxton, 2006; Statistics Canada, 2011). Furthermore, the application of no-till practices typically results in wetter root zone soil profiles as the water holding capacity of soil is increased due to a larger number of micro-pores. Nationally, the proportion of land prepared for seeding using no-till practices increased from 7% to 56% from 1991 to 2011 in Canada (Statistics Canada, 2011). The largest gains in no-till occurred in Saskatchewan and Alberta, but no-till seeding also increases rapidly in Ontario, Manitoba and British Columbia.

The management differences between CT and NT can lead to differences in soil physical properties. Several studies in Canada and the northern United States focused on measuring the difference in drainage between CT and NT using tile drain monitoring, lysimeters and infiltration, and have found inconsistent results (Arshad *et al.*, 1999; Patni *et al.*, 1996, Shipitalo and Edwards, 1993). McCoy *et al.* (2006) described soil water balances for CT and NT management systems in Elora Ontario where precipitation from a nearby weather station, evapotranspiration from eddy covariance system, change in water storage from water content reflectometers (WCR), runoff and change of water table level were all analyzed over multiple growing seasons. McCoy *et al.* (2006) reported that the amount of subsurface deep drainage for 2001-2003 of CT was slightly greater (about 9%) than the NT which could be due to enhanced interception by crop residue left on the surface of NT treatment. It is noted that fields were well drained with subsurface systematic drainage system with negligible slope. Using similar monthly water budget approach as described by McCoy *et al.* (2006), Jayasundara *et al.* (2007) reported 7-12% higher nitrogen (NO_3-N concentrations) leaching loss for CT compared to NT during 2000-2004 which is important for Ontario farmers for nutrient management plan. Therefore, it is understood that land management practice has important controls on soil moisture budgets.

The simultaneous heat and water (SHAW) model, a one dimensional vertical model was developed initially by Flerchinger and Saxton (1989) to simulate freezing and thawing of soils. SHAW has also been used for modeling agricultural water budgets as it can account for effects of tillage, residues and vegetation canopy over a wide range of conditions (Wang *et al.*, 2009; Parkin *et al.*, 1999). Given the large changes occurring land management practice over Canada, it is important to understand how sensitive hydrological simulation models are to land management practice on water budget simulations. Therefore, the overarching objective of this study is to evaluate the sensitivity and realism of the SHAW model water budget simulations to varying agricultural land management practices. The specific objectives of this study are: (i) to assess effects of CT and NT on rootzone soil moisture and soil temperature regimes, and (ii) to test SHAW's ability to simulate management effects on soil moisture and soil temperature distribution.

2.2. Materials and Methods

2.2.1 Treatments

The field study was initiated in early 2000, where two no tillage (NT) and 2 conventional tillage (CT) plots (each 100 m x 150 m) were established at the University of Guelph Research Station at Elora, Ontario, Canada (43˚38′29.05″N, 80˚24′46.03″W, 340 m). The experiment site was almost level with 0-1% slope towards North-West direction. The soil at the site is an imperfectly drained Guelph silt loam (Morwick and Richards, 1946). The soil parent material is 20-22 m in thickness above the bedrock and systematic tile drainage was installed at the site in 1960 at a drain spacing and depth of about 15 m and 0.75 m, respectively (McCoy *et al.*, 2006). Average

texture percentages of the test fields were sand = 32%, silt = 51%, and clay = 17% in 0-5 cm soil layer (Table 2.1). Soil physical properties of the both CT and NT plots were similar although these properties varied slightly spatially from location to location as well as in different soil depths within the field. McCoy (2002) reported that there was no significant change in the physical soil properties within those plots converted to NT during samplings between 1999 and 2002. The average field soil properties and literature-extracted parameters are shown in Table 2.1.

Table 2.1: Soil properties of CT and NT

Depth	Saturated hydro-conductivity (Ks)	Bulk density (ρ_s)	Porosity (θ_s)	Sand	Silt	Clay	Organic matter	Pore size distribution parameter (b)	Air entry potential (ψ_e)
m	cm h^{-1}	kg m^{-3}	m^3 m^{-3}	%	%	%	%		m
0-0.05	0.40	1550	0.45	32	51	17	2	3.34	-0.11
0.05-0.25	0.40	1550	0.45	32	51	17	1.6	3.34	-0.11
0.25-0.55	0.41	1610	0.41	42	43	15	1.1	3.72	-0.10
0.55-0.85	0.45	1660	0.40	44	42	14	0.6	4.23	-0.10

Source: Fallow *et al.*, 2003; McCoy, 2002; McCoy *et al.*, 2006

Prior to 2000, the site was in a traditional conventional tillage and the crop sequence (soybean-corn-winter wheat) was maintained on the no tillage and conventional tillage experimental plots. Over the conventional tillage plots, intensive tillage was practiced by moldboard ploughing in the fall to a depth of 15 cm followed by spring disking. In no tillage practice, seeds were planted with a no-till drill in one pass.

On 18 May 2010, the plots were planted with soybean at the rate of 81 lbs/acre (Dekalb DKB 00-99) along with a herbicide (Dual 2 Magnum @ 0.7 L/acre) in both the conventional (sites 1 & 4) and no tillage plots (sites 2 & 3). The crop residue affecting the plots was corn which was harvested in October 2009. The presence of heavy corn residue cover was evident in the no

tillage fields before planting of soybeans. Herbicide Weathermax (0.67L/acre) and Assure II (0.05L/acre) were applied in both managements on 15th June and 7th July of 2010 during vegetative growth of soybean (pers. comm. to Susantha). On 27th September 2010, soybean was harvested from both conventional and no tillage fields.

2.2.2 Instrumentation and Monitoring

The daily weather data, such as wind speed (km h^{-1}), solar radiation (W m^{-2}), relative humidity (%), air temperature (˚C) and precipitation (mm), were collected from a nearby meteorological station (approximately 200 m from the site) during growing season of 2010. The differing management plots were monitored from the beginning of April 2010 to the end of September 2010 using soil moisture and soil temperature sensors. The average soil data, including moisture content and temperature for CT and NT, were recorded every hour in 4 sets of instruments in four locations of 4 experimental plots. Multiple data sets were recorded to avoid missing data or malfunctioning of any sensor. Moreover, average data of each management was calculated to avoid errors. The installed instruments were: water content reflectometers (WCR) (Model CS615, Campbell Scientific Inc.) (Figure 2.1) and thermocouples (Model #107, Campbell Scientific Inc.) (McCoy *et al.*, 2006). The 30 cm long WCR waveguides (0.32 cm diameter, 3.2 cm apart) were installed vertically at three different depths within each treatment to give average soil moisture contents for the 0.10-0.40 m, 0.40-0.70 m and 0.70-1.00 m depths, and at an angle to give the average soil moisture content for 0-0.10 m soil depth. The thermocouples were installed at the midpoint of each soil depth range measured by the WCR, i.e., at 0.05, 0.25, 0.55 and 0.85 m depths. Data loggers recorded hourly values for soil moisture content and temperature measurements. The horizontal separation distance was maintained to allow

installation into undisturbed soil and to avoid interference of vertical moisture movement on subjacent probes. The details of installation and calibration of sensor with *in-situ* volumetric soil moisture measurements are presented in McCoy *et al.* (2006). It is noted that the WCR probes allowed for indirect measurement of soil moisture content, by using the effect of changing dielectric constant on applied electromagnetic waves. During plantation and harvesting operations of soybean, sensors in the top 0.05 m and 0.25 m of soil depths were removed and then reinstalled immediately thereafter.

Water Reflectometer

Figure 2.1: Installation of soil moisture sensor – Campbell Scientific model (CS 615).

2.2.3 The SHAW Model and Parameters for Simulations

Simultaneous Heat and Water (SHAW) model uses information on vegetation canopy, snow and surface residues to describe one-dimensional coupled water and heat flow in soils and is described fully in Flerchinger and Saxton (1989), Flerchinger (2000) and Flerchinger *et al.* (2003). In this study, the SHAW model requires local daily weather data (air temperature, relative humidity, wind speed, precipitation and solar radiation), estimated and recorded site characteristics (saturated hydraulic conductivity, pore size distribution index, air entry potential,

porosity, bulk density, texture, organic matter, etc.) and plant growth (height, dry biomass, leaf area index, etc.) data.

Inputs for SHAW simulations were determined primarily based on the available field measurements while other parameters were obtained from the literature (Tables 2.1-2.3). The fraction of soil surface covered by crop residues was assumed based on observation of no tillage plots. Dry biomass load in kg/ha and albedo of surface residues under NT were derived from previous studies (McCoy, 2002; Fernhout and Kurtz, 1999; Flerchinger, 2000) and is presented in Table 2.2. Soil samples representing the soil surface and major soil horizons were taken at the depths of 0.05, 0.25, 0.55 and 0.85 m in each treatment. The average bulk density, organic matter and particle size distribution were determined by standard methods and are referred to McCoy (2002). Saturated hydraulic conductivity, pore size distribution index and porosity were extracted from Rawls *et al.* (1982) based on texture of Guelph silt loam soil. As the purpose of this analysis was evaluate the ability of the model to simulate water budgets over differing tillage practices, a large parameter optimization exercise was not performed as part of this work. Rather soil hydrological parameter values were obtained from published sources and software documentation.

Table 2.2: Input parameters for SHAW modeling

Parameter	Conventional tillage	No tillage
Fraction of surface covered by residue	-	0.90
Albedo of residue	-	0.23
Dry weight of residue on surface, kg ha^{-1}	-	6,000
Thickness or depth of residue layer, cm	-	2

source: Flerchinger, 2000; McCoy, 2002

Table 2.3: Input parameters for soybean growth in CT and NT

Day of year 2010	Average height of plant	Average width of leaves	Dry biomass of plant	Leaf area index	Effective rooting depth
	m	cm	kg m^{-2}		m
Mar 31	0	0	0	0	0
May 18	0	0	0	0	0
May 30	0.1	2	0.03	0.1	0.1
Aug 27	0.75	10	1	2	1.6
Sep 27	0.7	1	1	0.8	1.5
Sep 28	0	0	0.2	0	1.4

source: Allen *et al.,* 1998; Mayaki *et al.,* 1976; Thies *et al.,* 1995

The SHAW model was used to simulate soil temperature and moisture content over the entire field experimental period. The soil domain or profile for the modeling was assumed as 3 m deep to allow uniform downward flow of soil water through the root zone soil depth where model (one-dimensional vertical type) neglected later flow during the execution as well as uniform drainage through existed subsurface tile drains since 1960 in the experimental sites. The domain was discretized into a total of 22 nodes, conforming to three morphological layers of 0 to 0.25 m, 0.25 to 0.55 m, and 0.55 to 0.85 m and corresponding to the positions of the soil moisture and temperature sensors. For water flow, a unit-gradient boundary condition was used for the lower boundary and a specified flux (observed precipitation) for the upper boundary (Flerchinger, 2000). Similarly for heat flow, a unit-gradient boundary condition was used for the lower boundary and atmospheric weather condition (field-observed air temperature) was used for the upper boundary condition. The initial conditions for moisture and heat flow consisted of observed soil moisture and temperature profiles on 01 April 2010. However, a simulation that initializing the model in the early spring with soil moisture at field capacity and at average air temperature over the various soil depths produced a simulation that was nearly identical to the simulations initialized with observed values. The variation between RMSEs was within 10%

while model initialized with observed soil moisture and soil temperature. The soybean was planted in both management conditions on May 18 and harvested on September 27 in 2010. Plant growth data for soybean in silt loam soil for this experiment were extracted from available literature (Allen *et al.*, 1998; Mayaki *et al.*, 1976; Thies *et al.*, 1995), and is shown in Table 2.3.

2.2.4 Statistical Analysis

Two-sample differences in means t-tests were used to determine differences in moisture contents and soil temperatures between CT and NT. It is noted that observations of both CT and NT are dependent within the individual successive samples throughout the same time series. Additionally, root mean square error (RMSE) to check accuracy and coefficient of determination of liner regression (R^2) to evaluate significant trends between SHAW-simulated and field-observed soil moisture and temperature at various depths under the CT and NT are reported to corroborate the results of the SHAW model with observations.

2.3. Results and Discussion

2.3.1 Observed Soil Moisture Content

Soil textural properties of the CT and NT plots were similar, except residues that covered about 90% of NT plots (Jayasundara *et al.*, 2007; McCoy, 2002; McCoy *et al.*, 2006). Residues in CT plots were removed and partially incorporated into soil during fall tillage using a disk ripper. Temporal variations of precipitation and soil moisture in the two treatments are shown in Figure 2.2. Precipitation from April to September 2010 in the experimental site was 550.8 mm; 768 mm precipitation was received from January – December 2010 that is within one standard deviation of the average annual rainfall totals for this region (863 ± 126 mm; Parkin *et al.*, 1999). Surface

soil moisture at 0.05 m and 0.25 m of both CT and NT had significantly greater response to occurrence of precipitation than measurements of soil moisture at 0.55 m and 0.85 m. The sensors were replaced after planting in the CT plot and NT plot (May 20, 2010), therefore recorded soil moisture data for the 0.05 m and 0.25 m of soil depths were only available from 20th May onward. These surface soil sensors were removed again from 20th September to 11th October during the harvesting activities. Therefore, periods of missing data are observed in Figure 2.2b and c. Sensors at 0.55 m and 0.85 m of soil depths were kept in CT and NT plots during planting and harvesting operations. The recording of data in sensors of NT plots started from 20th May and continued until end of the soybean growing season, i.e. 26th September (Figure 2.2).

In the CT treatment, the top 0.05 m and 0.25 m of soil dried during May and August months to about 0.18 m^3 m^{-3}, but the subsoil below 0.30 m retained moisture near 0.22 – 0.26 m^3 m^{-3}. Surface soil moisture at 0.05 m and 0.25 m showed significant response to the occurrence of precipitation. The surface soil was wetter in the CT than in the NT, in particular in beginning of summer i.e. until 10th July, however later in the year, the surface soil of NT remained relatively wetter than CT during the drying period (July-September) (Figure 2.2d). McCoy *et al.* (2006) also observed similar trends for 1-m profile soil water storage extracted from WCR sensors for CT and NT treatments during the dry year 2002. They reported that the drainage of CT was 24% higher than NT treatment and interception of CT was 6% lower than NT treatment during a drier year in 2002 at the same location. The surface soil moisture of NT remained comparatively wetter than CT during the drier period from August-September (Figure 2.2d) when the presence of crop residues has likely reduced surface evaporation as well as surface water run-off

(Reicosky and Saxton, 2006). The enhanced soil moisture at 0.25 m in the NT treatment in fall (Figure 2.2d) may be related to more available macropores in the undisturbed soil along due to dried roots of the previous crop. It is noted that several applications of herbicide was used to control weeds. Therefore, roots from previous crops at 0.25 m soil depth might intercept soil moisture in NT during dry period from middle of July to September. Moreover, Elliot *et al.* (2000) reported that preferential flow was slightly reduced by the tillage passes in CT due to the disruption of macropore continuity. Arshad *et al.* (1999) and Shipitalo and Edwards (1993) reported that steady-state infiltration in silt loam soil at surface was 30-60% greater under NT than under CT after 20 years of continuous management.

The soil moisture content below the 0.05 m depth was generally higher than that in the top 0.05 m for both CT and NT plots (Figure 2.2b and c). For the CT plot, soil moisture contents at 0.05 m and 0.25 m were similar and decreased from almost 0.30 m^3 m^{-3} in June to 0.12 m^3 m^{-3} at end of August. For the same period, soil moisture content at the top 0.05 m and 0.25 m in the NT plot also decreased from almost 0.30 to 0.15 m^3 m^{-3} while soil moisture content at 0.55 m was stable or varied between 0.15 and 0.21 m^3 m^{-3}. Low soil moisture values at end of August were due to relatively low precipitation and evapotranspiration of the maturing soybean crops. Soil moisture content at 0.85 m in both plots was above 0.20 m^3 m^{-3} most of the time.

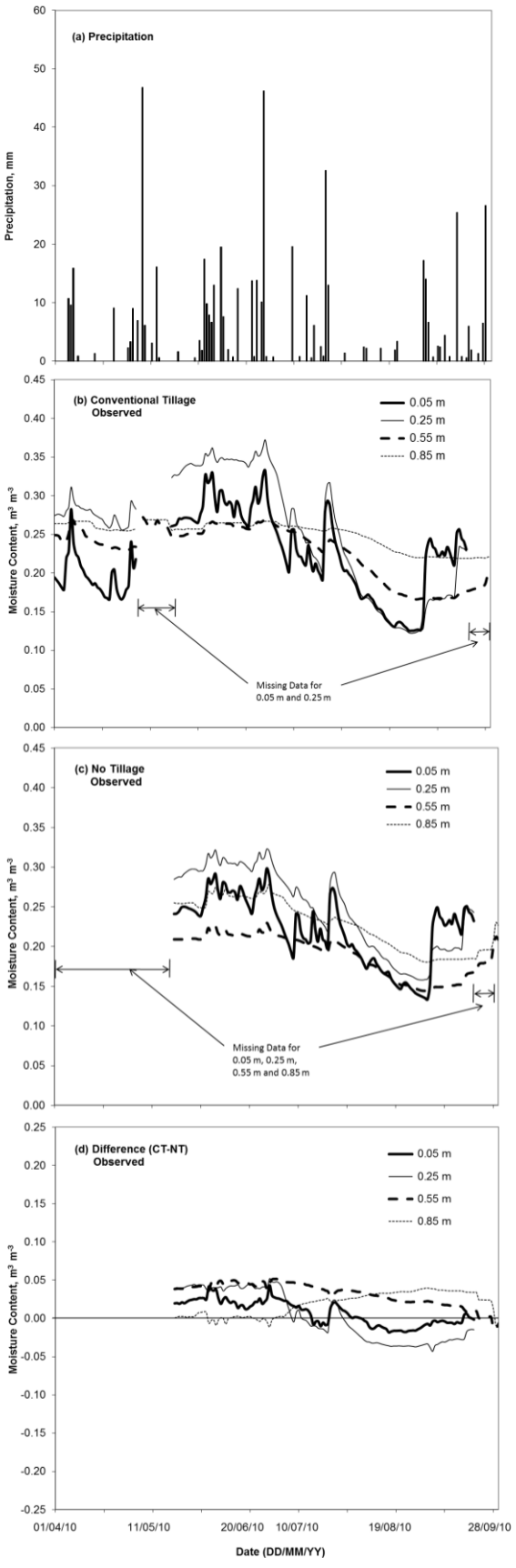

Figure 2.2: (a) Observed daily precipitation; (b) observed soil moisture at different depths in CT; (c) observed soil moisture at different depths in NT; and (d) difference in soil moisture between CT and NT.

The paired t-tests showed that, over the entire monitoring period from May to September 2010, the moisture contents measured with the Campbell Scientific probes at each depth except 0.25 m of soil depth were significantly different between the two treatments using a t-test (t-statistic > 5 for n = 124 where the t-critical value assuming two-tail = 1.97) (Figure 2.3a). At most depths, average moisture contents in CT were higher than in NT, but at the 0.25 m depth, average moisture contents of both treatments were found to be not significantly different (Figure 2.3a) where t-statistic = 0.97 for n = 124. The adoption of NT management practice in the experimental site was only about 10 years which may not be enough time to restore original hydraulic properties of NT soil especially at surface layers. The average moisture content differences are nearly equal between the treatments at the 0.05 m depth (in Figure 2.3a); however, at different time of the year differences are visible. For example, the higher soil moisture is observed in the CT during the early growing season (May-July) while higher soil moisture is observed in the NT during late growing season (August-September) (Figure 2.2d). After 20th July 2010, the soil moisture continuously decreased in both NT and CT until the onset of the rainfall beginning (3rd September 2010). Drury *et al.* (1999) also reported higher soil moisture for the no-tillage treatment during the drying period as the soil remained cooler and presence of residues.

2.3.2 Observed Soil Temperatures

The average soil temperatures at the various depths of NT in experimental site were consistently found to be cooler compared to CT plot (Figure 2.3b; t-statistic > 15; n=124) except 0.85 m of soil depth. Drury *et al.* (1999) reported that the daily average soil temperatures for clay loam soil at top soil (5-10 cm depths) were 1.6-1.9˚C warmer in the CT than corresponding NT. The very large difference in soil temperatures at 0.85 m was unexpected.

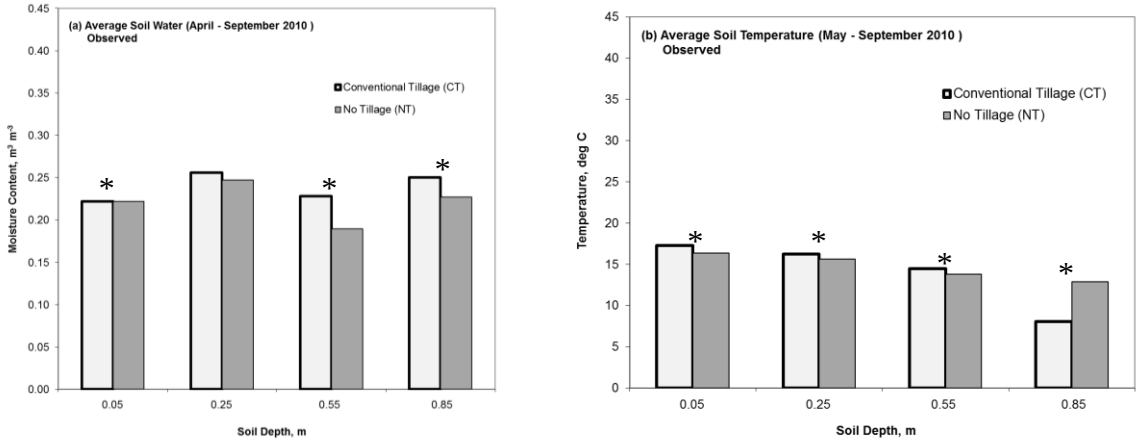

Figure 2.3: Averaged (a) moisture contents and (b) soil temperatures for conventional tillage (CT) and no tillage (NT) for 20 May to 20 September 2010 at different measurement depths. Asterisks denote significant difference at 0.05 probability level

2.3.3 Simulated Soil Moisture Contents

The SHAW model is physically-based model where soil moisture is mainly governed by porosity, pore size distribution index, air entry potential and saturated hydraulic conductivity (Flerchinger *et al.*, 2012). In this study, the SHAW-simulated moisture contents followed the general trend of the observational data (Figure 2.4a and b). For the NT treatment, soil moisture in each soil layer was better simulated than under CT possibly due to smaller variations in soil moisture content under NT treatment (Figure 2.4c and d). As shown in Figure 2.4, SHAW under predicted surface soil moisture at different soil depths of CT and NT (especially in wet period) which could be due to over prediction of soil evaporation or errors in precipitation records or inaccurate soil characteristics data. Wang *et al.* (2010) also experienced underestimation using SHAW in the early part (January – March) of the seasons in 2004 and 2005 and they reported it be typically due to inaccuracy of challenging snow measurements during winters.

For the CT treatment, SHAW under-estimated soil moisture for each soil depth during whole soybean growing season; however, the differences between the modeled results and observations were small (Figure 2.4c). Absolute differences in soil moisture between simulated and observed data were in most cases less than 0.05 m^3 m^{-3} (Figure 2.4c and d). Larger deviations between simulations and measured values were observed, mainly for the surface soil at 0.05 m depth, during rainy days in September. SHAW underestimated the moisture content in the seed zone at 0.05-0.25 m of soil depth and it continuously underestimated the moisture content in the root zone (Figure 2.4c and d). The minimum SHAW-simulated soil moisture for the 0.55 m depth was 0.10 m^3 m^{-3} for CT and 0.12 m^3 m^{-3} for NT (Figure 2.4a and b) during September which was almost below the wilting point (0.133 m^3 m^{-3}) for silt loam soil (Rawls *et al.*, 1982). Based on a sensitivity study of several model parameters including residue thickness, root depth and leaf area index, Wang *et al.* (2010) reported that the increase of residue thickness increased surface soil moisture regardless of leaf area index. Therefore, it is likely the increased residue thickness input into the SHAW for the NT simulations increased surface soil moisture at 0.05 m compared to CT (Figure 2.4a and b). Surface residue parameters are mainly influenced by tillage and its thickness is always an important factor, especially on near-surface soil moisture. From Figure 2.4e, simulated soil moisture of NT plot looks bit higher than that of CT plot which is due to effect of input parameters of SHAW model. The surface soil of NT remained relatively wetter (> 0.02 m^3 m^{-3}) than CT especially during the drying period (July-September). It is noted that observed surface soil moisture of NT also remained comparatively wetter than CT during the drier period from August-September (Figure 2.2d) due to presence of crop residues in NT plots.

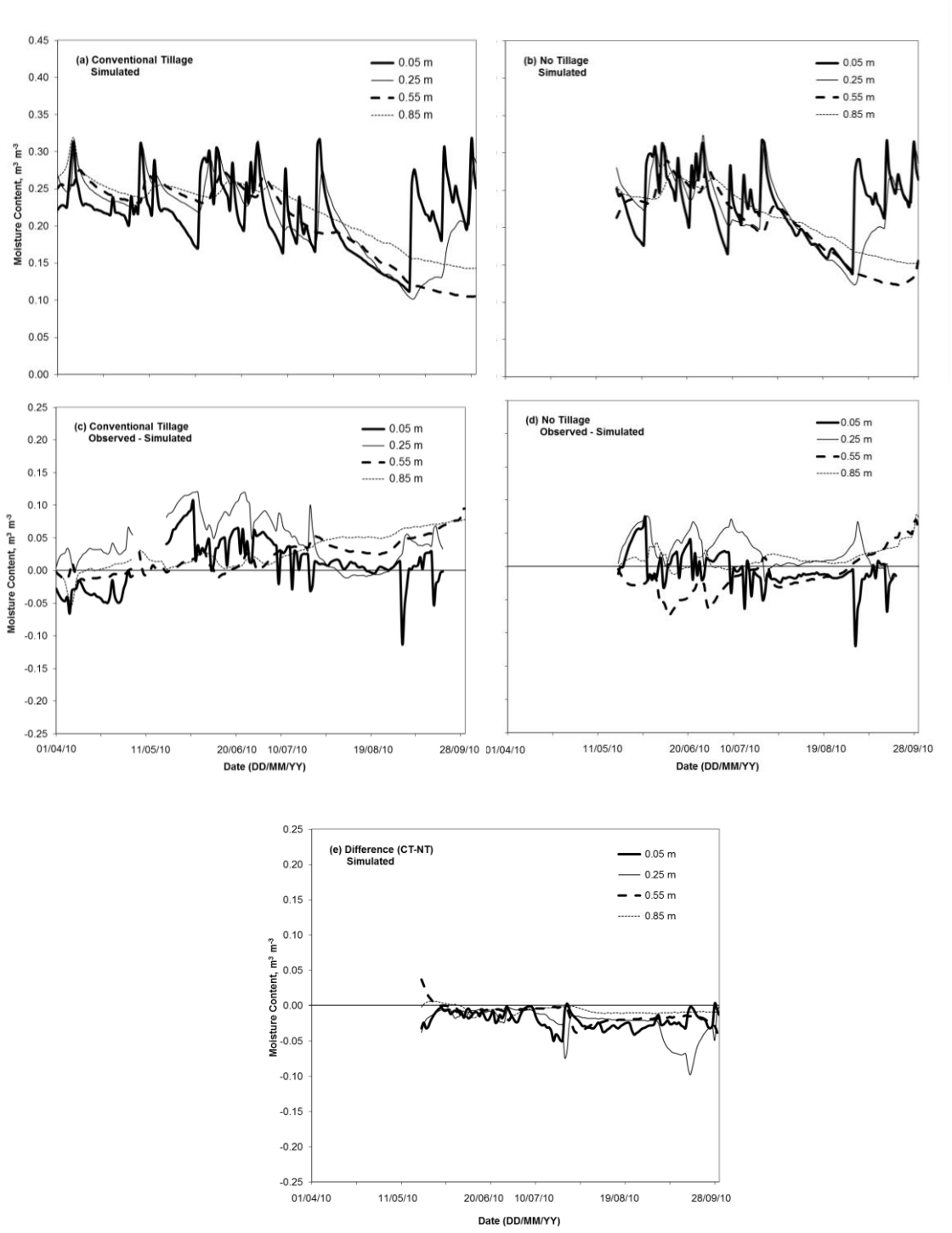

Figure 2.4: (a and b) Simulated moisture contents for conventional tillage (CT) and no tillage (NT), (c and d) differences between observed and simulated data, and (e) differences between simulated CT and NT data.

RMSE values for volumetric soil moisture content for all depths were in the range of 0.03 to 0.05 m^3 m^{-3} and 0.01 to 0.03 m^3 m^{-3} for CT and NT, respectively (Table 2.4). The low values of the RMSE confirm good agreement between SHAW-simulated and field-observed soil moisture contents. Of note, these results were obtained without extensive model calibration, which suggests that the SHAW model has a very good potential for soil moisture simulation in this region. However, it is noted that these results also benefit from initialization to observations; it is likely that a less realistic initialization have model drift. For the SHAW model, Li *et al.* (2012) reported that RMSD (root mean square deviation) varied from 0.016 to 0.042 m^3 m^{-3} for non-irrigated cultivation. It is noted that overall errors in 0.55 m and 0.85 m soil depths were smaller than those of surface soil depths for CT and NT treatments which may be attributed to lower temporal variation of soil moisture in subsoil.

Overall correlation between simulated and observed soil moisture was lower at surface soil compared to deeper soil depths (Table 2.4). The average correlation obtained in this study for CT and NT treatments for both treatments was 0.87** over the 1-m soil profile. These relationships are higher than those determined by Wang *et al.* (2010) who reported 0.81 for 1.2 m soil profile using SHAW. These results indicate that SHAW is able to simulate the seasonal progression of soil moisture in this region under different land management regimes.

Table 2.4: RMSE between SHAW-simulated and field-observed soil moisture and temperature

	Depth	RMSE		r	
	(m)	CT	NT	CT	NT
Moisture content (m^3 m^{-3})	0.05	0.0381	0.0266	0.7391	0.8248
	0.25	0.0599	0.0351	0.8847	0.8874
	0.55	0.0339	0.0331	0.9374	0.8482
	0.85	0.0397	0.0197	0.9400	0.9328
Average	0-1.00	0.0429	0.0286	0.8753	0.8733
Temperature (˚C)	0.05	2.5601	2.3901	0.9315	0.9331
	0.25	1.7290	1.9684	0.9631	0.9449
	0.55	1.2680	1.7805	0.9786	0.9505
	0.85	4.8673	1.5785	0.9813	0.9702
Average	0-1.00	2.6061	1.9294	0.9637	0.9497

2.3.4 Simulated Soil Temperatures

Observed and simulated soil temperatures are shown in Figure 2.5. The general trend of the soil temperature was well simulated by SHAW, although a few discrepancies between SHAW estimations and field observations were up to 5˚C at 0.85 m soil depth. Generally, observed soil temperatures were higher in CT than in NT at all soil depths which also reported by Drury *et al.* (1999) for top soil (0-0.10 m soil depth). SHAW tended to over-predict soil temperature during the soybean growing season. The discrepancies between observed and simulated soil temperature were most distinct in the surface layers as well as in 0.85 m soil depth. The reduced observed soil temperature compared to simulated soil temperature at 0.85 m soil depth was unexpected. The difference between observed and simulated soil temperature in NT may minimize by availability of reduced water or drainage at this depth. The input parameters for SHAW were very similar for the CT and the NT, except for the surface residues. SHAW simulated soil temperature of NT was slightly better than CT. However, overestimation of simulated soil temperature was observed at all soil depths in both treatments. Li *et al.* (2012) also reported overestimation of predicted soil temperature using SHAW model for 0.60 m soil profile. The RMSE values for soil temperature for different depths (Table 2.4) were in the range of 1.2 to 4.8˚C and 1.5 to 2.3˚C for the CT and

NT, respectively, with the largest discrepancy occurring at the lower most depth of 0.85 m in CT. However, as discussed previously an error in the sensor may have occurred. Besides 0.85 m depth in CT treatment, the accuracy of soil temperature prediction increased with soil depth for both CT and NT. The average RMSE of soil temperature from 1.5 to 2.6˚C simulated by SHAW was comparable to the results of the RMSD from 0.5 to 4.2˚C in Li *et al.* (2012). For the simulations performed the average correlation was above 0.94 (Table 2.4) suggesting that the trends of simulated soil temperature for CT and NT were very similar to the observed temporal pattern of soil temperature for all soil depths. Li *et al.* (2012) also reported SHAW predicted soil temperature showed 0.87 - 0.98 of correlation for the soil depth of 0.075 - 0.52 m and correlation increased with the increased of soil depth. The increased correlation at higher soil depth is due to the dampened fluctuation of soil temperature at those soil depths.

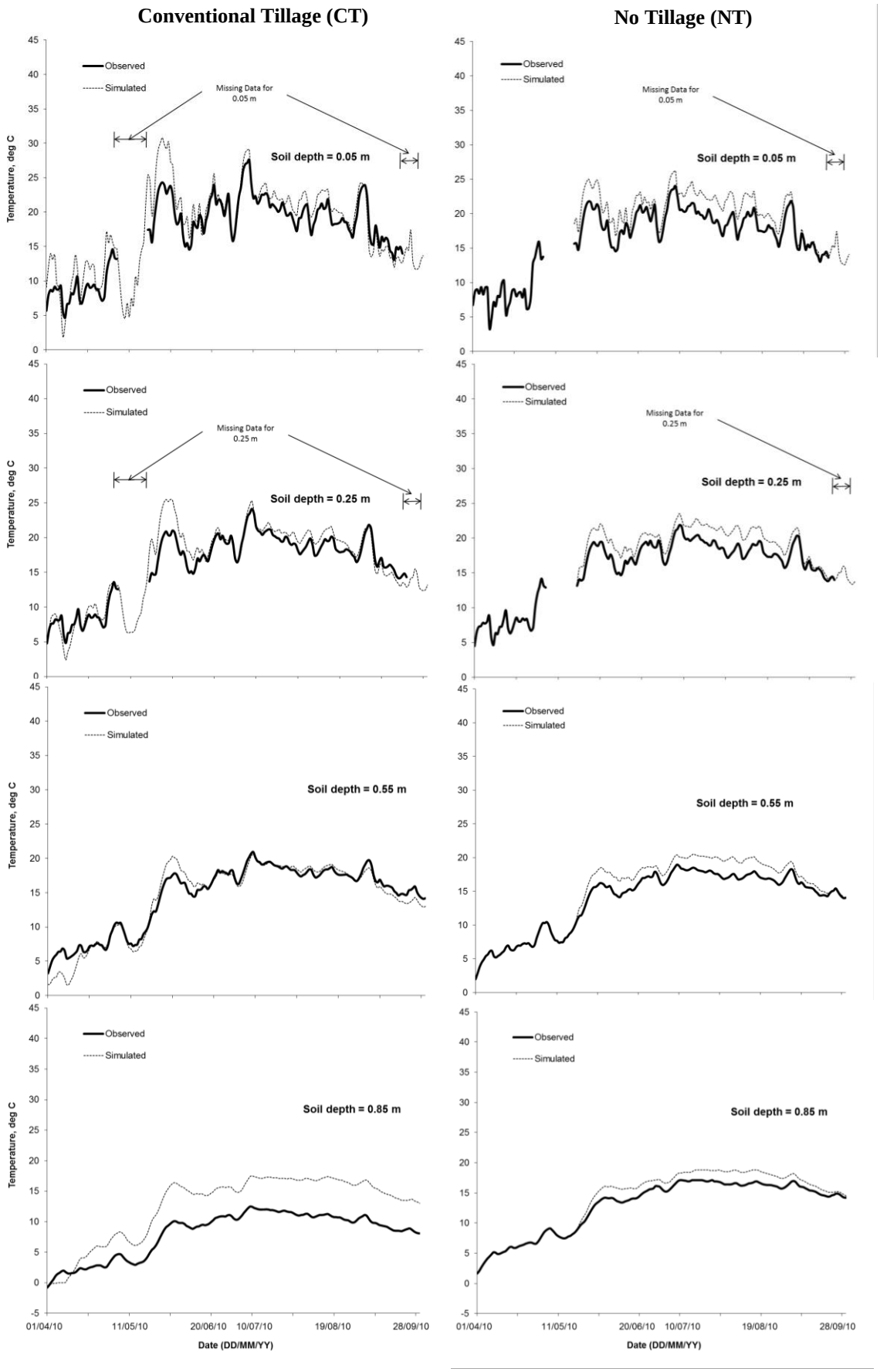

Figure 2.5: Observed and simulated soil temperatures (daily averages) at different depths for CT and NT.

2.4. Conclusions

This study documents some of the effects of tillage management systems on soil water budgets under a soybean crop system. Over the crop year, the NT treatment had higher soil moisture in the upper soil layers and particularly later in the growing season than observed in CT treatment. Simulations of these conditions using SHAW demonstrate that SHAW typically under-predicted soil moisture content at all soil depths except surface soil of NT. However, SHAW simulations of soil moisture content followed the general trend of the observed data suggesting that can be used for reasonable simulation of soil water budgets for this region under different land management practices. Generally, the absolute differences in soil moisture between observed and simulated data were mostly less than 0.05 m^3 m^{-3} over both treatments. For simulation of soil temperature, SHAW over-estimated soil temperatures for the CT and NT by up to 2.5˚C on average over the entire experimental period. Maximal deviations between measurements and simulations were up to 5˚C at the 0.85 m soil depth. The trend of soil temperatures, nonetheless, was well described by the SHAW model. Therefore, SHAW model has some capacity for the prediction of soil moisture and temperature under different agricultural management practices.

Chapter 3

Effect of Land Surface Heterogeneity on Simulated and Observed Brightness Temperature

Motivation

Sparse *in-situ* measurements are not sufficient to represent soil moisture for large areas as soil moisture varies widely both spatially and temporarily due to spatio-temporal variations in precipitation, soil texture, slope, vegetation, and agricultural management practices. Microwave remote sensing (at L-band) is useful to estimate soil moisture at large scales due its advantages in prediction accuracy for all weather monitoring and frequent availability over different satellite-based remote sensing techniques. The limitations of L-band passive microwave remote sensing are its sensitivity to the thermal emission from 2-5 cm soil depth and low spatial resolution (~40 km) of available satellites. Due to low spatial resolution, the retrieval of soil moisture or brightness temperature is affected by various land surface heterogeneities, like – variations in soil moisture, soil temperature, soil roughness and vegetation water content. There are limited studies that investigate the effect of land surface heterogeneity on retrieval of soil moisture accuracy. Given the sensitiveness of Simultaneous Heat and Water (SHAW) model to analyze water budget for 1-m soil profile of conventional and no tillage agricultural management practices (in Chapter 2), there is an opportunity to use the SHAW model to estimate soil moisture for incorporation into the Land Parameter Retrieval Model (LPRM) to estimate the brightness temperature associated with heterogeneous landscapes. It is necessary to investigate the impact of land surface heterogeneities on the brightness temperature errors obtained from the combined SHAW and LPRM models for in a region with variation in soil texture and crop cover. The errors are determined by comparing modeled brightness temperature with measurements made by the Soil Moisture and Ocean Salinity (SMOS) satellite.

Abstract

Soil moisture plays a significant role in productive crop growth and farm operations. Correct estimation of soil moisture is important and useful in irrigation scheduling, nutrient/ fertilizer management plan, site-specific management of disease and pests, monitoring of crop yields and indication of plant health. Due to limitations of *in-situ* soil moisture measurements, and low resolution of microwave remote sensing of soil moisture, a model that simulates soil moisture coupled with a radiative transfer model could potentially be used for downscaling passive microwave measurements to provide a higher resolution soil moisture product. The Soil Moisture Active Passive Validation Experiment 2012 (SMAPVEX12) provided an opportunity to evaluate spatial and temporal variations in soil moisture patterns across a region of similar size to the scale of two passive microwave pixels. There were two objectives for this study. The first was to investigate the ability of the Simultaneous Heat and Water (SHAW) model to simulate surface soil moisture as compared to *in situ* measurements for various soil texture and crops. The second was to assess the impact of land surface heterogeneity on brightness temperature. The SHAW model simulated soil moisture followed the general trends of the observed field data. The average root mean square error (RMSE) for surface soil moisture was 0.05 m^3 m^{-3}. The correlation between SHAW and *in situ* measurements were 0.38 to 0.86 for surface soil moisture. The lowest correlation for surface soil moisture was observed for sand soil. The horizontal polarized brightness temperature from a radiative transfer model, using soil moisture from the SHAW model, followed the general trends of the horizontal polarized SMOS brightness temperature (r = 0.72**). Accounting for land surface heterogeneities, sub-grid estimates of soil moisture and soil temperature were of critical importance and explained errors between the simulated brightness temperature and SMOS observations (r > 0.48**). Soil roughness and

vegetation water content have insignificant influence on the variation of brightness temperature difference.

Keywords: hydrological modeling (SHAW), soil moisture, forward radiative transfer model, brightness temperature, heterogeneity

3.1. Introduction

Knowledge of soil moisture is important for a number of agricultural applications including irrigation scheduling, site-specific management of some plant diseases and pests, crop yield predictions, and plant health (Moran *et al.*, 2004). Many studies report that sparse *in-situ* measurements are not sufficient to measure soil moisture for large areas as soil moisture varies widely, both spatially and temporally due to variations in precipitation, soil texture, slope, vegetation, and agricultural management practices (Jackson, 1990; Liu *et al.*, 2011; Klute, 1986; McCoy *et al.*, 2006). Therefore, measurements of soil moisture from satellite platforms that average over larger regions will have many potential benefits.

Remote sensing of soil moisture is based on the measurement of the dielectric properties of liquid water within the soil, which has a dielectric constant of ~80, contrary to dry soil with a dielectric constant < 4 at L-band (Wang and Schmugge, 1980). Among different satellite-based remote sensing techniques (optical, thermal infrared, active microwave), passive L-band microwave remote sensing is considered more advantageous for estimating soil moisture as it has shown higher accuracy, has less sensitivity to water vapor in the atmosphere, is able to estimate soil moisture where vegetation is present (limited to regions with less than 5 kg m^{-2} vegetation water content), and has higher return frequency (2-3 days) (Entekhabi *et al.*, 2010; Kerr *et al.*,

2012; Moran *et al.*, 2004; Njoku *et al.*, 2003). Active microwave remote sensing systems are more affected by surface roughness, topography and vegetation than passive systems (Dobson *et al.*, 1986; Dubois *et al.*, 1995; Oh *et al.*, 1992). A microwave radiometer measures the emitted energy (in the microwave frequency) from the land surface, which is dependent on surface soil moisture, surface temperature, surface roughness, vegetation water content, and vegetation structure (Jackson and Schmugge, 1991; Owe *et al.*, 2008; Wigneron *et al.*, 2001).

Currently, passive microwave L-band brightness temperatures at 1.4 GHz are available from the Soil Moisture and Ocean Salinity (SMOS) satellite with a temporal resolution of 2-3 days and a spatial resolution of 43 km (Kerr *et al.*, 2012). The SMOS satellite was launched by European Space Agency (ESA) in November 2009. With the aim of obtaining soil moisture measurements at a higher spatial resolution, the National Aeronautics and Space Administration (NASA) plans to launch the Soil Moisture Active Passive (SMAP) satellite in October 2014 (Entekhabi *et al.*, 2010). The SMAP mission will provide soil moisture products at low (36 km), high (3 km) and intermediate (9 km) spatial resolutions, using measurements from the radiometer, radar and a combination of radiometer and radar, respectively. The soil moisture products are required to be within $\pm$ 0.04 $m^3 m^{-3}$ of the actual soil moisture within the top five centimeters of the soil when the vegetation water content is $\leq$ 5 kg m^{-2} for a spatial resolution from ~10 km to ~40 km (Entekhabi *et al.*, 2010).

Due to limitations of *in-situ* measurements (low spatial resolution) and remotely sensed estimates of surface soil moisture (large spatial extent but low sensing depth), model driven soil moisture is necessary to understand detailed hydrologic process, and water budgets through the root zone

(Njoku *et al.*, 2003; Schlenz *et al*., 2012). One hydrological model that has been used successfully for modeling root zone hydrological process is the Simultaneous Heat And Water (SHAW) model, a physically based one-dimensional vertical model that was developed by Flerchinger and Saxton (1989) to simulate freezing and thawing of soils. This model requires either measured or estimated parameters and can be used with or without calibration for various applications. Flerchinger *et al.* (2012) and Wang *et al.* (2010) used the SHAW model to estimate soil moisture because it accounts for the effects of climate, residue, topography, tillage management, soil characteristics and vegetation canopy, and moreover, it has shown to successfully simulate heat movement, evapotranspiration, soil temperature, soil moisture and freezing depth in wide range of conditions including seeding germination, vegetation, weed emergence, irrigated and rain fed cultivation, etc. Compared to the Decision Support System for Agrotechnology Transfer-Cropping System Model (DSSAT-CSM), Wang *et al.* (2010) reported that the SHAW model improved the prediction of root zone soil moisture (RZSM) at 0-120 cm depth for conventional wheat cultivation with high correlation (r = 0.81). Li *et al.* (2012) reported that root mean square deviation (RMSD) between SHAW simulated soil moisture and observed soil moisture varied from 0.016 to 0.042 m^3 m^{-3} for non-irrigated rye.

Radiative transfer models are used to estimate surface soil moisture using measured brightness temperature (T_b) at microwave frequencies (Njoku *et al.*, 2003; Owe *et al.*, 2008). Owe *et al.* (2008) used the Land Parameter Retrieval Model (LPRM) and found that the daily average surface soil moisture from the T_b measured by the Advanced Microwave Scanning Radiometer for Earth Observing System (AMSR-E) satellite, at 6.96 GHz (C-band), compared well to ground measurements taken at 10 cm depth. They also reported that satellite observations were highly

sensitive to changes in soil moisture at the surface because the surface layer (<1 cm) dries much faster than deeper layers (>5 cm). The LPRM was also successfully used at the L-band frequency using SMOS scale observations from airborne flight to predict surface soil moisture at lower varied incidence angles (2 ~ 44˚) where canopy information was not required (De Jeu, *et al.*, 2009). Land surface heterogeneity produces some error in soil moisture retrieval at large footprint scales (e.g. SMOS observations), where uncertainty in soil moisture, soil temperature, soil texture, surface roughness and vegetation water content exist (Davenport *et al.*, 2008; Panciera *et al.*, 2011). However, there are a small number of studies that have assessed this problem of land surface heterogeneity using passive microwave data as most studies have been conducted in regions with smooth topography, partial vegetation and had limited ground sampling using airborne L-band data over an area the size of a SMOS pixel (Panciera *et al.*, 2011). After successful downscaling of low resolution heterogeneous SMOS observations to high resolution or point measurement, there is an opportunity to test its assimilation into land surface models for root zone soil moisture retrieval (Panciera *et al.*, 2008).

The limitation of remote sensing and models in estimating soil moisture are the result of various factors including: accuracy, uncertainty of observations, low spatial resolution, availability of satellite, etc. (Alavi *et al.*, 2009; Reichle and Koster, 2004; Zhan *et al.*, 2006; Liu *et al.*, 2011). Therefore, data assimilation (DA) of remote sensing data into process-based models is required to extract information to reduce errors and provided moisture at different soil depths and to make the data more accessible to users. In fact, the basic principle of data assimilation is to combine the information from measurements and models of the earth system into an optimal estimate of the geophysical fields of interest (Reichle, 2008). The satellite observed brightness temperatures

(T_b) are generally assimilated into Land Surface Models (LSMs) to improve soil moisture estimates due to uncertainties in land surface parameters in the retrieval algorithms (Richle, 2008; Richle *et al.*, 2008). For example, Dumedah *et al.* (2011) studied use of genetic algorithms (GAs) in data assimilation due to limitations of error in prediction. The first assimilation procedure generated a time series of soil moisture by assimilating brightness temperature from the Advanced Microwave Scanning Radiometer-Earth Observing System (AMSR-E) into the Land Parameter Retrieval Model (LPRM). The second procedure generated assimilated soil moisture by assimilating the soil moisture from LPRM into the Canadian Land Surface Scheme (CLASS) model. The retrieved soil moisture dataset was evaluated and it was found that the accuracy and temporal pattern of soil moisture compared to *in-situ* data was improved (overall r = 0.45 to 0.56 at 20 cm soil depth).

The Soil Moisture Active Passive Validation Experiment 2012 (SMAPVEX12) was a pre-launch validation campaign to evaluate soil moisture retrieval algorithms for the SMAP mission (McNairn *et al.*, 2013). The campaign was conducted from June 6 to July 17, 2012 (approximately 6 weeks), over a region approximately 15 km x 70 km in an agricultural region south of Winnipeg, Manitoba (Canada). The vegetation land cover consisted of a large variety of crop types, some permanent grasslands and mixed forest cover (McNairn *et al.*, 2013). Over the study region a very large range in soil textures is present ranging from sands to clays (Rowlandson *et al.*, 2013). Given the variety of land surfaces and soil textures, SMAPVEX12 provided an opportunity to evaluate the impacts of land surface heterogeneities on brightness temperature retrievals from SMOS. The main objective of this study was to estimate brightness temperature using a radiative transfer model connected to a hydrological model. The combined

model was used to evaluate the sensitivity of L-band brightness temperature estimates to observed variability in soil moisture, soil temperature, soil roughness and vegetation water content, and compare these estimates to SMOS observed brightness temperature. Two versions of the radiative transfer model were evaluated where one assumed heterogeneous land cover and the other homogeneous land cover in the simulation of brightness temperature.

3.2. Data and Methodology

3.2.1 SMAPVEX12 Field Campaign and Recorded Parameters

The SMAPVEX12 field campaign site was located near Elm Creek (98˚0´23˝W, 49˚40´48˝N), Manitoba (McNairn *et al.*, 2012). The experimental site is shown in Figure 3.1. The soil texture varied from heavy clay in the eastern portion of the study region to sandy soil in the west (AAFC, 2010). Changes in the topography of the region are minimal with a slope of 0-2% and NE aspect (AAFC, 2010; Walker, 2012). The major cultivated agricultural crops in the study area were cereals and oilseeds. Most of the crops were seeded in April/May and harvested in August/September. The typical field size varied from 20-30 to 50-60 hectares. The SMAPVEX12 measurements (soil and vegetation) were taken in 55 field sites, with continuous *in-situ* surface soil moisture measurements in 40 fields through installation of network stations for the duration of the campaign. The location of SMAPVEX12 site and temporary network stations are shown in Figure 3.1. Descriptions of the vegetation and soil samples taken during the field campaign can be found in McNairn *et al.* (2013) and Rowlandson *et al.* (2013).

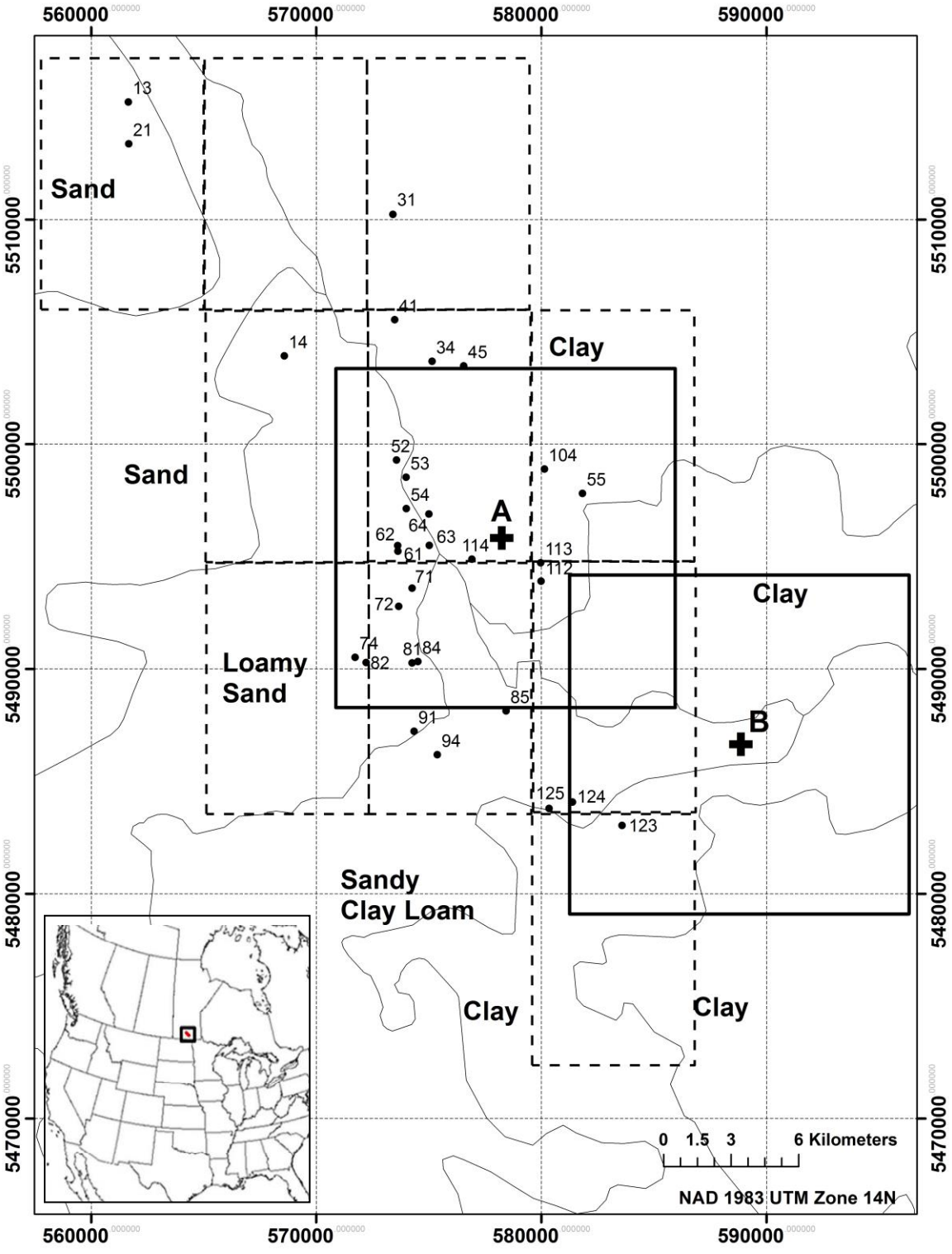

Figure 3.1: Location of SMAPVEX12 study site with field ID number (solid circle = *in-situ* temporary network station; solid cross = center of pixels A and B; solid square = 15 km x 15 km area of pixels; dotted rectangle = CaPA forecasted precipitation pixels, 7 km x 11 km; contours = areas of different soil type).

During the field experiment, temporary soil moisture stations were installed in 40 out of 55 SMAPVEX12 fields (Figure 3.1). However, for this study only 31 of the temporary soil moisture stations were used due to the malfunctioning sensors. The soil texture and crop type of each selected temporary network field site is shown in Table 3.1. These *in-situ* network sites (Figure 3.2) had Stevens Hydra Probes (Stevens Water Monitoring Systems, Inc., Portland, OR, USA) installed horizontally at approximately 5 cm depth and soil moisture was recorded hourly. The temporary stations were installed at the end of May and removed after field campaign in Mid-July 2012. Details regarding the calibration of the probes installed at the temporary network stations can be found in Rowlandson *et al.* (2013).

Table 3.1: Soil characteristics at 0.05 m depth and land coverage of 31 temporary network field sites during SMAPVEX12 campaign

Field	X	Y	Soil	Soil Texture		Bulk	Crop	VWC	Average Roughness	
				Sand	Clay	Density		Range	RMS height	Corr. length
	(m)	(m)		%	%	(kg m^{-3})		(kg m^{-2})	mm	mm
13	561656.95	5515231.78	Loamy sand	84.2	10.3	1.29	Pasture	0.08-0.12	0.50	9.20
14	568587.55	5503930.25	Sand	94.2	4.4	1.30	Soybean	0.11-0.91	0.86	11.75
21	561676.32	5513370.60	Sandy clay loam	51.0	34.6	1.27	Pasture	0.50-0.32	1.34	53.00
31	573410.34	5510233.43	Sandy clay	4.3	39.9	1.08	Wheat	1.60-2.31	0.59	7.25
34	575150.10	5503688.25	Heavy clay	4.4	66.8	0.88	Soybean	0.07-0.98	0.66	64.00
41	573490.04	5505534.18	Heavy clay	4.5	64.0	0.82	W. wheat	4.60-1.30	1.69	35.00
45	576559.71	5503481.39	Heavy clay	2.1	70.2	0.81	Wheat	2.00-2.36	0.85	6.50
52	573570.98	5499294.85	Sandy clay loam	52.3	29.6	1.20	Soybean	0.11-2.18	1.65	55.50
53	573999.22	5498529.79	Sandy clay loam	57.8	29.1	1.21	Corn	0.02-3.27	0.55	15.50
54	574006.07	5497135.74	Sandy loam	75.1	18.6	1.30	Corn	0.09-4.61	0.54	15.25
55	581830.20	5497814.33	Heavy clay	4.0	70.9	0.98	Wheat	1.15-2.29	0.90	8.00
61	573630.54	5495242.55	Loamy sand	83.3	11.8	1.34	Canola	0.90-2.75	0.75	9.00
62	573622.27	5495489.64	Sand	90.0	7.6	1.41	Corn	0.06-3.12	0.57	27.00
63	575031.72	5495495.80	Loamy sand	86.6	9.7	1.12	Soybean	0.06-0.98	0.65	14.00
64	575009.84	5496895.45	Sandy clay loam	61.5	28.7	1.18	Soybean	0.04-0.25	1.14	6.50
71	574262.46	5493599.96	Sand	93.5	6.3	1.40	Corn	0.02-3.01	0.55	36.25
72	573669.42	5492789.66	Sand	93.6	4.9	1.41	Corn	0.02-3.60	0.46	5.50
74	571733.87	5490523.75	Loamy sand	86.6	7.8	1.30	Wheat	1.20-2.30	1.20	14.00
81	574264.04	5490270.72	Loamy sand	84.8	9.6	1.16	Wheat	1.20-1.53	0.74	7.50
82	572218.29	5490289.89	Sandy loam	74.8	13.8	1.18	Soybean	0.04-2.28	0.78	8.50
84	574523.14	5490330.29	Sandy loam	73.1	16.7	1.34	Canola	0.59-3.18	0.83	8.00
85	578439.23	5488135.55	Clay	15.1	47.3	0.91	Wheat	1.92-1.59	0.96	8.50
91	574356.80	5487232.00	Loamy sand	87.9	7.9	1.07	Wheat	1.83-1.60	1.05	19.50
94	575381.92	5486192.06	Sandy loam	70.8	18.3	1.28	Corn	0.16-2.67	0.99	35.20
104	580140.29	5498897.62	Heavy clay	3.2	69.8	1.00	Wheat	0.20-3.67	0.95	8.00
112	579992.60	5493904.55	Heavy clay	3.4	65.7	0.97	Soybean	0.03-0.54	0.55	6.75
113	579971.64	5494727.50	Heavy clay	3.4	63.6	1.04	Soybean	0.02-0.22	0.90	18.25
114	576926.86	5494885.57	Clay	34.9	40.6	1.16	Soybean	0.05-0.92	0.40	28.70
123	583592.00	5483047.77	Heavy clay	6.9	61.8	0.80	Soybean	0.02-0.65	1.85	24.75
124	581383.22	5484080.19	Clay loam	26.6	37.7	0.95	Canola	3.20-5.50	1.30	9.50
125	580349.74	5483798.18	Clay loam	36.6	35.2	1.00	Canola	2.50-6.03	1.30	6.70

Note: X and Y followed Universal Transverse Mercator coordinate system (UTM Zone 14); soil texture and bulk density recorded closed to temporary network station; range of vegetation water content (VWC) varied from June to July; roughness parameters recorded during beginning of campaign; RMS = root mean square; Corr.= correlation

Figure 3.2: Temporary network station.

3.2.2 The SHAW Model and Required Parameters for Simulations

The SHAW model requires local hourly weather data (air temperature, relative humidity, wind speed, precipitation and solar radiation), estimated and recorded site characteristics (saturated hydraulic conductivity, pore size distribution index, air entry potential, porosity, bulk density, texture, organic matter, etc.) and plant growth (height, dry biomass, leaf area index, etc.) data. Using these parameters, the SHAW model describes the one-dimensional coupled water and heat flow in soils through vertical profile extending from top of plant canopy to specified soil depth (Flerchinger and Saxton, 1989; Flerchinger *et al.,* 2012). For details of model readers are referred to Flerchinger and Saxton (1989), Flerchinger (2000) and Flerchinger *et al.* (2003).

Hourly air temperature, wind speed, relative humidity, solar radiation and precipitation are used as the upper boundary in SHAW model to define heat and water fluxes (Flerchinger, 2000). Due to unavailability of complete required hourly weather data from nearby meteorological stations at Carman and Elm Creek, the available hourly weather data (excluding precipitation) used in this study were collected from St. Adolphe weather station, located approximately 70 km north-east

of the study region. Hourly precipitation data was extracted from 6-hour estimates at a 7 km x 11 km spatial resolution from the Canadian Precipitation Analysis (CaPA) product from Environment Canada. Ten CaPA pixels used in this study are indicated by dotted rectangles in Figure 3.1. The CaPA data is derived from statistical interpolation where Canadian Meteorological Center (CMC) regional model is used as the background field with rain-gauge measurements and radar extracted rain rates as observations (CaPA, 2013; Mahfouf *et al.*, 2007). CaPA data was used in this study due to an insufficient number of precipitation gauges within the study region.

Inputs for the SHAW model simulations were determined from the available field measurements (soil texture, bulk density, crop height, crop dry biomass, LAI) while other parameter values (pore size distribution index, air entry potential, porosity, organic matter, leaf width and crop root depth) were obtained from the literature. In fact, the determination of these other parameters are costly, difficult and impractical (Flerchinger *et al.,* 2012). The SHAW model was used to simulate soil moisture for each SMAPVEX12 agricultural field which contained an *in situ* soil moisture station during the field campaign period. The soil domain or profile for the SHAW model was set at 1.3 m deep. The 1.3 m soil profile was chosen in the SHAW model because some crop roots (e.g. corn) may extend below 1 m during the mature stage of the growing season (Allen *et al.*, 1998). The domain was discretized into a total of 15 nodes in the physically-based SHAW model calculating moisture at the 0-5 cm (0, 5, 10 cm) and 20-100 cm (20, 30, 40, 50, 60, 70, 80, 90, 100, 110, 120, 130 cm) soil depths which correspond to the surface soil moisture (SSM) and root zone, respectively. For water flow, a unit-gradient (gravity flow) boundary condition was used for the lower boundary and a specified flux (observed precipitation) for the

upper boundary. Similarly, a unit-gradient boundary condition was used for the lower boundary and a specified flux (observed air temperature) for the upper boundary (Flerchinger, 2000). The model was initialized May 1, 2012 where the conditions for water and heat flow were set at field capacity soil moisture (based on soil texture) and air temperature. It was assumed that model stabilized prior to start of the field campaign. For each site, manual calibration was followed to get better fit between simulated soil moisture and observed soil moisture trends by adjusting unknown soil parameters. Trial-and-error based calibration was performed where minor adjustments to pore size distribution index and air entry potential were made to obtain minimum RMSE (Root Mean Square Error) between daily observed and simulated soil moisture at 0.05 m soil depth. Ranges for the pore size distribution index, air entry potential, saturated hydraulic conductivity, porosity and organic matter are presented in Table 3.2 and based on literature indicated. For calibration results of the SHAW model, Flerchinger *et al.* (2012) reported that outcomes of trial-and-error method worked quite well in comparison with stepwise and parameter optimization algorithms (Monte Carlo simulations) methods, with the lowest root-mean-square deviation (RMSD) for loamy sand, sandy loam and silt loam. Many of the parameters necessary to run SHAW model were available from SMAPVEX12 field campaign and from the literature, and are listed in Table 3.2.

Table 3.2: Approximate range and source of input parameters of SHAW model

Input Parameters	Approximate Range	Source
Soil characteristics:		
Pore size distribution index	3.8 -12.22 (sand - clay)	Abdel-Nasser, 1999
Air entry potential, m	-0.009 - -0.71 (sand - clay)	Abdel-Nasser, 1999
Saturated hydraulic conductivity, cm/h	21 - 0.06 (sand - clay)	Rawls *et al.*, 1982
Porosity	0.43 -0.47 (sand - clay)	Rawls *et al.*, 1983
Bulk density, kg/cu. m	1.6 - 0.80 (sand - clay)	SMAPVEX12
Sand, %	3 - 95	SMAPVEX12
Silt, %	4 -90	SMAPVEX12
Clay, %	4 - 70	SMAPVEX12
Organic matter, %	0.10 – 10 (sand – clay)	AAFC, 2010
Plant characteristics:		
Height, m	0 - 2	SMAPVEX12
Leaf width, cm	0 - 8	Allen *et al.*, 1998
Dry biomass, kg/sq. m	0 - 1.4	SMAPVEX12
Leaf are index (LAI)	0 - 4	SMAPVEX12
Effective root depth, m	0 - 1.4	Allen *et al.*, 1998
Hourly weather data:		
Avg. air temperature, ˚C	3 - 28	St. Adolphe Station
Relative humidity, %	20 - 97	St. Adolphe Station
Wind speed, mile h^{-1}	1 - 25	St. Adolphe Station
Precipitation, inch	0 - 0.22	CaPA
Density of snow, g cm^{-2}	0	St. Adolphe Station
Solar radiation, W m^{-2}	0 - 700	St. Adolphe Station

The SHAW model for estimating surface soil moisture was validated by the root mean square error (RMSE) and evaluated its significant trends by correlation co-efficient (r) using the simulated and observed soil moisture values. The RMSE and r were defined as:

$$RMSE = \sqrt{\frac{\sum_{i=1}^{n}(x_i - y_i)^2}{n}} \qquad [3.1]$$

$$r = \frac{\sum_{i=1}^{n}\left((x_i - \bar{x})(y_i - \bar{y})\right)}{\sqrt{\sum_{i=1}^{n}(x_i - \bar{x})^2 \sum_{i=1}^{n}(y_i - \bar{y})^2}} \qquad [3.2]$$

where, x = observed soil moisture, y = simulated soil moisture, i = days of campaign period, and n = number days of field campaign.

3.2.3 Microwave Radiative Transfer Model

Soil microwave emission generally originates from the top surface layer where the emitting depth is governed by the dielectric characteristics of the near-surface moisture profile and is shallower for higher frequencies and for wetter soils. At the L-band (~1-2 GHz) frequency, the emitting depth is approximately 5 cm (Njoku *et al.*, 2003). Microwave emission is referred to as brightness temperature (T_b) which is a function of the physical temperature and the emissivity of radiating body (Owe *et al.*, 2001; Owe *et al.*, 2008). The horizontal polarization of T_b at low passive microwave frequency represents surface soil moisture with more accuracy than vertical polarization (Moran *et al.*, 2004; Owe *et al.*, 2008). Soil moisture is typically estimated from passive microwave observations of T_b using model inversions of radiative transfer models. The Land Parameter Retrieval Model (LPRM), a radiative transfer model, initially developed for the C-, X- or Ku bands frequency with higher incidence angle range of 50 – 55˚ (Owe *et al.*, 2001; Owe *et al.*, 2008) and used to successfully estimate soil moisture using brightness temperature observations from the Advanced Microwave Scanning Radiometer – Earth Observing System (AMSR-E) (Owe *et al.*, 2008), and has been used at L-band frequencies by De Jeu *et al.* (2009). The LPRM model is well described in Owe *et al.* (2001) and Owe *et al.* (2008). Adaptation to this model for this analysis and the necessary model parameters are described in Table 3.3.

Table 3.3: Values and source of input parameters of LPRM model for L-band frequency

Input Parameters	Approximate Range/Value	Source
Radiative characteristics:		
Frequency (f), GHz	1.4	Panciera *et al.*, 2011
Polarization mixing fraction (Q)	0	Wigneron *et al.*, 2001
Incidence angle (u), ˚	40	Panciera *et al.*, 2011
Soil characteristics (at 0.05 m soil depth):		
Soil moisture (W_s), $m^3\ m^{-3}$	0.03 – 0.43	SHAW estimation
Wilting point (WP)	0[#]	Wang and Schmugge, 1980
Soil/canopy temperature (T_s), ˚C	13.7 – 29.7	SHAW estimation
Porosity	0[#]	Wang and Schmugge, 1980
Bulk density, g cm^{-3}	1.6 - 0.80 (sand - clay)	SMAPVEX12
Sand (S)	0.03 – 0.95	SMAPVEX12
Clay (C)	0.04 – 0.70	SMAPVEX12
Average RMS height, mm	0.40 – 1.85 (sand – clay)	SMAPVEX12
Average correlation length, mm	5.50 – 64.00 (sand – clay)	SMAPVEX12
Plant characteristics (for selected 6 crops):		
Vegetation single scattering albedo (ω)	0	Mo *et al.*, 1982; ATBD, 2010
Vegetation parameter (b)	0.04 – 0.30	Jackson and Schmugge, 1991
Vegetation water content (Wv), kg m^{-2}	0.02 – 6.03	SMAPVEX12
Atmospheric characteristics:		
Atmospheric opacity (τ_a)	0.01	ATBD, 2010
Extraterrestrial brightness temperature, K	2.7	Martin, 2004
Weighted mean temperature (T_m), K	70.2+0.72 T_s	Bevis *et al.*, 1992

[#] values assigned 0, but model utilizes soil texture and bulk density to estimate

Soil surface roughness effects the microwave emission and scattering from the soil (Wigneron *et al.*, 2001). Wigneron *et al.* (2001) reported that the roughness parameter (h_s) is a function of surface root mean square (RMS) height (s), correlation length (l) and dynamics of surface soil moisture (W_s). They also reported that h_s was independent of incidence angle and polarization for rough surfaces at L-band frequency. For a wide range of surface soil moisture (0.03-0.35 $m^3\ m^{-3}$), they developed the following equation.

$$h_s = A \times \left(W_s^B\right) \times \left(\frac{s}{l}\right)^C \qquad [3.3]$$

where A=0.5761, B=-0.3457, and C=0.4230. The values of average RMS height and correlation length were obtained for each field in the SMAPVEX12 experiment when the field campaign started. In SMAPVEX12, roughness was measured using a 1-m portable pin-profilometer at two locations in each field to obtain the roughness parameters of RMS height (*s*) and correlation length (*l*). Average RMS height for Passive/Active L-band Sensor (PALS) flight is considered in this study where pin-profilometer placed perpendicular to the orbital track or low-altitude PALS flight lines in north-south direction (McNairn *et al.*, 2013). It is noted that the flight lines were almost similar to the directions of the SMOS satellite movement.

Vegetation emits microwave radiation, but also absorbs and scatters radiation coming from soil (Jackson and Schmugge, 1991). The canopy or vegetation transmissivity (Γ_c) is dependent on incidence angle and vegetation optical depth, where $\Gamma_c = \exp(-\tau/\cos u)$ and $0 \leq \Gamma_c \leq 1$ (Njoku *et al.*, 2003). The LPRM calculates the optical depth (τ) from Microwave Polarization Difference Index (MPDI) where MPDI is more than 0.01 for LAI < 4 at 6.6 GHz (Meesters *et al.*, 2005). In this study, optical depth (τ) is calculated from vegetation water content (W_v) and vegetation parameter (b) where measured vegetation water content is available on a weekly basis from individual SMAPVEX12 fields. Jackson and Schmugge (1991) described the relationship between optical depth and vegetation water content as:

$$\tau = b \times W_v \qquad [3.4]$$

Jackson and Schmugge (1991) reported b-parameters for different crops at 21 cm or 1.4 GHz wavelength (0.05 for wheat, 0.113 for corn, 0.087 for soybeans, 0.30 for short grass, 0.08 for canola, and 0.04 for oat) from various studies. The b-parameter is dependent on plant type and

wavelength (Jackson and Schmugge, 1991). Daily vegetation water content data (W_v) was determined using linear interpretation between SMAPVEX12 sampling dates.

3.2.3.1 SMOS Data

Dumedah *et al.* (2013) examined the potential error between the 15-km L1c gridded brightness temperature product and the actual 42-km SMOS footprint brightness temperature. They found that the RMSE was about 4.5K with R^2=0.97 for H-pol, with an RMSE closer to 5K for undulating land with high topographic roughness. Due to the similarities in brightness temperature between the 15-km gridded product and 42-km brightness temperature, the 15-km spatial resolution pixel is considered in this study. Two 15-km pixels fell within the agricultural portion of the SMAPVEX12 domain, and are labeled A and B in Figure 3.1. The UTM coordinates for the centers of pixels A and B are (578746.45mE, 5495840.72mN) and (589023.95mE, 5485991.21mN), respectively. The SMOS observations (processing level: Level 1c with version 5.0.5) were at a range of incidence angles (15 ~ 63°) during the SMAPVEX12 campaign period (01 June – 20 July). The brightness temperatures used in this study were restricted to incidence angles of 39.5~40.5˚ (≈ 40˚). The incidence angle was chosen as it will be the angle used for the SMAP mission. The brightness temperatures were available for night and day passes (6 am and 6 pm) during the period of the SMAPVEX12 campaign.

3.2.3.2 Heterogeneous and Homogeneous Pixels Approach

In this study, simulated coarse spatial resolution is considered as 15km x 15km pixels (2 squares A and B in Figure 3.1). During the SMAPVEX12 campaign, crop types for each field within the study domain were identified. Soil classification for the region is available from the Soil

Landscapes of Canada database (AAFC, 2010). The area under individual crops and soil class for each pixel was extracted in ArcGIS software and is shown in Table 3.4 and Figure 3.3. In each pixel, six major crops (forage crops or grass, oats, wheat, corn, canola and soybean) and three soil types (clay, sandy clay loam and loamy sand in pixels A and B) within individual pixel area are considered. The two heterogeneous pixel brightness temperatures were calculated from a total of 36 (6 crops x 3 soil texture classes x 2 pixels) different SHAW & LPRM model runs and the weighted land cover fractions of each of the 36 runs considered in each pixel (i.e. considering representative area of the heterogeneous characteristics of crops and soils within individual pixels). The soil moisture and soil temperature were extracted from the SHAW model, and vegetation water content and surface roughness were determined using the data obtained during the field campaign (Table 3.1). The minor missing areas in pixels A and B (in Figure 3.3) are homestead, wetland, broadleaf and other minor crops (sunflower, etc.).

Table 3.4: Area under individual crop and soil class for different pixels

Crop	Pixel Area (15 km x 15 km)					
	Soil	Pixel A (sq. km)	Area %	Soil	Pixel B (sq. km)	Area %
Forage Crops	Clay	1.30		Clay	2.73	
	Sandy Clay Loam	0.00		Sandy Clay Loam	0.00	
	Loamy Sand	1.90		Loamy Sand	0.00	
Sub-total		3.20	1.52		2.73	1.30
Oats	Clay	25.60		Clay	20.04	
	Sandy Clay Loam	0.00		Sandy Clay Loam	1.96	
	Loamy Sand	4.20		Loamy Sand	0.00	
Sub-total		29.80	14.14		22.00	10.49
Wheat	Clay	33.40		Clay	49.40	
	Sandy Clay Loam	5.40		Sandy Clay Loam	4.24	
	Loamy Sand	6.20		Loamy Sand	0.00	
Sub-total		45.00	21.35		53.64	25.56
Corn	Clay	5.40		Clay	11.40	
	Sandy Clay Loam	2.30		Sandy Clay Loam	7.45	
	Loamy Sand	15.80		Loamy Sand	0.00	
Sub-total		23.50	11.15		18.85	8.98
Canola	Clay	34.30		Clay	44.00	
	Sandy Clay Loam	6.60		Sandy Clay Loam	6.70	
	Loamy Sand	7.40		Loamy Sand	0.00	
Sub-total		48.30	22.91		50.70	24.16
Soybean	Clay	43.00		Clay	53.90	
	Sandy Clay Loam	4.60		Sandy Clay Loam	8.00	
	Loamy Sand	13.40		Loamy Sand	0.00	
Sub-total		61.00	28.94		61.90	29.50
Total		210.80	100.00		209.82	100.00

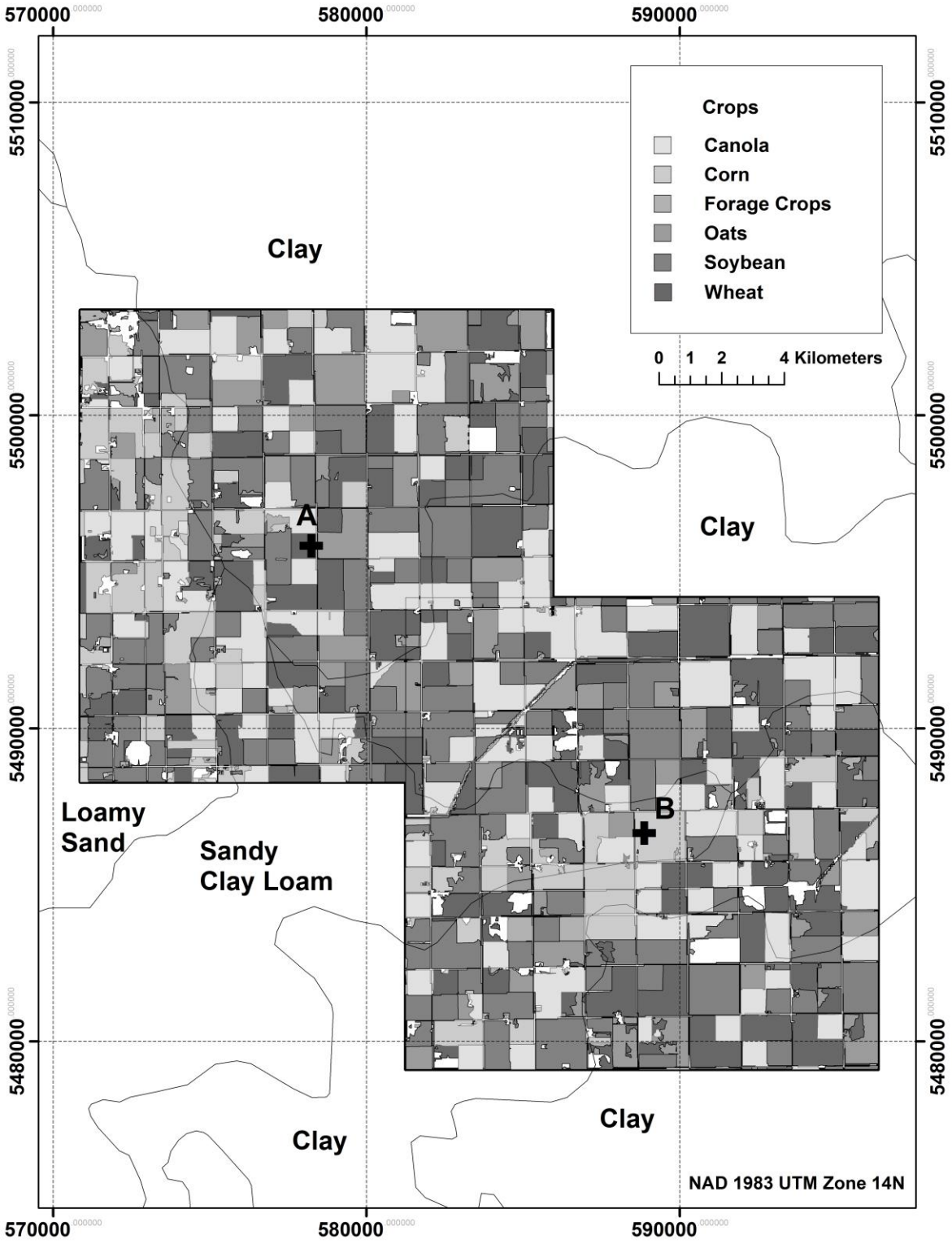

Figure 3.3: Area distribution of individual crops in 2 pixels.

For the homogeneous or traditional uniform pixel approach, the pixel is considered uniform in terms of land cover, soil texture, soil temperature, vegetation water content and surface roughness. Therefore, pixel average soil texture (sand, silt and clay) was calculated based on the weighted soil fractions of clay, sandy clay loam and loamy sand of the individual pixels (calculated from Table 3.4) and presented in Table 3.5. The average soil texture of pixels A and B was found to be clay. The uniform vegetation for each pixel was determined by selecting the most dominant crop within the pixel area. The crop type for pixel A and pixel B was determined to be soybean as it was about 29% of total area for pixel A, and 30% of total area for pixel B. The average soil moisture and soil temperature (extracted from SHAW model), vegetation water content and surface roughness were determined using the data obtained from these soil types and individual crops observed during the field campaign (Table 3.1). The two homogeneous pixel brightness temperatures were calculated from a total of 2 (1 crop x 1 soil texture class x 2 pixels) different SHAW and LPRM model runs.

Table 3.5: Crops and average soil texture of 2 pixels

		Average soil texture				
	Crops	Sand	Silt	Clay	Total	Soil class
Pixel A	Soybean	28.43	22.77	48.80	100.00	clay
Pixel B	Soybean	12.89	27.84	59.27	100.00	clay

The two horizontal polarized brightness temperatures simulated for heterogeneous and homogeneous conditions was calculated for each pixel. In model validation of the SHAW coupled LPRM simulations, RMSE and correlation were calculated between each simulated brightness temperature (from both the heterogeneous and uniform pixel scenarios) and compared to SMOS observations. The H-pol brightness temperature difference was calculated from

individual pixel brightness temperature (for heterogeneous and homogeneous) and the SMOS observations.

3.3. Results

3.3.1 Corroboration of SHAW Simulated Surface Soil Moisture with Observations

During the SMAPVEX12 experiment, surface soil moisture at 5 cm depth was recorded in 31 temporary network stations continuously from 6th June to 15th July, 2012. Average precipitation and surface soil moisture of the 31 fields and the variation in surface soil moisture during the campaign are shown in Figures 3.4a-c. The average CaPA precipitation for the region is presented Figure 3.4a. It indicated that a long drying period that followed a heavy rainfall on June 10 (56 mm) during the beginning of campaign and further scattered rainfall occurred toward the end of the campaign (Figure 3.4a). Therefore, observed surface soil moisture ranged from saturation to very dry conditions. The range of the daily surface soil moisture observed throughout the campaign is shown in Figure 3.4b. This plot shows the mean, minimum and maximum daily surface soil moisture observations of 31 fields and illustrates soil wetting and drying conditions. The average observed surface soil moisture of 31 fields showed comparatively higher (~ 0.30 m^3 m^{-3}) in the beginning of June and lower (~0.20 m^3 m^{-3}) in July which was due to the occurrence of precipitation. The trend of observed average soil moisture is found to be similar to that trend presented by McNarin *et al.* (2013) for 40,000 measurements taken over 55 fields using hand held soil moisture monitoring probes over a 0-6 cm soil depth for the almost same duration. Figure 3.4c shows the variability in the soil moisture for individual field for the entire campaign where precipitation of individual CaPA pixels were considered for individual field during SHAW model execution. The variation of temporal surface soil moisture varied

widely, especially in heavy clay soils (e.g. fields 55, 113, 114). Sandy fields exhibited lower range of surface soil moisture (e.g. fields 13, 14, 62, 71, 72).

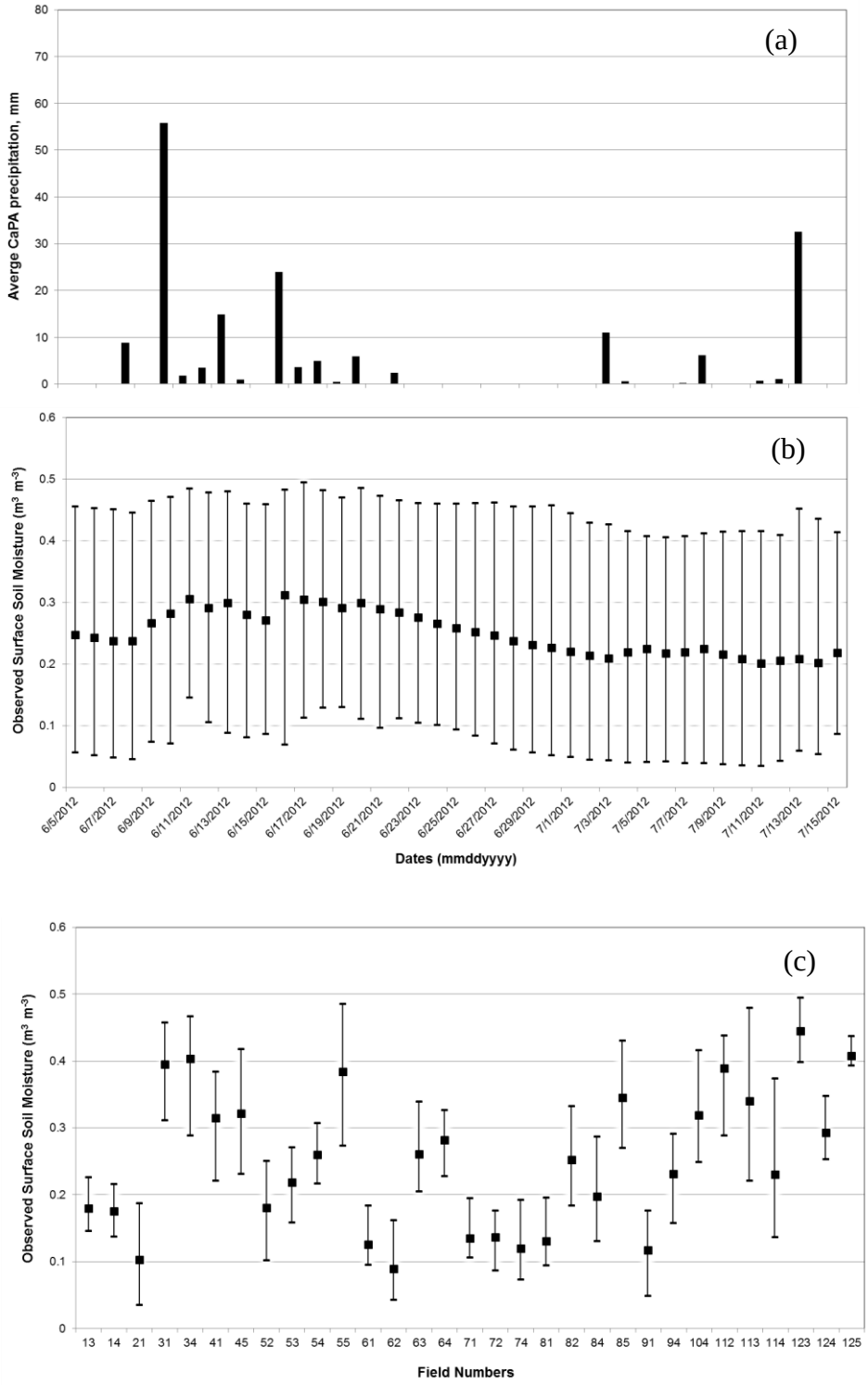

Figure 3.4: (a) average CaPA precipitation throughout SMAPVEX12 campaign; (b) surface soil moisture mean and range over the 31 agricultural fields; (c) mean and range of surface soil moisture conditions over each of the 31 sample fields during the experiment.

Before coupling the SHAW simulations of soil moisture to the LPRM, the simulated soil moisture time series was compared to *in-situ* data for each of the 31 fields. The time series of the daily mean simulated and *in situ* dataset is shown in Figure 3.5a, the error bars represent simulated minimum and maximum surface soil moisture of the 31 agricultural fields and the observations during the time period is shown as the solid line. Generally, the time series is well represented, however, SHAW overpredicted soil moisture at 0.05 m soil depths during wet period (until middle of June). Li *et al.* (2012) also found that the SHAW over predicted soil moisture due to an under prediction of soil evaporation. Based on Figure 3.5a, some of the deviation between observed and simulated surface soil moisture could be related to the lower spatial variability of CaPA precipitation (a 10 km product) than would be observed at the scale of the fields; this is, particularly evident on July 3 and July 13-15, where large local storms were not well represented in the CaPA precipitation data.

The comparison between SHAW simulated surface soil moisture and the *in situ* dataset is shown in Figure 3.5b. The simulated dataset is well distributed around the *in situ* soil moisture although higher errors are observed for the sandier soils. The average RMSE and *r* over all of the simulated fields was 0.0548 m^3 m^{-3} and 0.6951** (i.e., significant at 0.01 probability level), respectively. This relationship is bit lower than those determined by Wang *et al.* (2010) who reported a correlation of 0.75** for 0-0.15 m soil profile using SHAW for clay loam soil. In general, fields with fine textured soils, i.e. clay and loamy soils (in middle and east side of SMAPVEX12 site) had much lower RMSE (<0.05 m^3 m^{-3}) and higher correlation (>0.7) between observed and estimated surface soil moisture than fields with sandier textures. Of note, much of the increased RMSE and reduced correlation are due to use of forecasted CaPA weather data for

all fields. For comparison, the *in-situ* precipitation data (from Fields 11, 22 and 85) used over these fields resulting in reduced RMSE (and increased *r*) was observed between observed and simulated surface soil moistures. However, for the purpose of this research, using of operationally available precipitation products (e.g. CaPA) will be of use for future applications particularly in regions where less precipitation data is available. Further simulations and evaluation of the SHAW model for 6 fields (varied from clay soil to loamy sand soils) to predict root-zone soil moisture at 0.05m, 0.20m, 0.50m and 1.00m soil depths is shown in Appendices A.5a-6c.

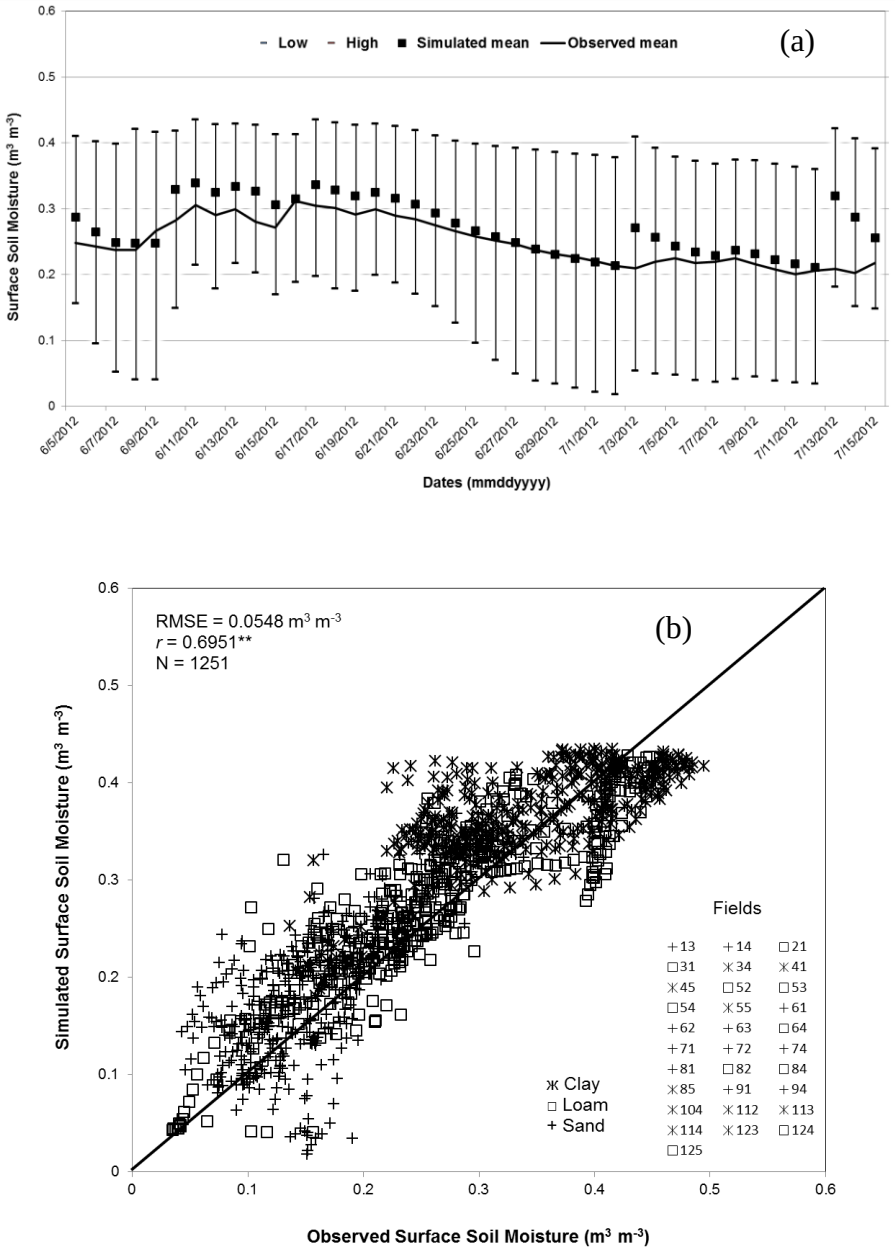

Figure 3.5: (a) Time series of daily surface soil moisture (5-cm depth) estimates from SHAW (bars) and daily mean observed (*in situ*) soil moisture (line) of 31 agricultural fields for time period 6 June – 15 July 2012; (b) Comparison among daily simulated and observed surface soil moisture over the 31 fields for the same data period.

3.3.2 Validation of Pixel Brightness Temperature

Time series of simulated horizontal polarized brightness temperatures from the SHAW coupled to the LPRM (S_LPRM) and SMOS observations over the 2 pixels (A and B) is shown in Figure 3.6. The general trends of the heterogeneous and homogeneous brightness temperatures were well simulated by the coupled system, although a few discrepancies exist particularly toward the end of June (at medium soil moisture conditions). Generally, SMOS brightness temperatures (T_b) were higher than the simulated brightness temperature (T_b) which was also experienced by Schlenz *et al.* (2012) while using the coupled land surface model (Processes of Radiation, Mass and Energy Transfer, PROMET) and radiative transfer model (L-band Microwave Emission of the Biosphere, L-MEB) to compare with SMOS L1c processed Tb observations (version 5.0.4) during a SMOS Validation Campaign in April-October 2011 for the 40˚ look angle at Upper Danube Catchment of southern Germany.

The RMSE and correlation between simulated brightness temperature and SMOS observations for the two pixels (A and B) are shown in Table 3.6. Over the SMAPVEX12 experiment, the RMSE was lower and the correlations were higher for heterogeneous simulations than those simulated using a homogeneous assumption. Pixel A shows lowest RMSE (4.6K) and higher correlation (0.74) for heterogeneous condition. This pixel contained clay soil with 68% clay, 9% sandy clay loam and 23% loamy sand. Considering both pixels, the heterogeneous simulations contained the lowest RMSE (4.72K) and highest correlation (0.72) compared to homogeneous pixels (RMSE = 7.12K, r = 0.71) when compared with SMOS observations. Panciera *et al.* (2011) also reported that soil moisture retrieval error was less for simulated heterogeneous pixel

(RMSE=2.5%v/v) compared to uniform pixel (RMSE=3.1%v/v) when 40 km spatial resolution was extracted from air borne observations.

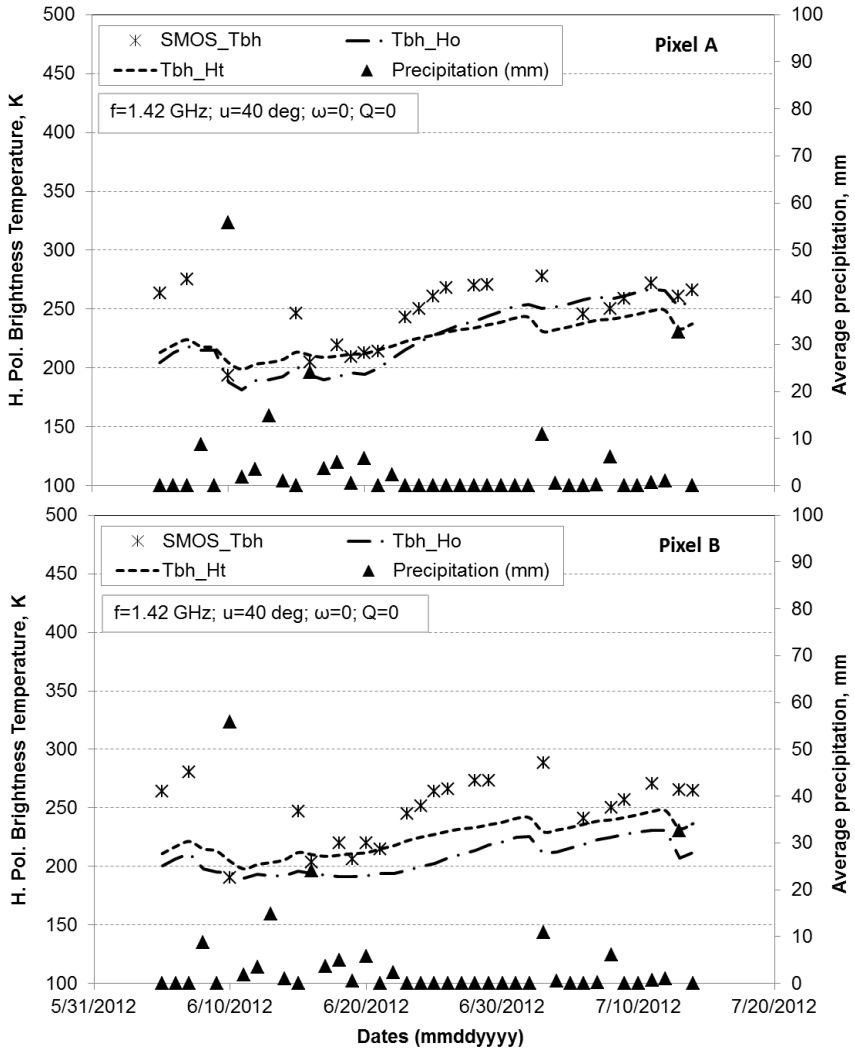

Figure 3.6: The time series of modeled brightness temperature (heterogeneous and homogeneous pixels) and SMOS brightness temperatures during 5 June – 14 July 2012 for the 40° look angle. Note: T_{bh_Ht}=horizontal polarized brightness temperature of heterogeneous pixels; T_{bh_Ho}=horiozantal polarized brightness temperature of homogenous pixels.

Table 3.6: RMSE and correlation among modeled and SMOS brightness temperature

Pixel	T_{bh_Ht}			T_{bh_Ho}		
	RMSE (K)	*r*	N	RMSE (K)	*r*	N
A	4.61	0.74	22	7.76	0.78	22
B	4.82	0.69	23	6.47	0.64	23
Average	4.72	0.72		7.12	0.71	

Note: T_{bh_Ht}=horizontal polarized brightness temperature of heterogeneous pixels;

T_{bh_Ho}=horiozantal polarized brightness temperature of homogenous pixels

3.3.3 Effect of Land Surface Heterogeneity on Difference Between Simulated and Observed Brightness Temperature

The t-Test statistics between heterogeneous and homogenous brightness temperature for pixels A and B is shown in Table 3.7. Based on the results for each of the pixels, the brightness temperature differences between heterogeneous and homogenous assumptions are significantly different from each other at the 0.01 probability level. The homogeneous pixels have higher larger errors than the heterogeneous pixels. Panciera *et al.* (2011) also experienced same phenomenon using Polarimetric L-band Multibeam Radiometer (PLMR) observations integrated at SMOS pixel scale for different land surface factors. Low (2008) also reported that fractional land use affects the quality of surface soil moisture retrievals conducted for a synthetic study using L-band passive microwave brightness temperature at 40 km spatial resolution. In the following section, these errors are examined relative to the spatial variations of land surface heterogeneities or parameters observed in the catchment.

Table 3.7: t-Test statistics between heterogeneous and homogeneous brightness temperature differences

	df	t-Test	t-critical
Pixel A	21	-51.16**	2.83
Pixel B	21	-17.35**	2.83

** = significant at 0.01 probability level

Table 3.8 presents correlations between the model errors (SMOS T_b observed minus T_b estimated using the homogeneous pixel approach) and the variability of physical characteristics within each of the SMOS pixels. Evaluated physical characteristics include the variations among *in-situ* surface soil moisture, *in-situ* surface soil temperature, soil roughness and vegetation water content based on observations taken during the SMAPVEX12 campaign. The correlation between the T_b errors and the variability of the observed soil moisture within the two pixels was 0.66** (Pearson's *r*, $p<0.05$) and is shown in Figure 3.7. Panciera *et al.* (2011) reported no significant correlation between retrieval error and pixel heterogeneity representing variation of soil moisture, however, a significant relationship is observed in this study.

Table 3.8: Correlation (*r*) between variations of land surface characteristics and T_b difference (n = 44)

	$T_{bh\_diff\_Ho}$ (K)
CV of Surface Soil Moisture, %	0.66**
CV of Surface Soil Temperature, %	0.48**
CV of Soil Roughness, %	-0.27
CV of Vegetation Water Content, %	-0.03

Note: $T_{bh\_diff\_Ho}$ = difference between SMOS observation and horizontal polarized brightness temperature of homogenous pixels

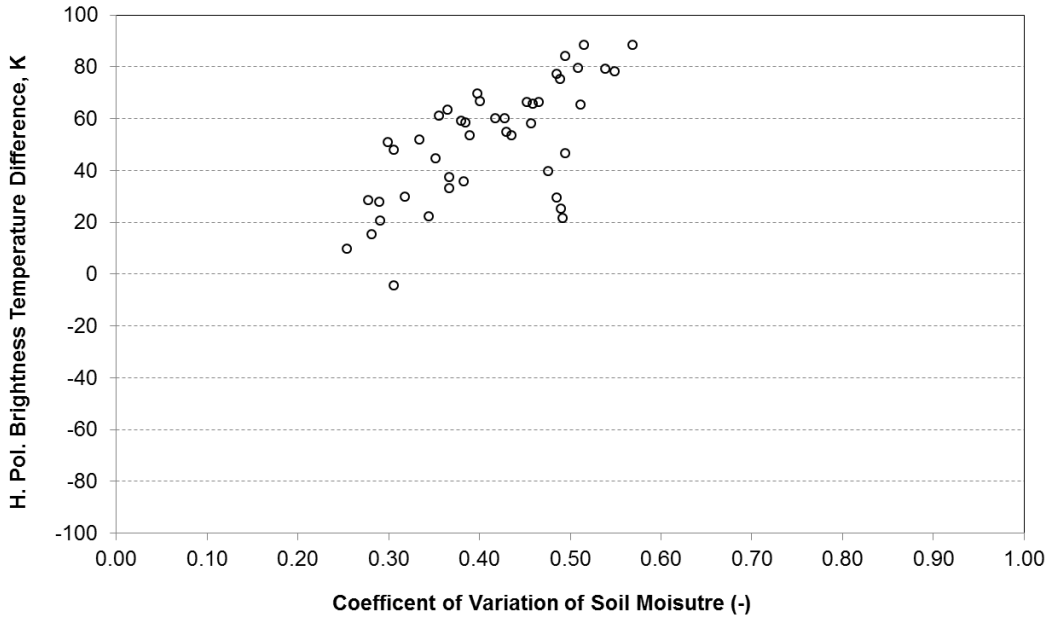

Figure 3.7: Relationship between horizontal polarized brightness temperature difference and homogeneity (coefficient of variation) of observed surface soil moisture for A and B pixels.

As shown in Table 3.8, there is statistical correlation (r = 0.48**) between differences in simulated T_b to SMOS and variation of soil temperature in the pixel. Very low variation of soil temperature was observed (Figure 3.8) following large precipitation events (55 mm) on the 11th June and the highest variation observed over dry soils (25th June); errors in retrieval followed this pattern. Panciera *et al.* (2011) reported low spatial variability of soil temperature with negligible effect on soil moisture retrieval and in contrast to their results, variation of soil temperature has found to be significant effect on brightness temperature difference in this study.

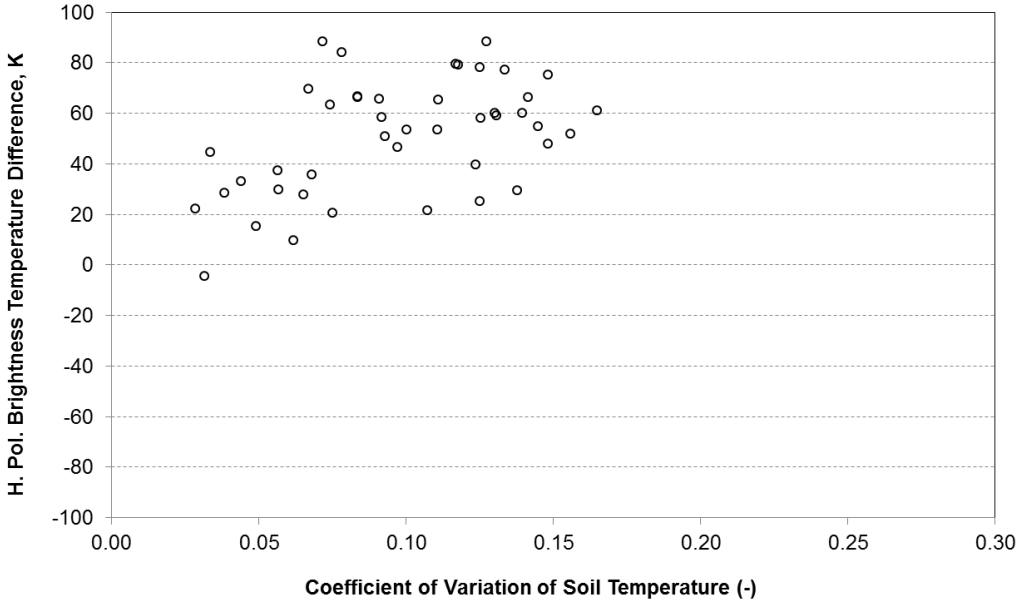

Figure 3.8: Relationship between horizontal polarized brightness temperature difference and homogeneity (coefficient of variation) of observed surface soil temperature for A and B pixels.

Insignificant correlations between retrieval error (differences between SMOS and model) were observed for measured variation of soil roughness and vegetation water content (Table 3.8). Due to insignificant correlation, the variation of soil roughness shows little or almost no effect on the brightness temperature retrieval in this study. In Figure 3.9, the higher variation of soil roughness observed in pixel B where higher amount of clay content (59%) was found (Table 3.5). The soil moisture of clay fields was also varied widely (Figure 3.3). Denvenport *et al.* (2008) similarly reported that heterogeneity in soil roughness using surface height variation at L-band wavelength has small effect on soil moisture retrieval.

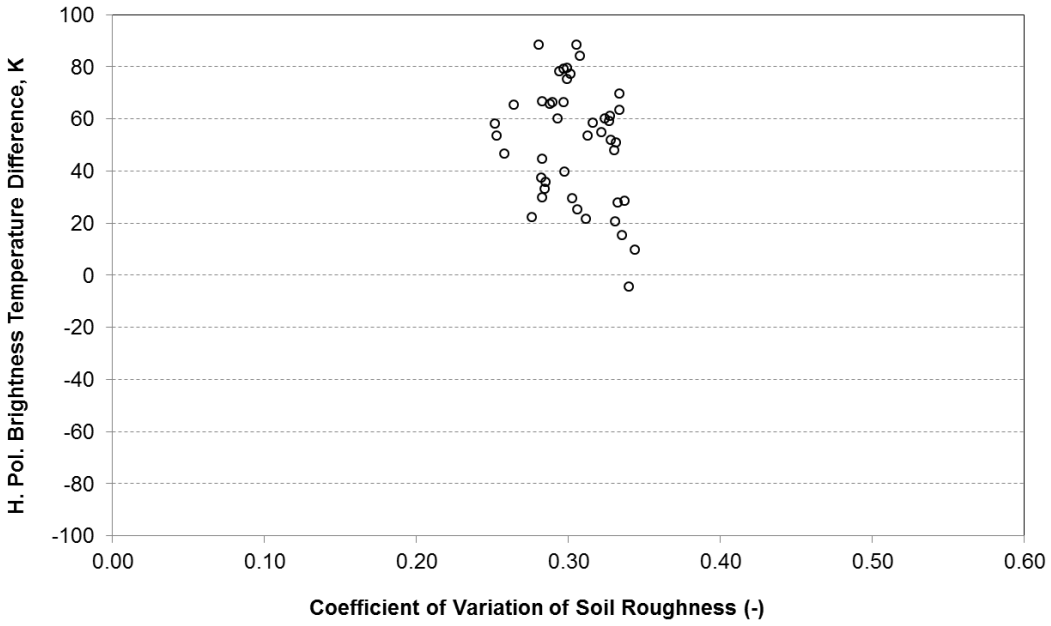

Figure 3.9: Relationship between horizontal polarized brightness temperature difference and homogeneity (coefficient of variation) of soil roughness for A and B pixels.

There is no significant relationship between the variation of vegetation water content and the difference in brightness temperature for various agricultural crops growing during SMAPVEX12 campaign (Table 3.8; Figure 3.10). On the contrary, Panciera *et al.* (2011) reported significant soil moisture retrieval error (RMSE=7%v/v) for the variation of vegetation optical depth in pixel composed by 50% grassland and 50% forest fraction. However, given the focus on agricultural crops less variation is anticipated in this study.

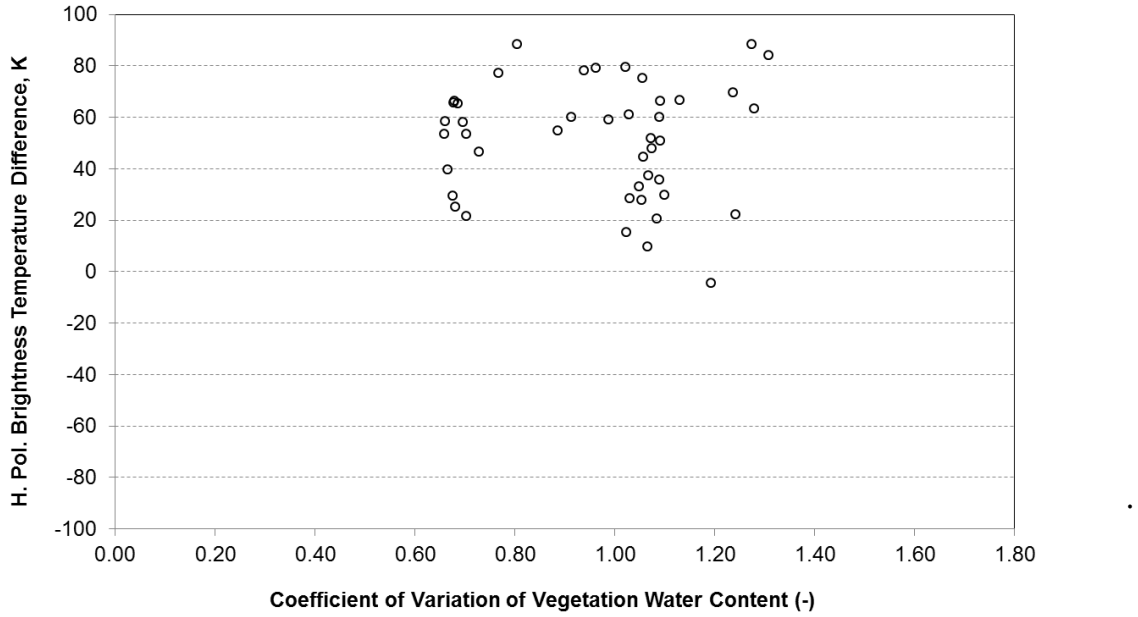

Figure 3.10: Relationship between horizontal polarized brightness temperature difference and homogeneity (coefficient of variation) of vegetation water content for A and B pixels.

3.4 Conclusions

In this study, a model for simulating L-band T_b was developed through coupling the SHAW hydrological process model with the LPRM (radiative transfer model). The sensitivity of this combined system to variability at the sub-SMOS pixel scale was assessed using ground data collected during the SMAPVEX12 field campaign. Two coupled simulations were developed for estimating T_b at the scale of the SMOS sensor. The first simulation used average parameters at the SMOS pixel scale over the agricultural sites and the second attempted to model for the observed sub-grid variability. For simulated brightness temperature, the SHAW model coupled with radiative transfer model under-predicted brightness temperature compared to SMOS observations for the region with average RMSE of 4.7K for heterogeneous land covers whereas

higher average RMSE (7.1 K) was found to be for homogeneous land covers. The trend of SMOS brightness temperatures, nonetheless, was well described by the SHAW coupled radiative transfer model with correlation over 0.72 (for the heterogeneous simulations). Relationships between model error and variability of parameters observed during SMAPVEX12 suggest that sub-grid estimates of soil moisture and soil temperature were of critical importance and explained errors between the homogeneous model and observations. During SMAPVEX12, these parameters were strongly influenced by soil texture (McNairn *et al.*, 2012). Therefore, it is suggested that enhanced modelling of sub-grid variability using systems such as that described heterogeneity has some capacity to improve the prediction of brightness temperature over a SMOS pixel. This has importance for improving downscaling approaches or for data assimilation that attempt to optimize between observations and model estimates of brightness temperature.

Chapter 4

Conclusions

4.1 Summary and Conclusions

Changes in agricultural practices across North America, including the wide spread adoption of no-till practices, has an impact on the storage of soil moisture. The effects of agricultural practices and soil management practices are typically not included in many hydrological models, particularly in models used for large scale monitoring such as those used in assimilation systems for hydrometeorology or seasonal water prediction. In order to evaluate the impact of differences in agricultural practices on hydrological budgets it is necessary to understand how well these processes are currently simulated in available hydrological models.

Chapter 2 documents some of the effects of tillage on the soil water budget under soybean where CT and NT experiments were carried out in silt loam soil at Elora, Ontario. The soil characteristics, weather data and plant growth data were available from field measurements as well as from literature. The SHAW model was used to predict soil moisture and soil temperature for 1-m soil profile, and validated with available continuous soil moisture and soil temperature data from installed electrical sensors in the fields. Results showed that NT had higher soil moisture in upper soil layers particularly later in the growing season than observed in CT treatment. However, SHAW simulations of soil moisture content followed the general trend of the observed data suggesting that SHAW can be used for reasonable simulation of soil water budgets for this region under different land management practices. Generally, the average differences in soil moisture between observed and simulated data were mostly less than 0.05 m^3 m^{-3} over both treatments. For simulation of soil temperature, SHAW over-predicted soil temperatures for the CT and NT by up to 2.5˚C on average over the entire experimental period.

Remote sensing systems, such as - the Soil Moisture and Ocean Salinity (SMOS) mission, are currently making near surface observations of the soil moisture state over much of the Earth's land surface. Improvements to observation systems such as SMOS are being driven by process studies to understand the influences of land surface characteristics within a satellite pixel and how these parameters influence the retrieval of microwave brightness temperatures that are used for obtaining soil moisture. A model such as SHAW, as detailed in Chapter 2, was shown to produce accurate simulations of the agricultural water budgets, in Chapter 3 this model was used to evaluate the impact of agricultural practices on variability of soil moisture and other parameters at the sub-SMOS scale pixel level and to evaluate the sensitivity of this variability on the estimation of microwave brightness temperature.

The impact of sub-SMOS scale (~15 km) grid variability on the simulation of microwave brightness temperature was evaluated through the following procedure. In step 1, the SHAW model was used to predict surface soil moisture (at 0.05 m soil depth) with available weather data, soil characteristics and plant growth data from over 31 agricultural fields under wide range of crops (soybean, wheat, corn, canola, corn and grass) and soil textures (sand, loam and clay soils) under the SMAMPVEX12 campaign in Manitoba. The simulated soil moisture was validated with available observed soil moisture data from installed electrical sensors in individual fields. The outputs from the SHAW model indicated that the RMSE was less than 0.05 m^3 m^{-3} for surface soil moisture for the study region. In step 2, the estimates (surface soil moisture and surface soil temperature) from the SHAW model were used in the LPRM along with soil roughness (RMS height and correlation length) and vegetation water content available from SMAPVEX12 campaign, to obtain simulated brightness temperature of individual fields.

For the heterogeneous assumption, simulated brightness temperature was the summation of the products of the weighted area fraction of individual crop area within sub-SMOS scale (~15 km) grid and calculated simulated brightness temperature of individual crop fields. Similarly, for the homogeneous assumption, simulated brightness temperature at the same spatial scale (~ 15 km) was calculated based on average soil texture and average crop of the pixel. The simulated brightness temperature of two individual pixels within the agricultural land management area was then validated with the available SMOS observations. The outputs from SHAW coupled LPRM model indicated that simulated brightness temperature was under-predicted compared to SMOS observations for the region with an average RMSE of 4.3K for heterogeneous land covers. The trend of SMOS brightness temperatures, nonetheless, was well described by the SHAW coupled radiative transfer model with correlation over 0.72 for the heterogeneous simulations. Relationships between model error and variability of parameters observed during SMAPVEX12 suggest that sub-grid estimates of soil moisture and soil temperature were of critical importance and explained errors between the homogeneous model and observations.

It is suggested that enhanced modelling of sub-grid variability using systems such as that described above has some capacity to improve the prediction of brightness temperature over a SMOS pixel. The further development and application of models like SHAW that can be used to accurately simulate the spatial and temporal variations of soil moisture within a satellite pixel will have importance for improving downscaling approaches or for data assimilation systems that attempt to optimize between observations and model estimates of brightness temperature.

4.2 Research Contributions

The study has developed new approach with integration of hydrological model (SHAW) and LPRM to improve accuracy of soil moisture prediction for different agricultural management (conventional and no tillage) practices including heterogeneity of *in-situ* soil moisture, soil temperature, soil texture, soil roughness and vegetation water content. The proposed integrated model could reduce the error in estimation of soil moisture, with improved parameterization. Improved estimation of soil moisture will help farmers to understand the availability of soil moisture or soil nutrients for plant growth, as well as to understand how this affects crop yield. This research is expected to enhance our understanding of the impact of land management practices for improved hydrological process, and how modelling this land surface heterogeneity can improve simulation of microwave brightness temperatures for data assimilation systems.

Bibliography

AAFC. 2010. Soil Landscapes of Canada version 3.2. Soil Landscapes of Canada Working Group, Agriculture and Agri-Food Canada, http://sis.agr.gc.ca/cansis/nsdb/slc/v3.2/index.html

Abdel-Nasser, G. 1999. Air-entry potential (ψ_e) in relation to basic soil physical properties: prediction using pedotransfer functions. *J. Agric. Sci.*, Mansoura Univ., Vol. **24**(12): 7809-7822.

Allen, R.G., L.S. Pereira, D. Raes and M. Smith. 1998. Crop evapotranspiration – Guidelines for computing crop water requirements. FAO Irrigation and Drainage Paper 56, Rome, Italy.

Alavi, N., J.S Warland and A.A. Berg. 2009. Assimilation of Soil Moisture and Temperature Data into Land Surface Models: A Survey. Chapter to Springer book on "Data Assimilation for Atmospheric, Oceanic, and Hydrologic Applications" edited by Seon Ki Park. doi: 0.1007/978-3-540-71056-1_22.

Arshad, M.A., A.J. Franzluebbers and R.H. Aooz. 1999. Components of surface soil structure under conventional and no-tillage in northwestern Canada. *Soil & tillage Research*, **53**: 41-47Chatfield, Chris. 1999. The Analysis of Time Series – An Introduction (5th Ed.), Chapman & Hall/CRC Press.

ATBD. 2010. Algorithm Theoretical Basis Document (ATBD) for the SMOS Level 2 Soil Moisture Processor Development Continuation Project. Array Systems Computing Inc., Toronto, Canada

Bevis, M., S. Businger, T.A. Herring, C. Rocken, R.A. Anthes and R.H. Ware. 1992. GPS Meteorology: Remote sensing of atmospheric water vapor using the global position system. *Jr. of Geophysical Research*, Vol. **97**(D14): 15,787-15,801.

CaPA. 2013. Canadian precipitation analysis (CaPA). Data Access Integration. http://loki.qc.ec.gc.ca/DAI/capa-e.html

Davenport, I.J., M.J. Sandells and RJ. Gurney. 2008. The effects of scene heterogeneity on soil moisture retrieval from passive microwave data. *Advances in Water Resources*, Vol. **31**: 1494-1502.

De Jeu, R.A.M., T.R.H. Holmes, R. Panciera and J.P. Walker. 2009. Parameterization of the Land Parameter Retrieval Model for L-Band Observations Using the NAFE'05 Data Set. *IEEE Geoscience and Remote Sensing Letters*, Vol. **6**(4): 630-634.

Dobson, M.C. and F.T. Ulaby. 1986. Active microwave soil moisture research. *IEEE Transactions on Geoscience and Remote Sensing*, Vol. **GE-23** (1): 23-36.

Drewitt, G., A.A. Berg , W.J. Merryfield and W. Lee. 2012. Effect of Realistic Soil Moisture Initialization on the Canadian CanCM3 Seasonal Forecast Model. *Atmosphere-Ocean*, **50**(4), 466-474.

Drury, C.F., C.S. Tan, W.T. Welacky, T.O. Oloya, A.S. Hamell and S.E. Weaver. 1999. Red clover and tillage influences on soil temperature, water content and corn emergence. *Agron. J.*, **91**: 101-108.

Dubois, P.E., J. van Zyl and T. Engman. 1995. Measuring soil moisture with imaging radars. *IEEE Transactions on Geoscience and Remote Sensing*, Vol. **33** (4): 915-926.

Dumedah, G., A.A. Berg and M. Wineberg. 2011. An integrated framework for a joint assimilation of brightness temperature and soil moisture using the Non-dominated Sorting Genetic Algorithm-II. *Journal of Hydrometeorology*, Vol. **12**: 1596-1609.

Dumedah, G., J.P. Walker and C. Rudiger. 2013. Can SMOS Data be Used Directly on the 15-km Discrete Global Grid? *IEEE Transactions on Geoscience and Remote Sensing* (in press).

Entekhabi, D., E. Njoku, P. O'Neill, K. Kellogg, W. Crow, W. Edelstein, J. Entin, S. Goodmand, T. Jackson, J. Johnson, J. Kimball, J. Peipmeier, R. Koster, N. Martin, K. McDonald, M. Moghaddam, S. Moran, R. Reichle, J. Shi, M. Spencer, S. Thurman, L. Tsang, J. van Zyl. 2010. The Soil Moisture Active Passive SMAP mission. Proc IEEE., **98**(5), 704-716.

Elliot, J.A., A.J. Cessna, W. Nicholaichuk and L.C. tollenfson. 2000. Leaching rates and preferential flow of selected herbicides through tilled and untilled soils. *J. Environ. Qual.*, **29**: 1650-1656.

Fallow, D.J., D.M. Brown, G.W. Parkin, J.D. Lauzon and C. Wagner-Riddle. 2003. Identification of critical regions for water quality monitoring with respect to seasonal and annual water surplus. Dept. of Land Resource Science, OAC, University of Guelph, LRS Contribution No. 2003-1

Fernhout, P.D. and C.F. Kurtz. 1999. Garden with Insight v1.0 Help: soil patch next day functions: Calculate today's albedo. http://www.kurtz-fernhout.com/help100/00000536.htm. Accessed Dec 2012.

Flerchinger, G.N. 2000. The Simultaneous Heat and Water (SHAW) Model: User's Manual and Technical Documentation. Technical Report NWRC 2000-09 &10. Northwest Watershed Research Center, USDA Agricultural Research Service, Boise, Idaho.

Flerchinger, G.N. and K.E. Saxton. 1989. Simultaneous heat and water model of a freezing snow-residue-soil system I. Theory and Development. *Transactions of the ASAE*, **32**(2): 573-578.

Flerchinger, G.N., T.J. Sauer and R.A. Aiken. 2003. Effects of crop residue cover and architecture on heat and water transfer at the soil surface. *Geoderma*, **116**(1-2): 217-233.

Flerchinger, G.N., T.G. Caldwell, J. Cho and S.P. Hardegree. 2012. Simultaneous Heat and Water (SHAW) Model: Model Use, Calibration, and Validation. *Transactions of the ASABE*, Vol. **55**(4): 1395-1411.

Fuentes, J.P., M. Flury and D.F. Bezdicek. 2004. Hydraulic properties in a silt loam soil under natural prairie, conventional till and no-till. *Soil Sci. Soc. Am. J.*, **68**:1679-1688.

Jayasundara, S., C. Wagner-Riddle, G. Parkin, P. vonBertoldi, J. Warland, B. Kay and P. Voroney. 2007. Minimizing nitrogen losses from a corn-soybean-winter wheat rotation with best management practices. *Nutr Cycle Agroecosyst*, **79**: 141-159.

Jackson, T.J. 1990. Laboratory evaluation of a field-portable dielectric/soil moisture probe. *IEEE Transactions on Geoscience and Remote Sensing*, **28**: 241-245.

Jackson, T.J. and T.J. Shmugge. 1991. Vegetation effects on the microwave emission of soils. *Remote Sens. Environ*, **36**: 203-212.

Jayasundara, S., C. Wagner-Riddle, G. Parkin, P. vonBertoldi, J. Warland, B. Kay and P. Voroney. 2007. Minimizing nitrogen losses from a corn-soybean-winter wheat rotation with best management practices. *Nutr Cycle Agroecosyst*, **79**: 141-159.

Kerr, Y.H., P. Waldteufel, P. Richaume, J.P. Wigneron, P. Ferrazzoli, A. Mahmodi, A.A. Bitar, C. Gruhier, S.E. Juglea, D. leroux, A. Mialon and S. Delwart. 2012. The SMOS soil moisture

retrieval algorithm. *IEEE Transactions on Geoscience and Remote Sensing*, Vol. **50** (5): 1348-1403.

Klute, A. 1986. *Methods of Soil Analysis, Part 1: Physical and Mineralogical Methods*. American Society of Agronomy, Madison, Wisconsisn, U.S.

Koster, R.D., S.P.P. Mahanama, T.J. Yamada, G. BALSAMO, A.A. Berg, M. Boisserie, P.A. Dirmyer, F.J. Doblas-Reyes, G. Drewitt, C.T. Gordon, Z. Guo, J.-H. Jeong, W.-S. Lee, Z. Li, L. Luo, S. Malyshev, W.J. Merryfield, S.I. Seneviratne, T. Stanelle, B.J.J.M. Van De Hurk, F. Vitart and E.F. Wood. 2011. The Second Phase of the Global Land–Atmosphere Coupling Experiment: Soil Moisture Contributions to Subseasonal Forecast Skill. *Journal of Hydrometeorology*. Vol. **12**: 805-822. DOI: 10.1175/2011JHM1365.1

Li, Z., L. Ma, G.N. Flerchinger, L.R. Ahuja, H. Wang and Z. Li. 2012. Simulation of overwinter soil water and soil temperature with SHAW and RZ-SHAW. *Soil Sci. Soc. Am. J.*, **76**: 1548-1563.

Liu, Q., R.H. Reichle, R. Bindlish, M.H. Cosh, W.T. Crow, R.D Jeu, G. J.M.D. Lannoy, G.J. Huffman and T.J. Jackson. 2011. The contributions of precipitation and soil moisture observations to the skill of soil moisture estimates in a land data assimilation system. *Journal of Hydrometeorology*, Vol. **12**:750-765. doi:10.1175/JH-D10-05000.1

Mahfouf, J., B. Brasnett and S. Gagnon. 2007. A Canadian Precipitation Analysis (CaPA) project: Description and preliminary results. *Atmosphere-Ocean*, **45**(1): 1-17.

Manitoba. 2013. Manitoba 2011 Flood Review – Task Force Report. Report to the Ministry of Infrastructure and Transportation, April 2013. http://www.gov.mb.ca/asset_library/en/2011flood/flood_review_task_force_report.pdf

Martin, S. 2004. An introduction to Ocean Remote Sensing. Cambridge University Press, Cambridge. UK.

Mayaki, W.C., Teare I.D. and L.R. Stone. 1976. Top and root growth of irrigated and nonirrigated soybeans. *Crop Sci*, **16**:92-94.

McCoy, A.J. 2002. An assessment of drainage and runoff under conventional and no-till agricultural practices. MSc Thesis. University of Guelph.

McCoy, A.J., G. Parkin, C. Wagner-Riddle, J. Warland, J. Lauzon, P. von Bertoldi, D. Fallow and S. Jayasundara. 2006. Using automated soil water content measurements to estimate soil water budgets. *Can. J. Soil Sci.* **86**: 47-56.

McNairn, H., T.J. Jackson, G. Wiseman, S. Belair, A. Berg, P. Bullock, A. Colliander, M.H. Cosh, S. Kim, R. Magagi, M. Moghaddam, J.R. Adams, S. Homayouni, E. Ojo, T. Rowlandson, J. Shang, K. Goita and M. Hosseini. 2013. The soil moisture active passive validation experiment 2012 (SMAPVEX12): Pre-launch calibration and validation of the SMAP satellite. *IEEE Transactions on Geoscience and Remote Sensing*, (*in press*).

Meesters, A.G.C.A., R.A.M. de Jeu and M. Owe. 2005. Analytical derivation of the vegetation optical depth from the microwave polarization difference index. *IEEE Geoscience and Remote Sensing*, Vol. **2**(2): 121-123.

Mo, T., B.J. Choudhury, T.J. Schmugge and J.R.Wang. 1982. A model for microwave emission from vegetation-covered fields. *Journal of Geophysical Research*, **87**(C13):11,229-11,237.

Moran, M.S., C.D. Peters-Lidard, J.M. Watts and S. McElroy. 2004. Estimating soil moisture at the watershed scale with satellite-based radar and land surface models. *Can. J. Remote Sensing*, Vol. **20**(5): 805-826.

Morwick, F.F. and N.R. Richards. 1946. Soil survey of Wellington County. Report no. 35 of the Ontario Soil Survey. Canada Department of Agriculture and The Ontario Agriculture College.

Njoku, E.G., T.J. Jackson, V. Lakshmi, T.K. Chan and S.V. Nghiem. 2003. Soil Moisture Retrieval From AMSR-E. *IEEE Transactions on Geoscience and Remote Sensing*, Vol. **41**(2): 215-229.

Oh, Y., K. Sarabandi and F.T. Ulaby. 1992. An empirical model and an inversion technique for radar scattering from bare soil surfaces. *IEEE Transactions on Geoscience and Remote Sensing*, Vol. **30**(2): 370-381.

Owe, M., R. de Jeu and J. Walker. 2001. A methodology for surface soil moisture and vegetation optical depth retrieval using the microwave polarization difference index. *IEEE Transactions on Geoscience and Remote Sensing*, Vol. **39**(8): 1643-1654.

Owe, M., R. de Jeu and T. Holmes. 2008. Multisensor historical climatology of satellite-derived global land surface moisture. *Jr. of Geophysical Research*, Vol. **113**, doi:10.1029/2007JF000769.

Panciera, R., J.P. Walker, J.D. Kalma, E.J. Kim, J.M. Hacker, O. Merlin, M. Berger and N. Skou. 2008. The NAFE'05/CoSMOS Data Set: Toward SMOS Soil Moisture Retrieval, Downscaling, and Assimilation. *IEEE Transactions on Geoscience and Remote Sensing*, Vol. **46**(3): 736-745.

Panciera, R., J.P. Walker, J. Kalma and E. Kim. 2011. A proposed extension to the soil moisture and ocean salinity level 2 algorithm for mixed forest and moderate vegetation pixels. *Remote Sensing of Environment*, Vol. **115** (2011): 3343-3354.

Parking, G.W., C. Wagner-Riddle, D.J. Fallow and D.M. Brown. 1999. Estimated seasonal and annual water surplus in Ontario. *Can. Water Res. Jr.*, Vol. **24**(4): 277-291.

Patni, N.K., L. Masse and P.Y. Jui. 1996. Tile effluent quality and chemical losses under conventional and no tillage – Part 1: Flow and nitrate. *Trans. ASAE*, **39**: 1665-1672.

Rawls, W.J., D.L. Brakensiek and K.E. Saxton. 1982. Estimation of soil water properties. *Transactions of the ASAE*, Vol. **25**(5): 1316-1320.

Reichle, R.H. and R.D. Koster. 2004. Bias reduction in short records of satellite soil moisture. *Geopys Res Lett*, **31**:L19501. doi: 10.1029/2004GL020938.

Reichle, R.H. 2008. Data assimilation methods in the Earth sciences. *Advances in Water Resources*, doi:10.1016/j.advwatres.2008.01.001

Reichle, R.H., W.T. Crow, R.D. Koster, H.O. Sharif and S.P.P. Mahanama. 2008. Contribution of soil moisture retrievals to land data assimilation products. *Geophysical Research Letters*. **35** (L01404), doi:10.1029/2007GL031986.

Reicosky, D.C. and K.E. Saxton. 2006. The benefits of no-tillage. eBook on 'No-tillage seeding in conservation agriculture'. doi: 10.1079/9781845931162.0011.

Rowlandson, T.L., A.A. berg, P.R. Bullock, E.R. Ojo, H. McNairn, G. Wiseman and M.H. Cosh. 2013. Evaluation of several calibration procedures for a portable soil moisture sensor. *Jr. of Hydrology*, Vol. **498**: 335-344.

Schlenz, F., J.T. dall'Amico, W. Mauser and A. Loew. 2012. Analysis of SMOS brightness temperature and vegetation optical depth data with coupled land surface and radiative transfer models in Southern Germany. *Hydrol. Earth Syst. Sci.*, **16**: 3517-3533.

Shipitalo, M.J. and W.M. Edwards. 1993. Seasonal patterns of water and chemical movement in tilled and no-till column lysimters. *Soil Sci. Soc. Am. J.*, **57**: 218-223.

Statistics Canada 2011. No-till practices increased. Chapter 5. http://www.statcan.gc.ca/pub/95-640-x/2012002/05-eng.htm

Thies, J.E., P.W. Singleton and B.B. Bohlool. 1995. Phenology, growth, and yield of field-grown soybean and bush bean as a function of varying modes of N nutrition. *Soil Biol. Biochem.*, Vol. **27** (4/5): 575-583.

Topp, G.C., J.L. Davis and A.P. Annan. 1980. Electromagnetic determination of soil water content: measurements in Coaxial Transmission Lines. *Water Res. Research*, Vol. **16**(3): 574-582.

USDA. 2012. U.S. Drought 2012: Farm and Food Impacts. USDA Economic Research Service, United States Department of Agriculture. http://www.ers.usda.gov/topics/in-the-news/us-drought-2012-farm-and-food-impacts.aspx#.UgPhq_nqksI

Walker, B.D. 2012. Agri-environmental monitoring – Manitoba, Methodology and Landscape Descriptions. BeauTerre Soilscapes Consulting Inc. submitted to Agri-environmental Services Branch, Agriculture and Agri-Food Canada. March 2012.

Wang, H., G.N. Flerchinger, R. Lemke, K. Brandt, T. Goddard and C. Sprout. 2010. Improving SHAW long-term soil moisture prediction for continuous wheat rotations, Alberta, Canada. *Can. J. Soil Sci.*, **90**: 37-53.

Wang, J.R. and T.J. Schmugge. 1980. An empirical model for the complex dielectric permittivity of soil as a function water content. *IIIE Transactions on Geoscience and Remote Sensing*, Vol. **GE-18** (4): 288-295.

Wigneron, J., L. Laguerre and Y. H. Kerr. 2001. A simple parameterization of the L-band microwave emission from rough agricultural soils. *IEEE Transactions on Geoscience and Remote Sensing*, Vol. **39**(40: 1697-1707.

Zhan, X. et al. 2006. A Method for Retrieving High-Resolution Surface Soil Moisuture from Hydros L-Bank Radiometer and Radar Observations. *IEEE Trans Geosci Remote Sens* **44**:1564-1544.

Appendices

A.1 SHAW input files for CT

File: Trial.inp

```
1 0 0
TRIAL.SIT
TRIAL.WEA
TRIAL.MOI
TRIAL.TMP
 24  0 24 24  0 24 24  0  0  6  0  0  1
OUT.OUT
PROFIL.OUT
TEMP.OUT
MOIST.OUT
MATRIC.OUT
ENERGY.OUT
WATER.OUT
WFLOW.OUT
ROOTXT.OUT
```

File: Trial.sit

```
SITE WITH SOYBEAN DURING 2010-2011   ** (CONVENTIONAL TILLAGE, ELORA)                    LINE A
 91  00  110  34  111              ****** SIMULATION PERIOD                             LINE B
 43 38   0.15  225.0  12.0  340.        ****** LOCATION                                 LINE C
 2  0  0  22  0  00.010  1  0   0   0   1   0   0    ***** NODES                        LINE D
 0.4  2.0  0.00                ******* WEATHER CHARACTERISTICS                         LINE E
 1   -53.72  1.32   0.2           ***** PLANT GROWTH / CANOPY                          LINE F
 1   1   0.23  7.0  100.  5.0  -100.   2.0E05   3.0E05  **** SOYBEAN                  LINE F1-1
 1   1   0.25  7.0  100.  5.0  -300.   6.7E05   1.7E06  **** WBARLEY                  LINE F1-2
 soyb.110
 wbar.110
 1.0  .15                          ****** SNOW                                        LINE G
 1  1  0.15 0.0                     ****** SOIL                                        LINE J
 0.00  3.34  -0.11 0.40 1550. 0.45  32. 51. 17. 2.0                                   LINE J-1
 0.05  3.34  -0.11 0.40 1550. 0.45  32. 51. 17. 2.0                                   LINE J-2
 0.10  3.34  -0.11 0.40 1550. 0.45  32. 51. 17. 2.0                                   LINE J-3
 0.25  3.34  -0.11 0.40 1550. 0.45  32. 51. 17. 1.6                                   LINE J-4
 0.40  3.34  -0.11 0.40 1550. 0.45  32. 51. 17. 1.6                                   LINE J-5
 0.55  3.72  -0.1  0.41 1610. 0.41  42. 43. 15. 1.1                                   LINE J-6
 0.70  3.72  -0.1  0.41 1610. 0.41  42. 43. 15. 1.1                                   LINE J-7
 0.85  4.23  -0.1  0.45 1660. 0.40  44. 42. 14. 0.6                                   LINE J-8
 1.00  4.23  -0.1  0.45 1660. 0.40  44. 42. 14. 0.6                                   LINE J-9
 1.15  4.23  -0.1  0.45 1660. 0.40  44. 42. 14. 0.6                                   LINE J-10
 1.30  4.23  -0.1  0.45 1660. 0.40  44. 42. 14. 0.6                                   LINE J-11
 1.45  4.23  -0.1  0.45 1660. 0.40  44. 42. 14. 0.6                                   LINE J-12
 1.60  4.23  -0.1  0.45 1660. 0.40  44. 42. 14. 0.6                                   LINE J-13
 1.75  4.23  -0.1  0.45 1660. 0.40  44. 42. 14. 0.6                                   LINE J-14
 1.90  4.23  -0.1  0.45 1660. 0.40  44. 42. 14. 0.6                                   LINE J-15
 2.05  4.23  -0.1  0.45 1660. 0.40  44. 42. 14. 0.6                                   LINE J-16
 2.20  4.23  -0.1  0.45 1660. 0.40  44. 42. 14. 0.6                                   LINE J-17
 2.35  4.23  -0.1  0.45 1660. 0.40  44. 42. 14. 0.6                                   LINE J-18
 2.50  4.23  -0.1  0.45 1660. 0.40  44. 42. 14. 0.6                                   LINE J-19
 2.65  4.23  -0.1  0.45 1660. 0.40  44. 42. 14. 0.6                                   LINE J-20
 2.80  4.23  -0.1  0.45 1660. 0.40  44. 42. 14. 0.6                                   LINE J-21
 2.95  4.23  -0.1  0.45 1660. 0.40  44. 42. 14. 0.6                                   LINE J-22
```

File: Trial.moi

```
91      0       110     0.195   0.195   0.274   0.274   0.249   0.249   0.264   0.264   0.264   0.264
        0.264   0.264   0.264   0.264   0.264   0.264   0.264   0.264   0.264   0.264   0.264   0.264
35      0       111     0.026   0.026   0.194   0.194   0.228   0.228   0.228   0.228   0.228   0.228
        0.228   0.228   0.228   0.228   0.228   0.228   0.228   0.228   0.228   0.228   0.228   0.228
```

File: Trial.tmp

```
91      0       110     5.2     5.2     4.4     4.4     3       3       -0.9    -0.9    1       1
        1       1       1       1       1       1       1       1       1       1       1       1
35      0       111     -1.4    -1.4    -0.6    -0.6    1.3     1.3     2.1     2.1     2.1     2.1
        2.1     2.1     2.1     2.1     2.1     2.1     2.1     2.1     2.1     2.1     2.1     2.1
```

File: Trial.wea

1	110	-0.7	-13	-6.8958	310.495032	0.059055118	46.272852
2	110	-12.9	-15.9	-17.35	411.097032	0	80.90226
3	110	-9.7	-15.6	-14.446	430.353	0	45.416376
4	110	-8.3	-12.5	-13.313	308.632032	0	78.680052
5	110	-6	-10.7	-9.9167	291.253968	0.023622047	61.45794

……
……

File: soyb.110

90	110	0	0	0	0	0	MAR 31
138	110	0	0	0	0	0	MAY 18
150	110	0.1	2	0.03	0.1	0.1	MAY 30
234	110	0.75	10	1	2	1.6	AUG 22
270	110	0.7	1	1	0.8	1.5	SEP 27
271	110	0	0	0.2	0	1.4	SEP 28
38	111	0	0	0	0	0	FEB 7

File: wbar.110

80	110	0	0	0	0	0
150	110	0	0	0	0	0
275	110	0	0	0	0	0
303	110	0.05	0.5	0.05	0.5	0.1
34	111	0.05	0.8	0.05	0.5	0.1
143	111	0.6	1.5	0.3	2.5	1.25
178	111	0.8	1.5	0.85	0.7	1.5
200	111	0	0	0.05	0	0.9

A.2 Observed and Simulated Soil Moisture of CT and NT plots at different soil depths

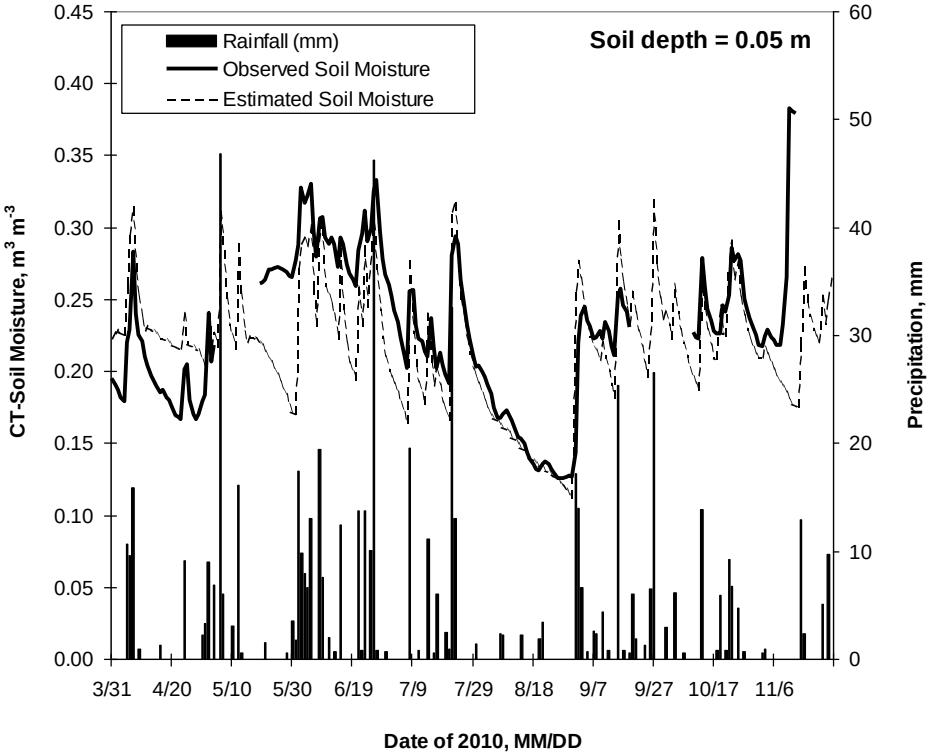

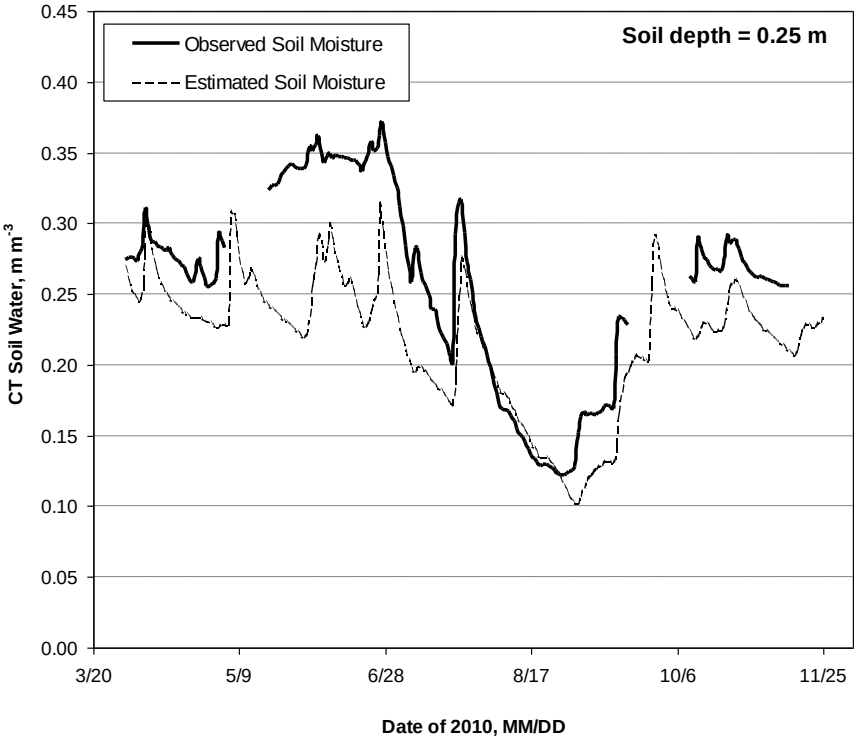

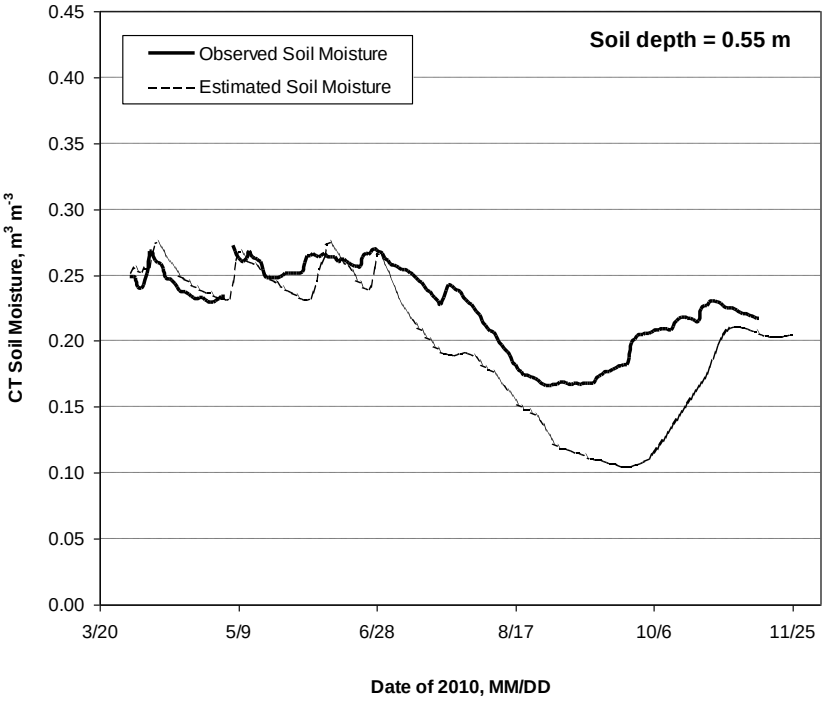
Soil depth = 0.55 m
Observed Soil Moisture
Estimated Soil Moisture
CT Soil Moisture, m3 m-3
0.45
0.40
0.35
0.30
0.25
0.20
0.15
0.10
0.05
0.00
3/20
5/9
6/28
8/17
10/6
11/25
Date of 2010, MM/DD

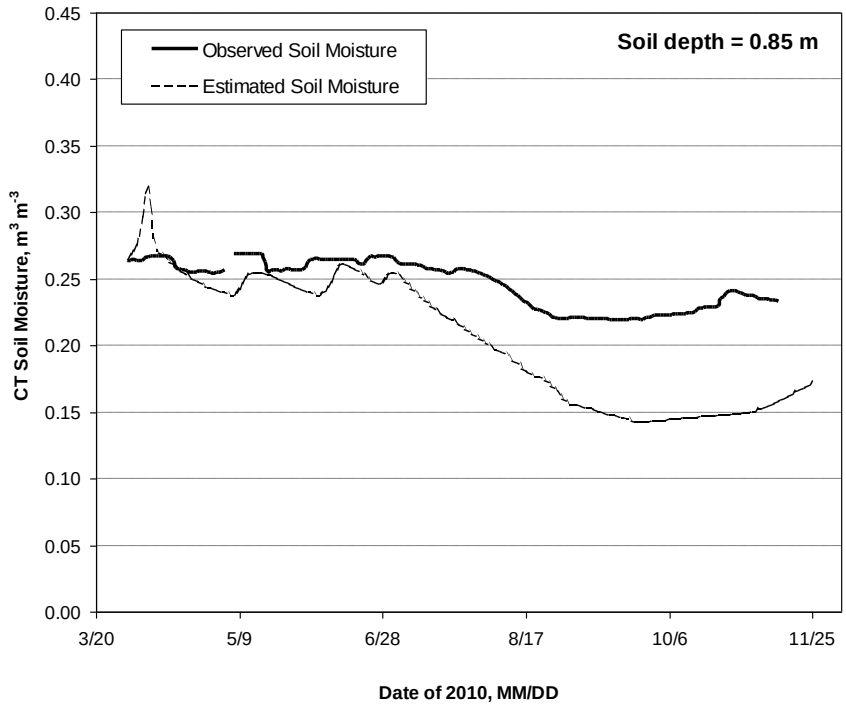
Soil depth = 0.85 m
Observed Soil Moisture
Estimated Soil Moisture
CT Soil Moisture, m3 m-3
0.45
0.40
0.35
0.30
0.25
0.20
0.15
0.10
0.05
0.00
3/20
5/9
6/28
8/17
10/6
11/25
Date of 2010, MM/DD

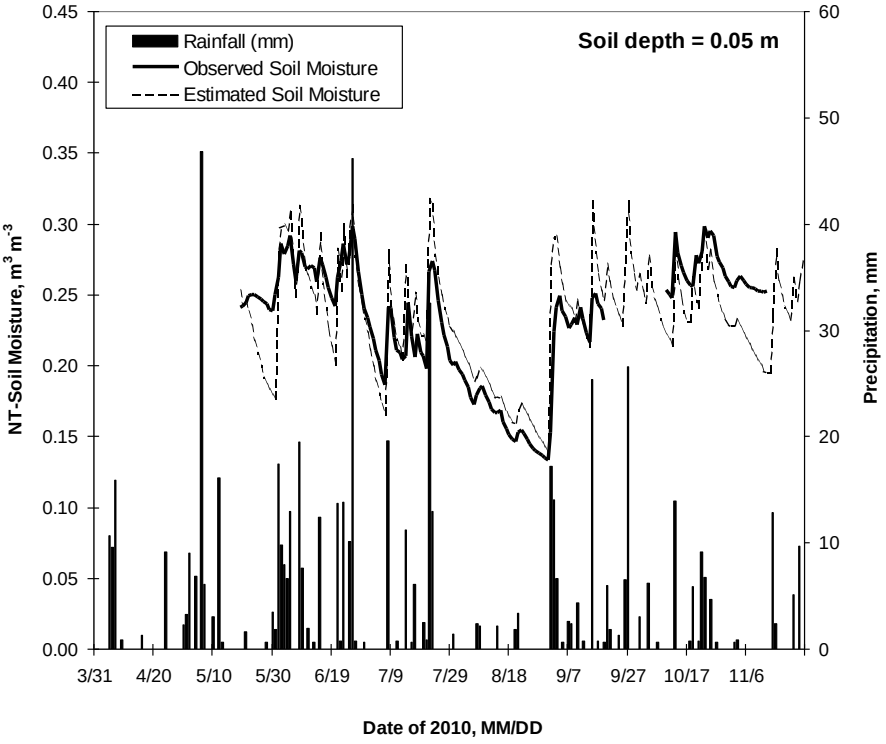
Rainfall (mm)
Observed Soil Moisture
Estimated Soil Moisture
Soil depth = 0.05 m
NT-Soil Moisture, m3 m-3
Precipitation, mm
0.45
0.40
0.35
0.30
0.25
0.20
0.15
0.10
0.05
0.00
60
50
40
30
20
10
0
3/31
4/20
5/10
5/30
6/19
7/9
7/29
8/18
9/7
9/27
10/17
11/6
Date of 2010, MM/DD

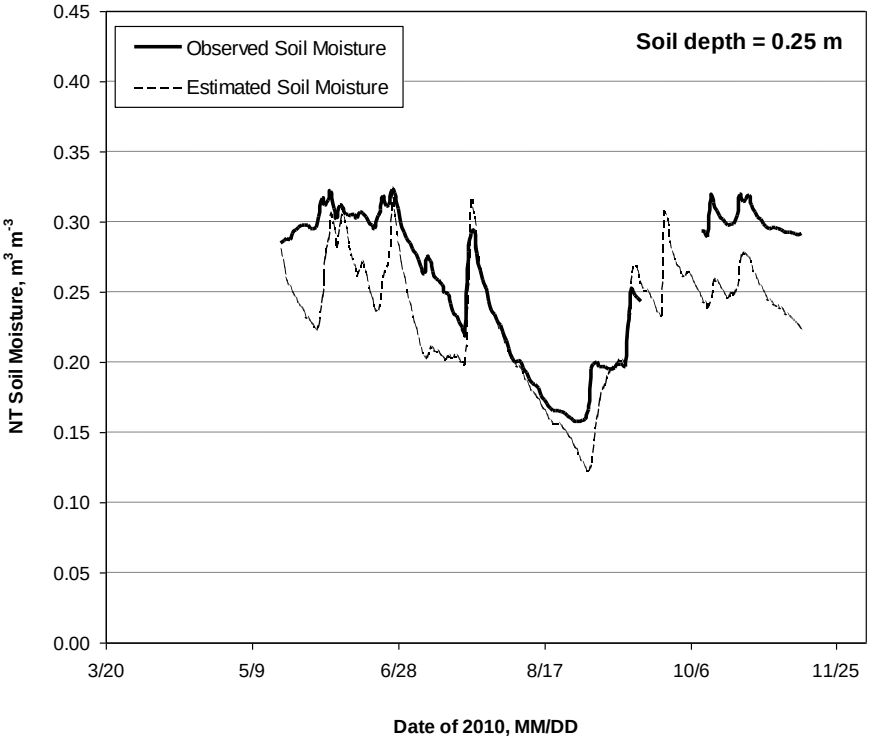
Observed Soil Moisture
Estimated Soil Moisture
Soil depth = 0.25 m
NT Soil Moisture, m3 m-3
0.45
0.40
0.35
0.30
0.25
0.20
0.15
0.10
0.05
0.00
3/20
5/9
6/28
8/17
10/6
11/25
Date of 2010, MM/DD

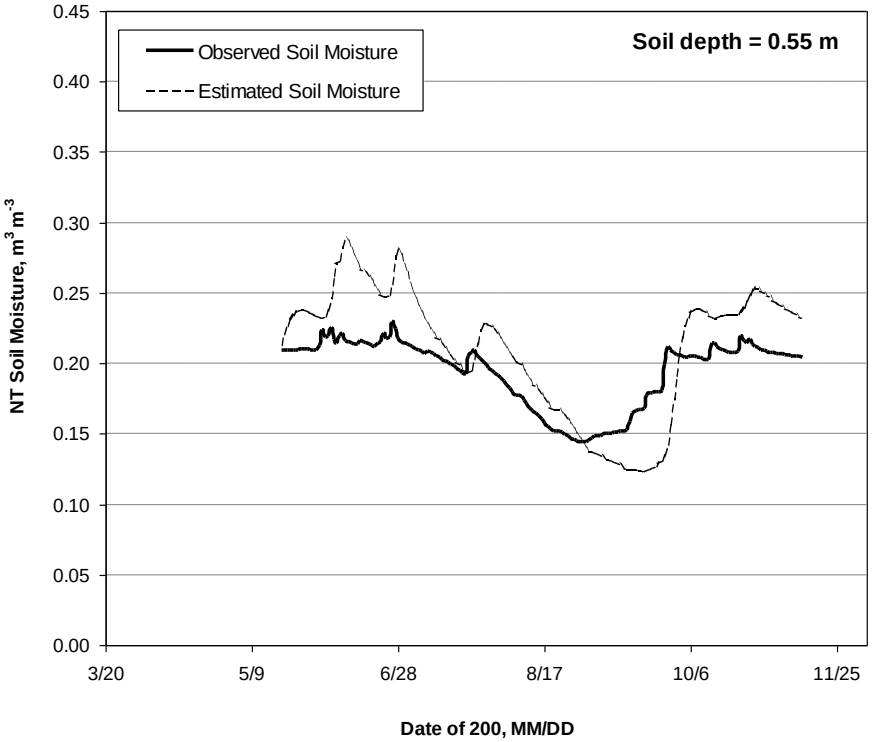
Soil depth = 0.55 m
Observed Soil Moisture
Estimated Soil Moisture
NT Soil Moisture, m3 m-3
0.45
0.40
0.35
0.30
0.25
0.20
0.15
0.10
0.05
0.00
3/20
5/9
6/28
8/17
10/6
11/25
Date of 200, MM/DD

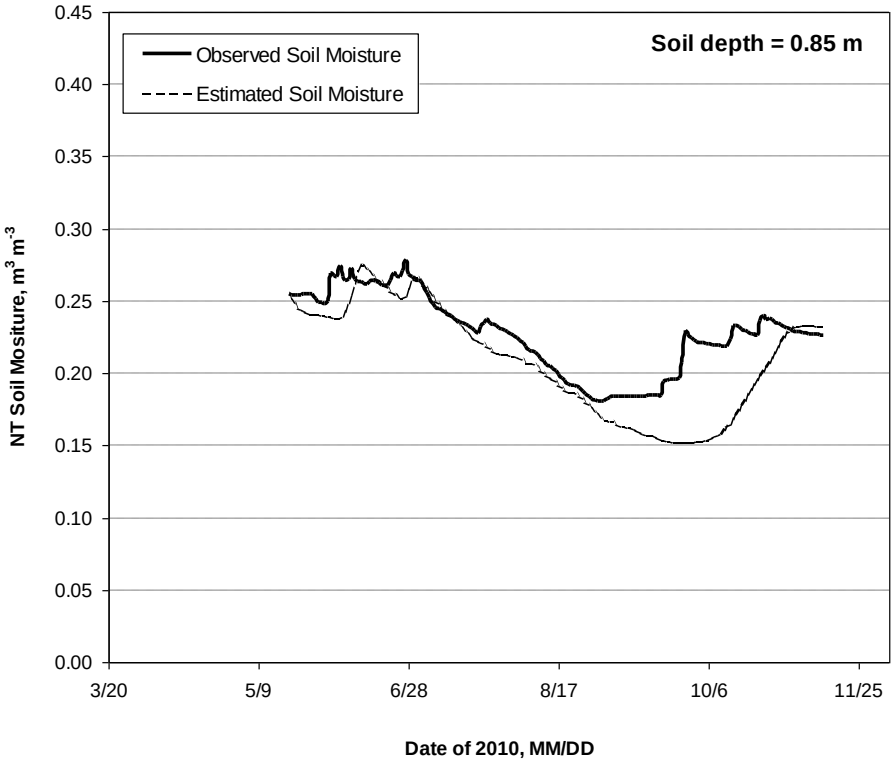
Soil depth = 0.85 m
Observed Soil Moisture
Estimated Soil Moisture
NT Soil Mositure, m3 m-3
0.45
0.40
0.35
0.30
0.25
0.20
0.15
0.10
0.05
0.00
3/20
5/9
6/28
8/17
10/6
11/25
Date of 2010, MM/DD

A.3 SHAW input files and LPRM files for sample SMAPVEX12 Field 52

File: Trial.inp

```
0 0 0
TRIAL.SIT
TRIAL.WEA
TRIAL.MOI
TRIAL.TMP
 24  0 24 24  0 24 24  0  0  6  0  0  1
OUT.OUT
PROFIL.OUT
TEMP.OUT
MOIST.OUT
MATRIC.OUT
ENERGY.OUT
WATER.OUT
WFLOW.OUT
ROOTXT.OUT
```

File: Trial.sit

```
SITE WITH SOYBEAN DURING 2012      ****** (MANITOBA Field 52)                LINE A
 123  00  112  273  112              ****** SIMULATION PERIOD                 LINE B
 49 39.84  0.15  225.0  12.5  268       ****** LOCATION                      LINE C
 1  0  0  15  0  0.01   1  0   0   0   1   0   0    ***** NODES              LINE D
 0.4  2.0  0.00                ****** WEATHER CHARACTERISTICS                LINE E
 1   -53.72  1.32   0.2           ***** PLANT GROWTH / CANOPY                LINE F
 1   1   0.23  7.0  100.  5.0  -100.   2.0E05   3.0E05  **** SOYBEAN         LINE F1-1
 soyb.112
 1.0  .15                            ****** SNOW                             LINE G
 1  1  0.15 0.0                        ****** SOIL                           LINE J
 0.00  4.0  -0.2   0.43  1200.  0.398 52.3 18.1 29.6  2.4                    LINE J-1
 0.05  4.0  -0.2   0.43  1200.  0.398 52.3 18.1 29.6  2.4                    LINE J-2
 0.10  4.0  -0.2   0.43  1200.  0.398 52.3 18.1 29.6  2.4                    LINE J-3
 0.20  4.0  -0.2   0.43  1200.  0.398 52.3 18.1 29.6   2.5                   LINE J-4
 0.30  4.0  -0.2   0.43  1200.  0.398 52.3 18.1 29.6   2.5                   LINE J-5
 0.40  4.0  -0.2   0.43  1200.  0.398 52.3 18.1 29.6   2.5                   LINE J-6
 0.50  4.0  -0.2   0.43  1200.  0.398 52.3 18.1 29.6   0.17                  LINE J-7
 0.60  4.0  -0.2   0.43  1200.  0.398 52.3 18.1 29.6   0.17                  LINE J-8
 0.70  4.0  -0.2   0.43  1200.  0.398 52.3 18.1 29.6   0.17                  LINE J-9
 0.80  4.0  -0.2   0.43  1200.  0.398 52.3 18.1 29.6   0.17                  LINE J-10
 0.90  4.0  -0.2   0.43  1200.  0.398 52.3 18.1 29.6   0.17                  LINE J-11
 1.00  4.0  -0.2   0.43  1200.  0.398 52.3 18.1 29.6   0.17                  LINE J-12
 1.10  4.0  -0.2   0.43  1200.  0.398 52.3 18.1 29.6   0.17                  LINE J-13
 1.20  4.0  -0.2   0.43  1200.  0.398 52.3 18.1 29.6   0.17                  LINE J-14
 1.30  4.0  -0.2   0.43  1200.  0.398 52.3 18.1 29.6   0.17                  LINE J-15
```

File: Trial.moi

```
123    00          112       0.49      0.49      0.498     0.498     0.398     0.365     0.365     0.365     0.365     0.379
           0.379     0.379     0.379     0.379     0.379
273    24          112       0.28      0.28      0.329     0.329     0.329     0.178     0.178     0.178     0.178     0.366
           0.366     0.366     0.366     0.366     0.366
```

File: Trial.tmp

```
123   00        112     12      11.5    11.5    15.22   15.22   13.14   13.14   13.14   13.14   11.10
        11.10   11.10   11.10   11.10   11.10
273   24        112     18      20.84   20.84   20.25   20.25   19.3    19.3    19.3    19.3    17.25
        17.25   17.25   17.25   17.25   17.25
```

File: soyb.112

```
90    112     0       0       0       0       0       APR 01
139   112     0       0       0       0       0       MAY 18
165   112     0.14    2       0.02    0.1     0.10    JUN 13
182   112     0.36     5      0.016   0.33    0.15    JUN 30
191   112     0.62    6        0.15   0.77    0.4     JUL 09
200   112     0.75    6       0.20    1.2      0.5    JUL 18
272   112     0       0       0       0       0.3     SEP 28
275   112     0       0       0       0       0.2     OCT 01
```

File: Trial.wea

```
122   0 112   12.2    8.0769  74      0       0       0
122   1 112   10.6    6.8343  85      0       0       0
122   2 112   10.2    6.8343  86      0       0       0
122   3 112   10.2    4.3491  84      0       0       0
122   4 112   10.1    8.0769  84      0       0       0
122   5 112   10.4    11.8047 83      0       0       0
.....
.....
```

File: LPRM_Tb_SMAPVEX12.m

```
%Filename=LPRM_BrightnessTemp.m
%Calculate daily brightness temperature for 2012 for SMAPVEX12 plots
clear all;
P=0;              % porosity of the soil
WP=0;             % soil moisture content at wilting point
f=1.4;            % frequency (SMOS)
BD=1.2;           % bulk density in g/cu.cm
mpdi=NaN;         % microwave polarization difference index
S=0.523;          % sand in %
C=0.296;          % clay in %
Q=0;              % polarization mixing fraction
w=0;              % vegetation single scattering albedo
opt_atm=0.01;     % zenith atmospheric opacity f (water vapor)
u=0.698131701;    % incidence angle in rad. or 40 deg
b=0.087;          % vegetation parameter (corn)
ps=1.65;          % average RMS height
pl=55.5;          % average correlation length (cm)
p=dlmread('C:\SMAPX12\Field_52_sm_st_vw.csv'); % file contains Julian day,
soil moisture (SHAW simulated), soil temperature (SHAW simulated) and
vegetation water content
JD = p(:,1);
sm = p(:,2);
T = p(:,3)+273.15;
wv=p(:,4);
h= 0.5761*((p(:,2)).^(-0.3475))*(ps/pl).^(0.4230);
[Tb,opt]=forward_sw(mpdi,T,sm,P,WP,S,C,BD,h,Q,w,opt_atm,f,u,wv,b);
```

File: forward_sw.m

```
function [Tb,opt]=forward_sw(mpdi,T,sm,P,WP,S,C,BD,h,Q,w,opt_atm,f,u,wv,b)

% Forward model to predict Tb and Optical Depth
% INPUT:
%   mpdi,                                                        [-]
%   T, Soil Temperature at 1.25cm                                [K]
%   sm, Water content of the soil                                [m3/m3]
%   P, Porosity of the soil (if unknown, fill in 0, give BD)     [m3/m3]
%   WP, Water content at wilting point (if unknown, fill in 0)   [m3/m3]
%   S, C, Sand and Clay content (if Wilting Point unknown)       [m3/m3]
%   BD, Bulk density (if Porosity unknown)                       [g/cm3]
%   h, empirical roughness parameter (0-0.2)                     [-]
%   Q, polarization mixing fraction (0-0.2)                      [-]
%   w, vegetation single scattering albedo (<0.12)               [-]
%   b, vegetation parameter at 1.4GHz or 21 cm (0.0-2.0)         [-]
%   wv, vegetation water content                                 [kg/m2]
%   opt_atm, zenith atmospheric opacity f(water vapor)           [-]
%   f, Frequency of Radiometer                                   [GHz]
%   u, Incidence angle                                           [rad]
% OUTPUT:
%   opt, Optical Depth                                           [-]
%   Tb, Brightness Temperature  (H)                              [K]

% REFERENCE : M. Owe, R. de Jeu and T. Holmes, (2008). "Multisensor
%  historical climatology of satellite-derived global land surface
%  moisture", J. Geophys. Res., 113, F01002, doi:10.1029/2007JF000769.
% AUTHOR : May 2006, T. Holmes, Vrije Universiteit Amsterdam
% CHANGES : December 2006, T. Holmes
%           in kcurven : if mpdi<1e-9, mpdi=1e-9; end
% ---------------------------------------------------------------------

    % Dielectric Constant of the soil [-]
    e=wang(P,WP,T,f,sm,BD,S,C); % complex
    k=abs(e); % absolute value
    % Smooth Surface Reflectivity
    [Rh,Rv]=fresnel(k,u);
    % Rough Surface Emissivity
    [eh,ev]=emissivity(Rh,Rv,h,Q);
    % Vegetation Optical Depth at nadir
    opt=swapan(b,wv);
    % Vegetation Transmissivity
    trans_v=exp(-opt./cos(u));
    % Predicted Tb(H)
    Tb=radtrans(T,eh,trans_v,w,opt_atm,u);

%------- END OF MAIN FUNCTION ------------------

function Tb=radtrans(Ts,e,trans_v,w,opt_atm,u)
% Radiative transfer equation (Kirdiashev et al., 1979) (Mo et al., 1982)
% Assumption: Tcanopy = Tsoil and single scattering
    Tc=Ts;
    % Emitted Brightness Temperature from soil/vegetation
    Tb = Ts.*e.*trans_v ...
```

```
        + (1-w).*Tc.*(1-trans_v) + (1-e).*(1-w).*Tc.*(1-trans_v).*trans_v;
    if opt_atm>0
    % Atmospheric Contribution
    [trans_atm,Textra,Tup,Tdn]=atmosphere(Ts,opt_atm,u);
    % Measured Brightness Temperature by spaceborn radiometer
    Tb= trans_atm*( Tb + (1-e).*(Tdn+Textra.*trans_atm).*trans_v.*trans_v ) +
Tup;
    end

function  [trans_atm,Textra,Tup,Tdn]=atmosphere(Ts,opt_atm,u)
% Atmospheric Contribution to Tb as measured by spaceborn radiometer
    % Atmospheric Transmissivity
    trans_atm=exp(-opt_atm./cos(u));
    % Weighted mean temperature of atmosphere [K] (Bevis et al., 1992)
    Tm=70.2+0.72*Ts;
    % Upwelling brightness temperature from atmosphere [K]
    Tup=Tm*(1-trans_atm);
    Tdn=Tup;
    % Extraterrestrial Brightness Temperature [K] (Ulaby, 1981)
    Textra=2.7;

function opt=swapan(b,wv)
%Jackson & O'Neill (1990) Model to predict Optical Depth
% REFERENCE : Jackson, T.J. and T.J. Schmugge. 1991. "Vegetation effects on
%  the microwave emission of soils", Remote Sens. Environ. 36: 203-212.
    opt=b*wv;

function [eh,ev]=emissivity(Rh,Rv,h,Q)
% Rough Surface Emissivity (Choudhury et al., 1979), (Wang and Choudhury,
1981)
    eh=1-((1-Q)*Rh+Q*Rv).*exp(-h);
    ev=1-((1-Q)*Rv+Q*Rh).*exp(-h);

function [Rh,Rv]=fresnel(k,u)
% Fresnel Law
    Rh=((cos(u)-sqrt(k-sin(u)^2))./(cos(u)+sqrt(k-sin(u)^2))).^2;
    Rv=((k.*cos(u)-sqrt(k-sin(u)^2))./(k.*cos(u)+sqrt(k-sin(u)^2))).^2;
```

File: wang.m

```
function e=wang(P,WP,T,f,Wc,BD,Sand,Clay)

% e=wang(P,WP,T,f,Wc,BD,Sand,Clay)
% Wang and Schmugge model (1980)
%
% INPUT
%   P = porosity of the soil (if unknown, fill in 0, give BD)    [m3/m3]
%   WP = soil moisture content at wilting point                  [m3/m3]
%       (if unknown, fill in 0, give Sand,Clay)
%   T = Temperature of soil water                                [Kelvin]
%   f = Frequency                                                [GHz]
%   Wc = Water content of the soil                               [m3/m3]
%   BD = Bulk density (if Porosity unknown)                      [g/cm3]
%   Sand,Clay = Sand and Clay content (if Wilting Point unknown) [m3/m3]
```

```
% OUTPUT
%   e = complex Dielectric Constant of the soil (real+imag)      [-]
% AUTHOR : 2005, T. Holmes, Vrije Universiteit

% frequency conversion [GHz] to [Hz]
f=f.*1e9;

% calculate porosity if unknown
if (P==0 & length(P)==1), P=1-(BD/2.65);
else
i=find(P==0);
if (isempty(i)==0 && length(BD)==length(P)); P(i)=1-(BD(i)/2.65); end
end
% calculate wilting point if unknown (Wang and Schmugge,1980)
if (WP==0 & length(WP)==1), WP=0.06774-0.064.*Sand+0.478.*Clay;
else
i=find(WP==0);
if (isempty(i)==0 && length(Sand)==length(WP) && length(Sand)==length(WP))
    WP(i)=0.06774-0.064.*Sand(i)+0.478.*Clay(i); end
end

% definitions:
ei=3.2+0.1i;    %dielectric constant of ice (Wang and Schmugge, 1980)
ea=1+0i;        %dielectric constant of air (Wang and Schmugge, 1980)
er=5.5+0.2i;    %dielectric constant of rock (Wang and Schmugge, 1980)

% dielectric constant of water (Ulaby, Vol III p2020)
[ew]=debye(T,f);

% The final Wang Schmugge model
% ----------------------
% fit parameter (Wang and Schmugge,1980)
y=-0.57.*WP+0.481;
% transition moisture (Wang and Schmugge,1980)
Wt=0.49.*WP+0.165;
% dielectric constant of the initially absorbed water (Wc <= Wt)
ex=ei+(ew-ei).*(Wc./Wt).*y;
% dielectric constant of the soil (Wc <= Wt)
e1=Wc.*ex+(P-Wc).*ea+(1-P).*er; %(Wc <= Wt)
% dielectric constant of the initially absorbed water (Wc > Wt)
ex=ei+(ew-ei).*y;
% dielectric constant of the soil (Wc > Wt)
e=Wt.*ex+(Wc-Wt).*ew+(P-Wc).*ea+(1-P).*er; %(Wc > Wt)
% combine (Wc <= Wt) & (Wc > Wt)
if (length(Wc)>1 || length(Wt)>1 )
    z=find(Wc <= Wt);
    e(z)=e1(z);
elseif Wc<Wt
    e=e1;
end
% ----------------------

function [ew]=debye(T,f)
%Calculation of dielectric constant of water (Ulaby, Vol III p2020)
```

```
% Debye Equation

% convert Temperature from Kelvin to Celcius
T=T-273.15;
% high frequency limit of the dielectric constant of pure water
ewinf=4.9;
%relaxation time of pure water  (Stogryn, 1970)
relt=(1.1109e-10)-(3.824e-12).*T+(6.938e-14).*(T.^2)-(5.096e-16).*(T.^3);
%Static dielectric constant of pure water
ewo=88.045-0.4147.*T+(6.295e-4).*(T.^2)+(1.075e-5).*(T.^3);
%real part of the dielectric constant of pure water
ewr=ewinf+((ewo-ewinf)./(1+(relt.*f).^2));
%imaginary part of the dielectric constant of pure water
ewc=(relt.*f.*(ewo-ewinf)./(1+(relt.*f).^2));
%dielectric constant of water
ew=ewr+ewc*i;
```

A.4 Observed and simulated surface soil moisture at 0.05 m soil depth, and simulated brightness temperature of individual temporary network sites

Field 13 (Pasture) – Loamy Sand (using CaPA precipitation, pixel 9_4) [RMSE=0.0325; R^2=0.7344] [note: h = average of daily roughness parameter (h_s)]

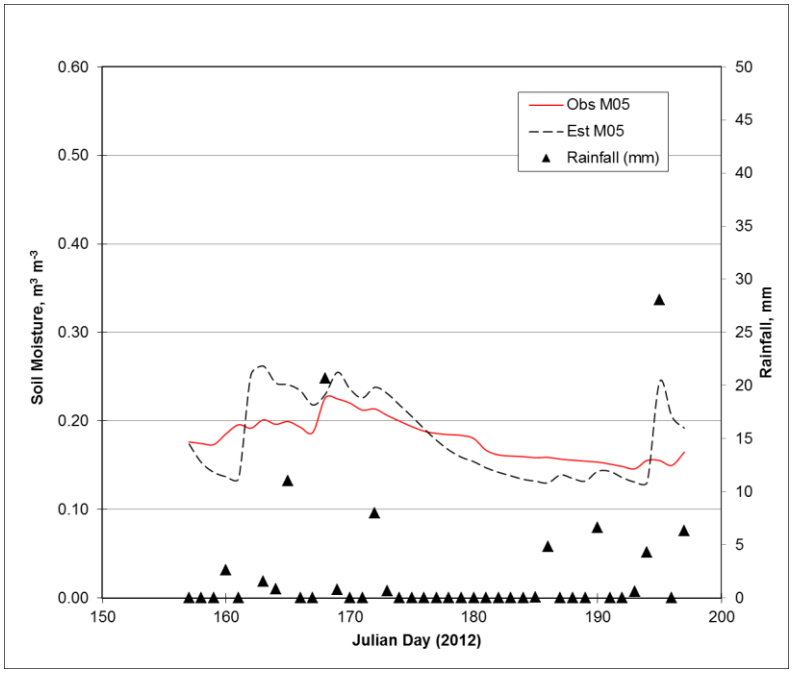

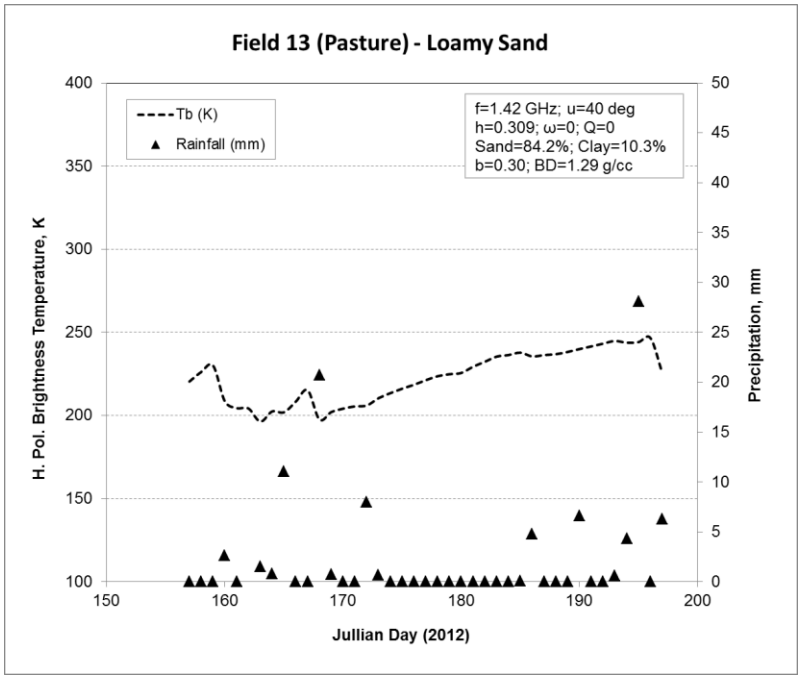

Field 14 (Soybean) – Sandy Soil (using CaPA precipitation, pixel 10_5) [RMSE=0.0768; R^2=0.8138]

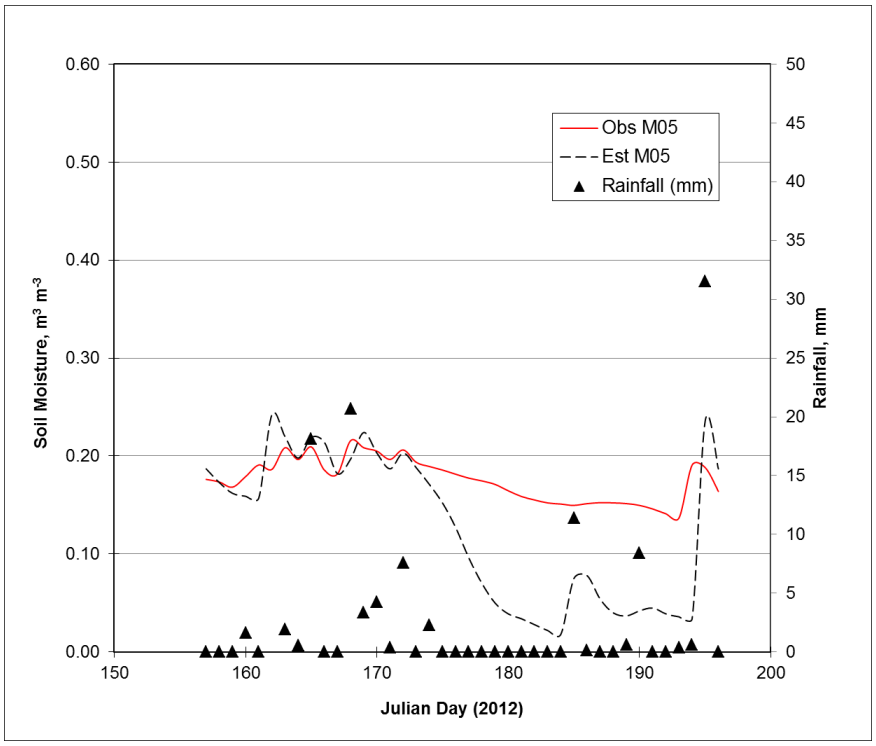

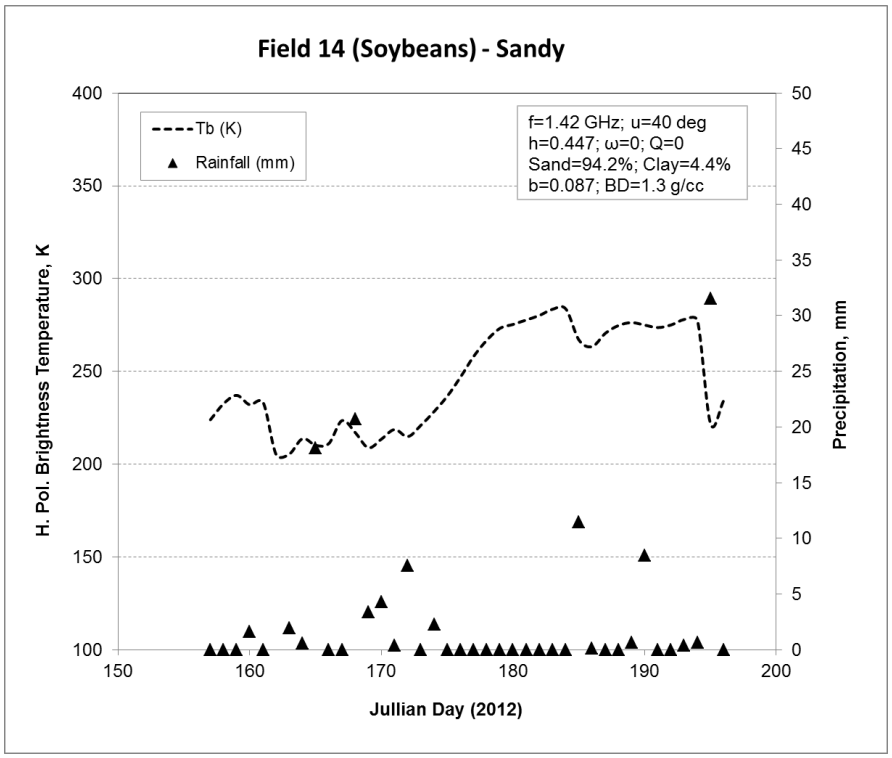

Field 21 (Pasture) – Sandy Clay Loam (using CaPA precipitation, pixel 9_4) [RMSE=0.0651; R^2=0.8207]

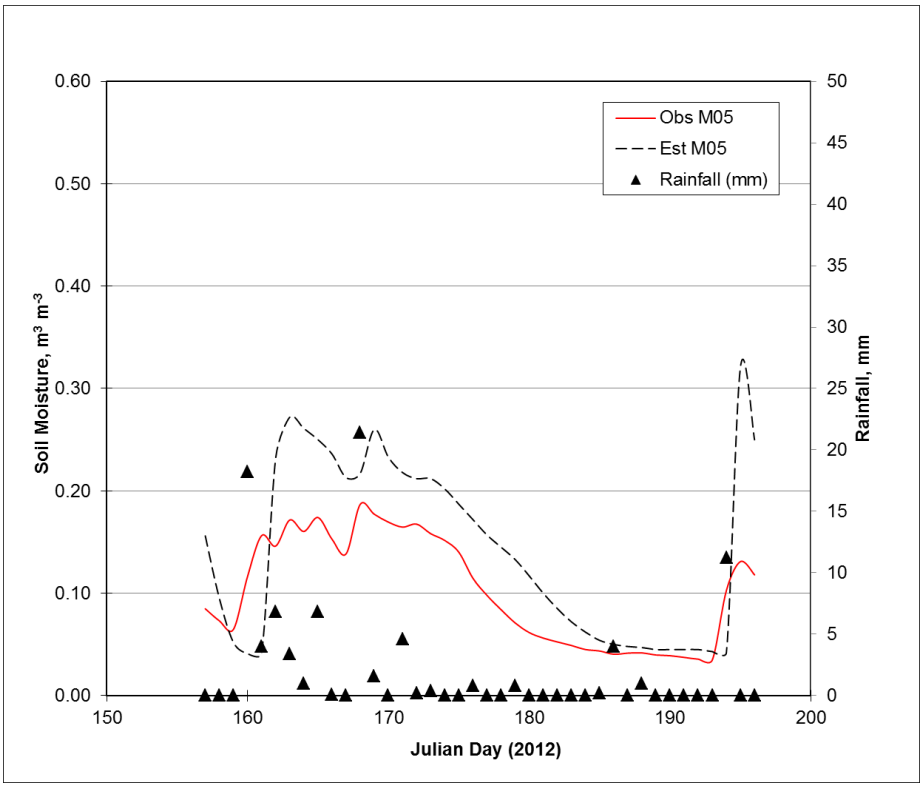

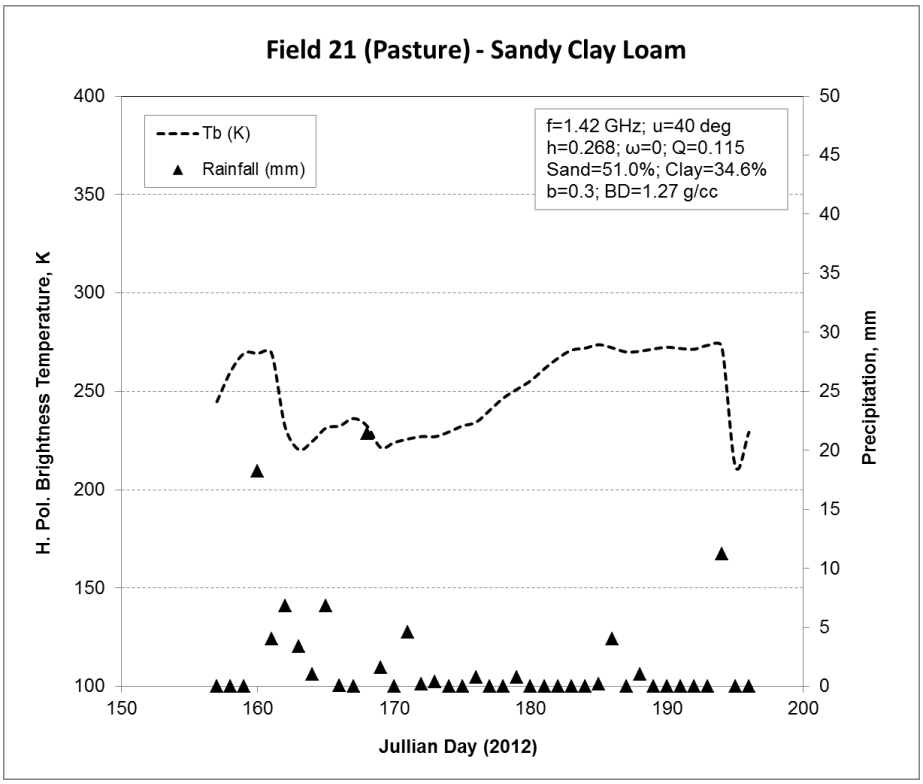

Field 31 (Wheat) – Sandy Clay (using CaPA precipitation, pixel 11_4) [RMSE=0.0422; R^2=0.8203]

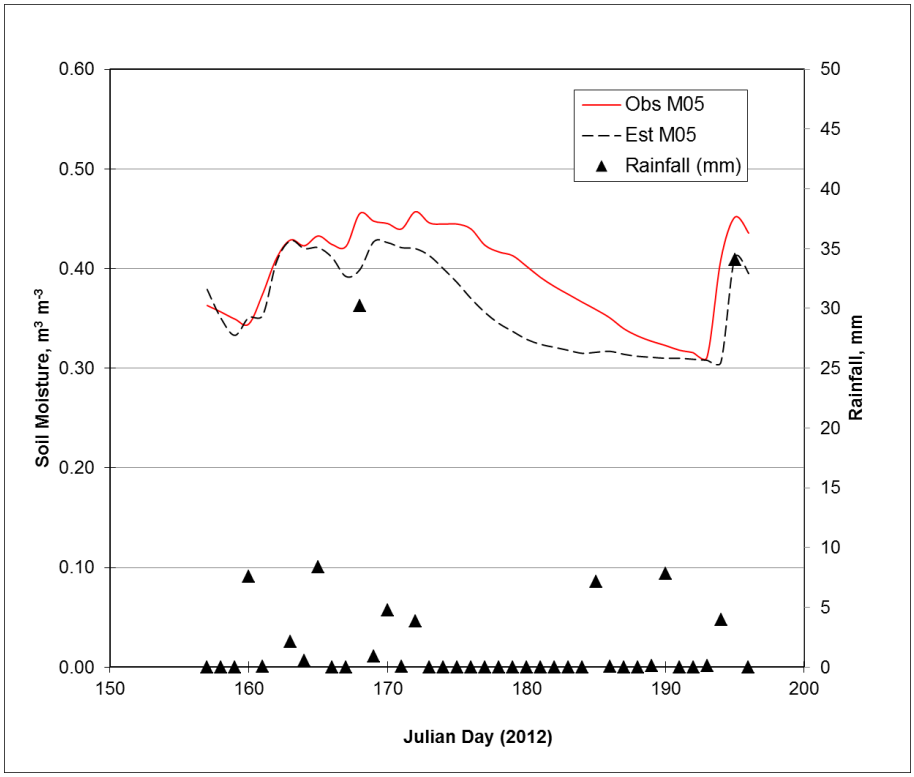

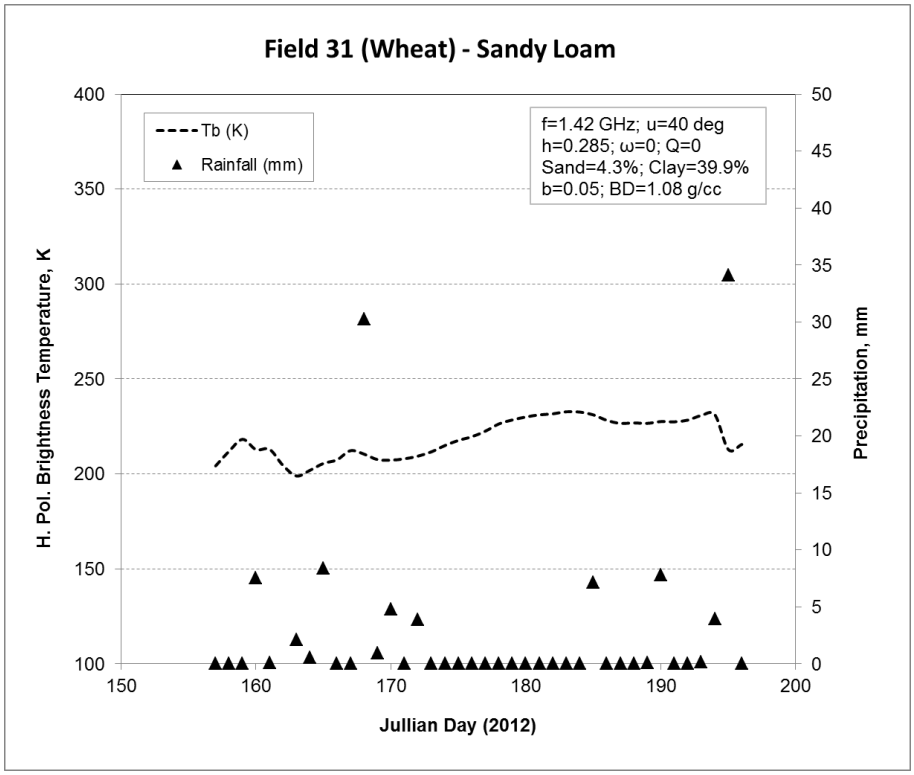

Field 34 (Soybean) – Heavy clay soil (using CaPA precipitation, pixel 11_5) [RMSE=0.0540; R^2=0.5849]

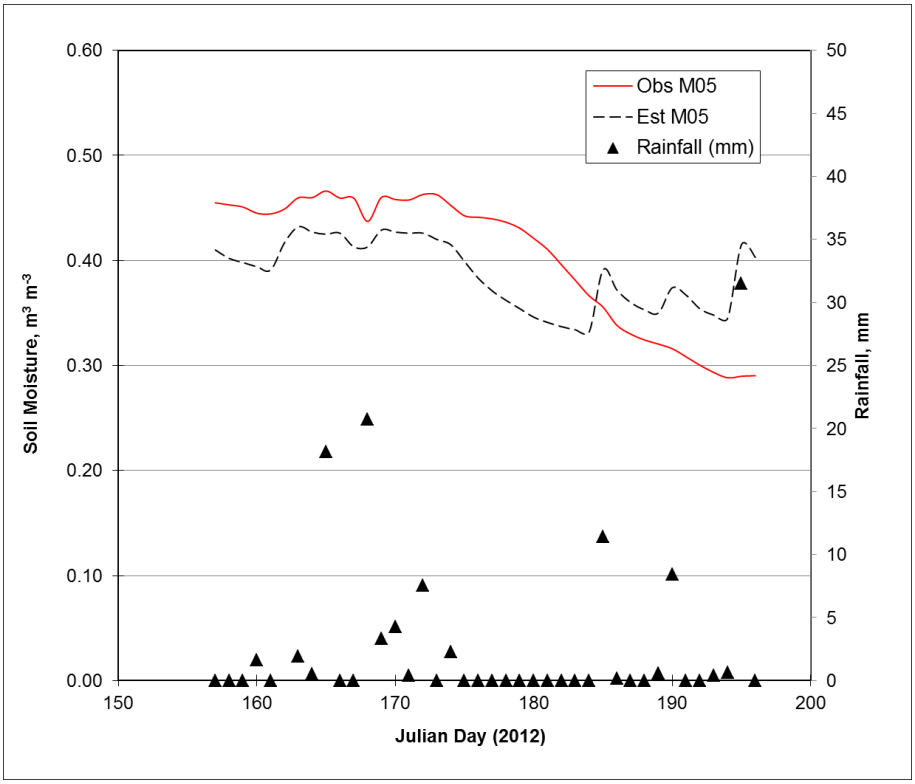

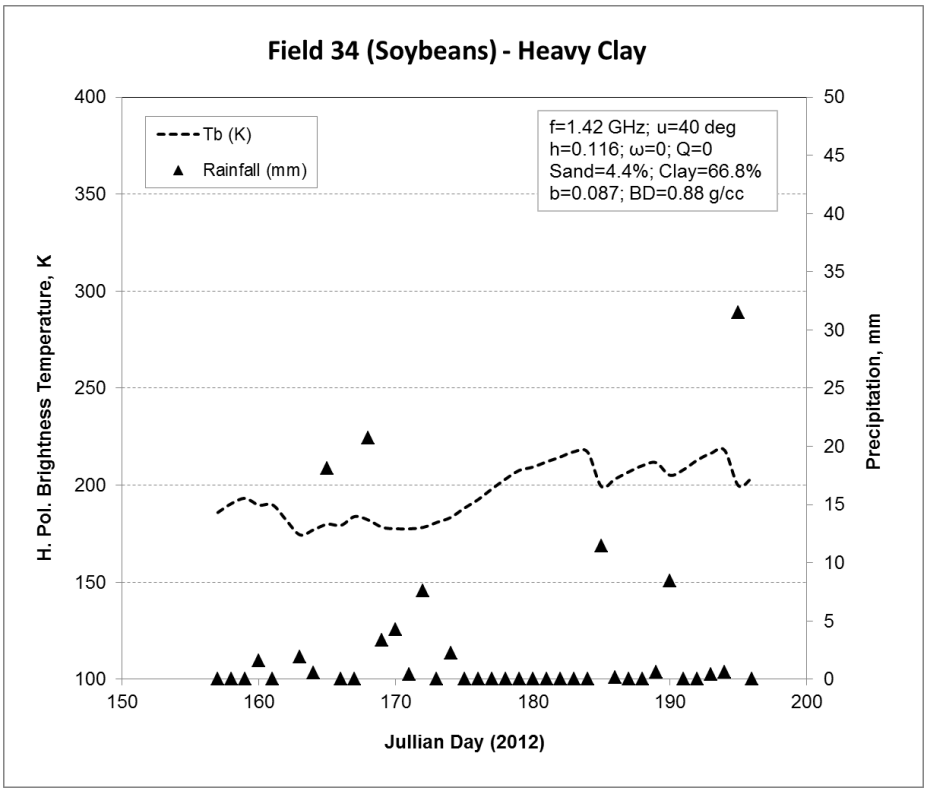

Field 41 (Winter Wheat) – Heavy Clay (using CaPA precipitation, pixel 11_5) [RMSE=0.0694; R^2=0.822]

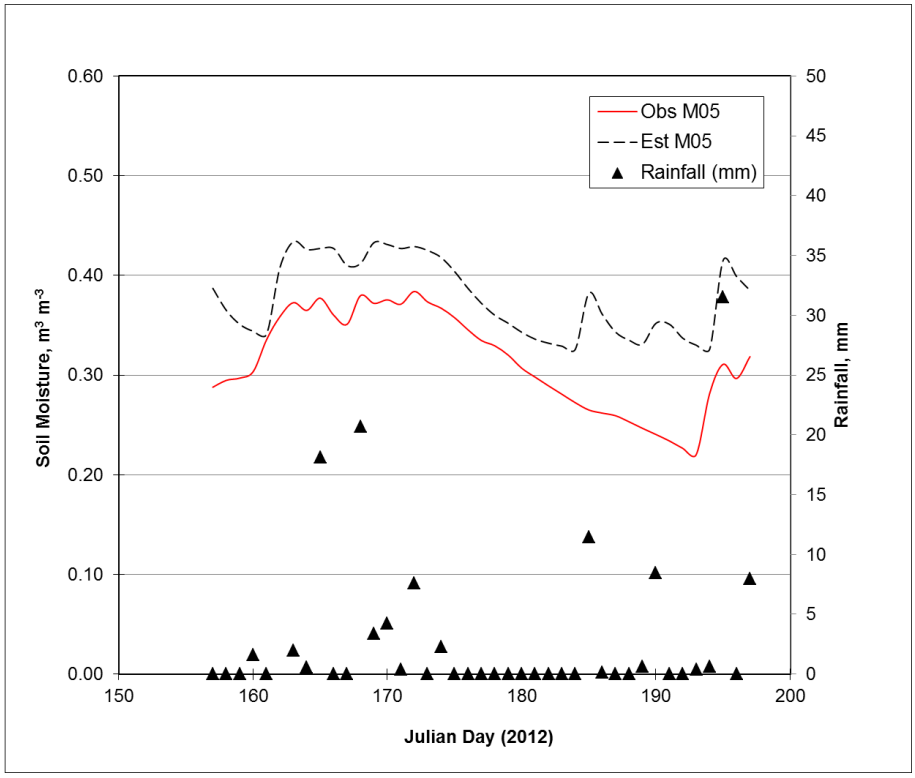

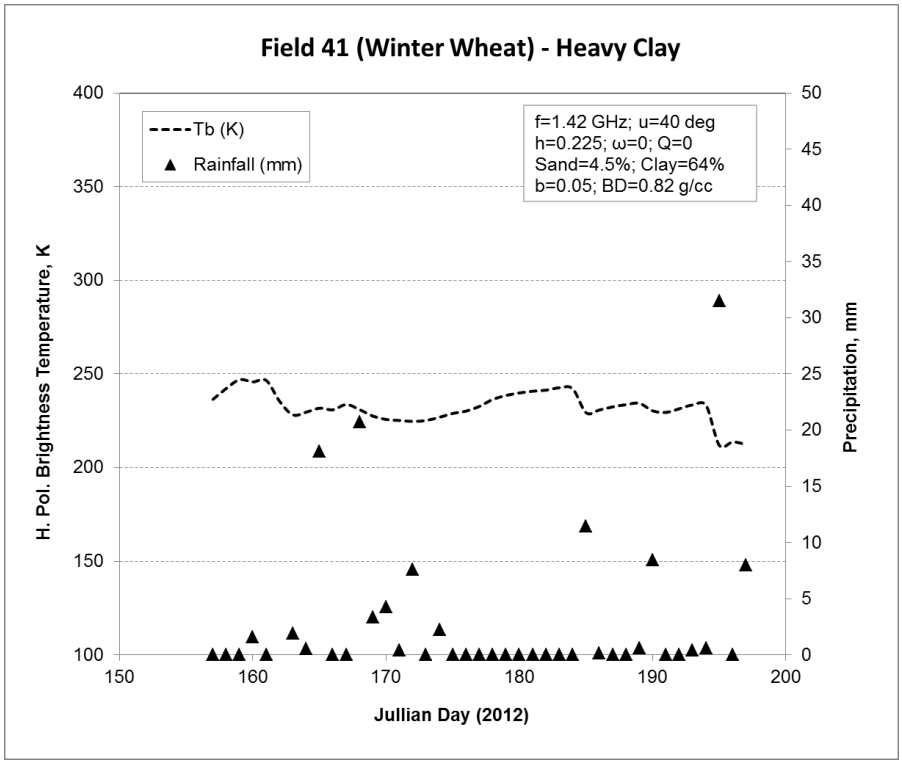

Field 45 (Wheat) – Heavy Clay (using CaPA precipitation, pixel 11_5) [RMSE=0.0742; R^2=0.7199]

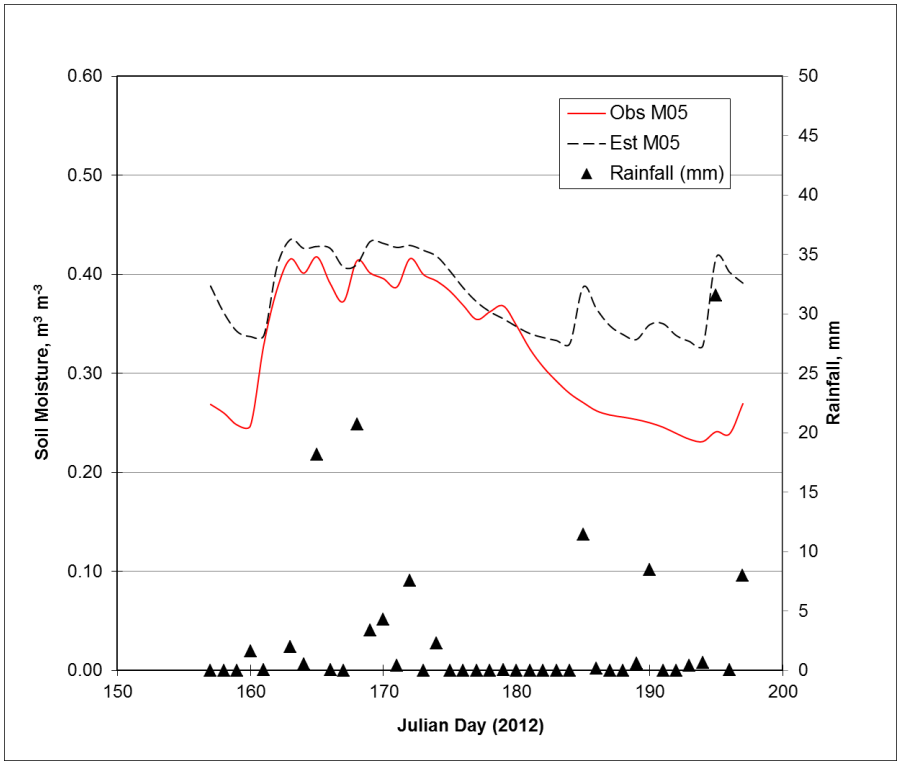

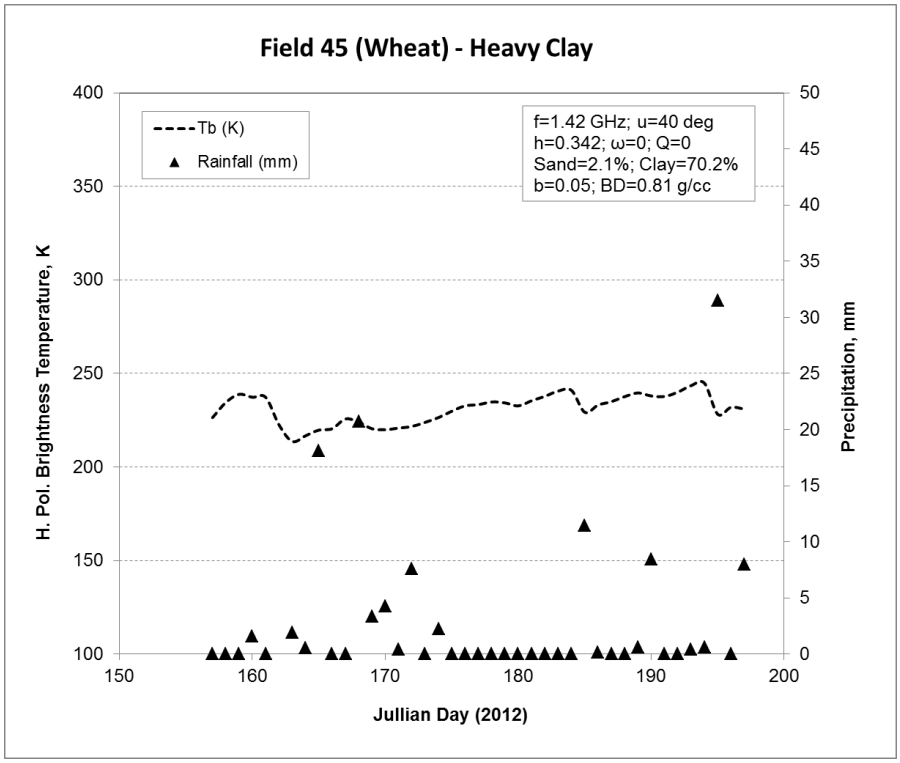

Field 52 (Soybean) – Sandy Clay Loam (using CaPA precipitation, pixel 11_5) [RMSE=0.0551; R^2=0.7646]

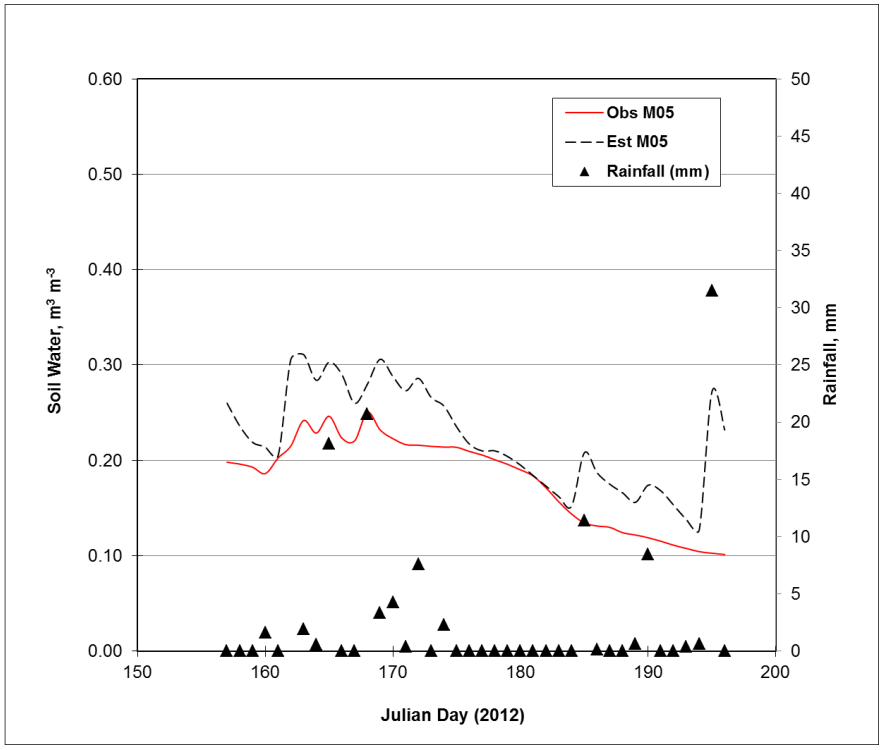

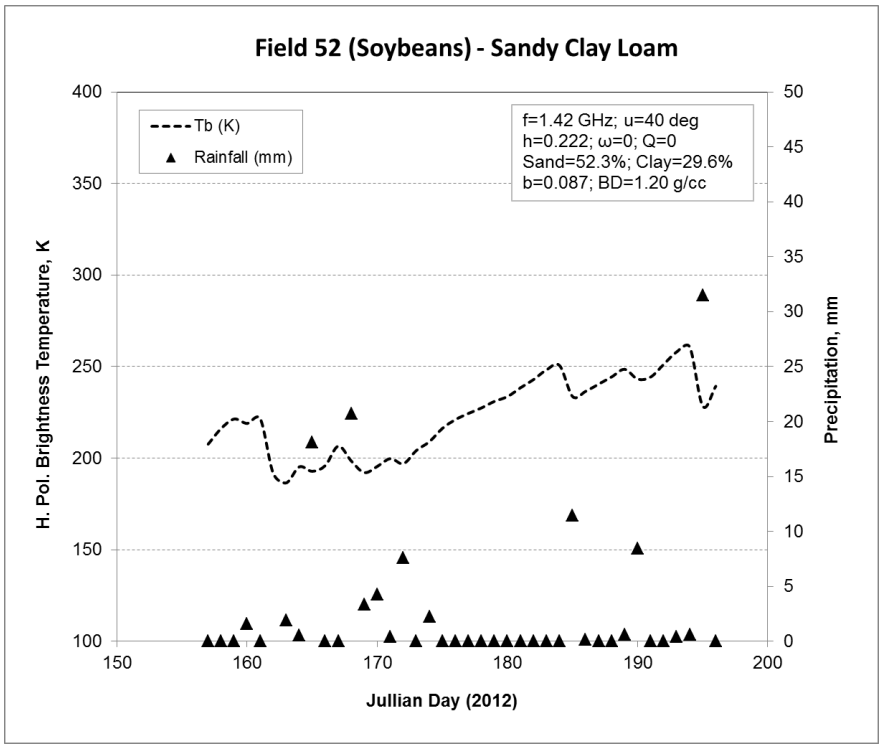

Field 53 (Corn) – Sandy Clay Loam (using CaPA precipitation, pixel 11_5) [RMSE=0.0419; R^2=0.7125]

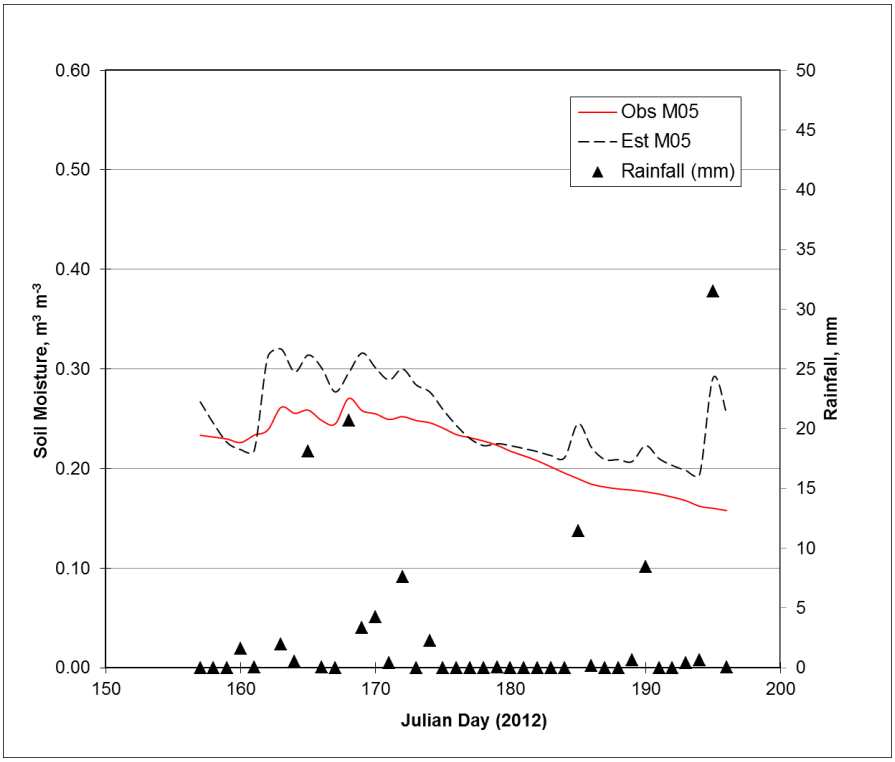

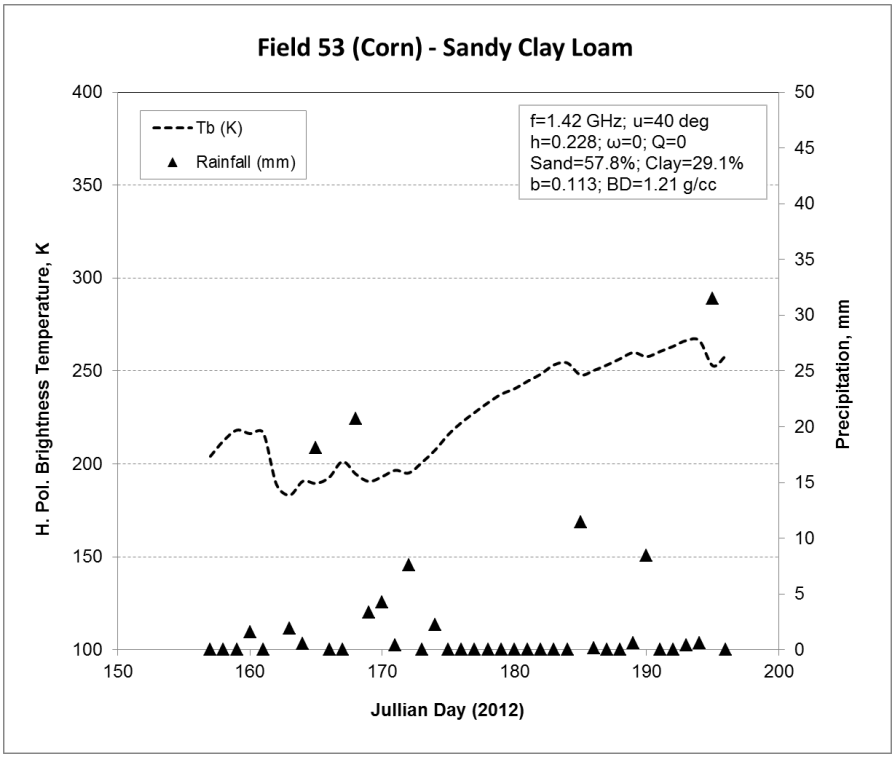

Field 54 (Corn) – Sandy Loam (using CaPA precipitation, pixel 11_5) [RMSE=0.0365; R^2=0.8109]

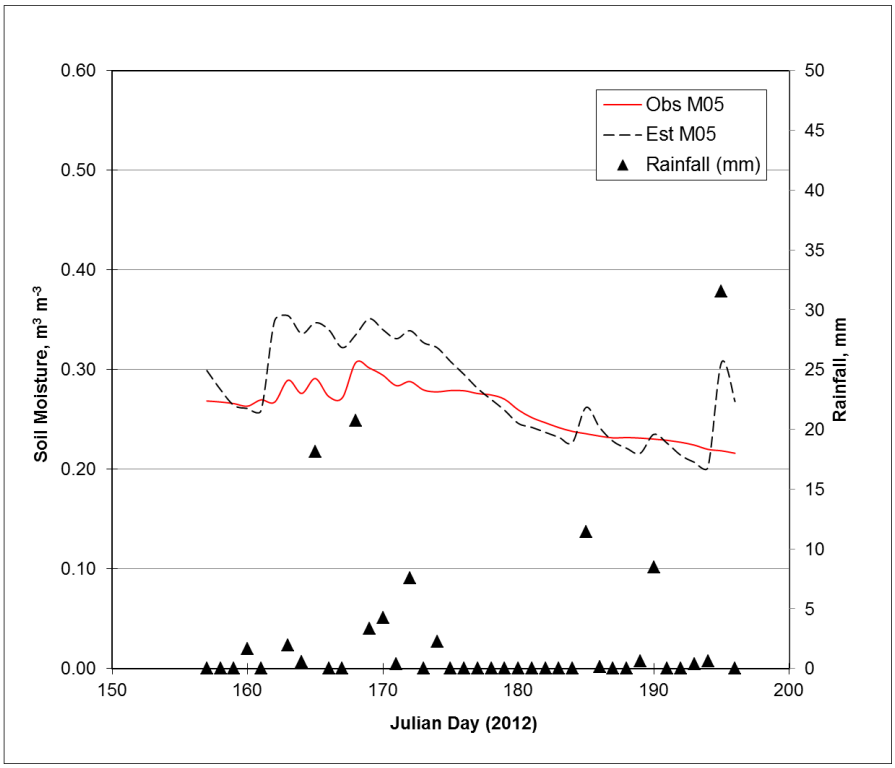

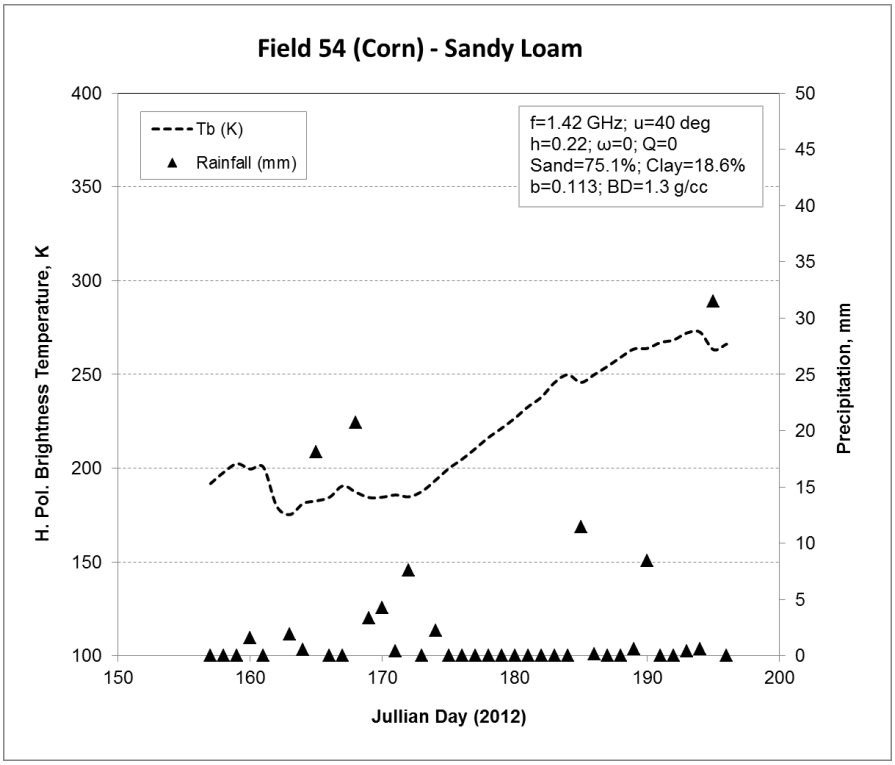

Field 55 (Wheat) – Heavy Clay (using CaPA precipitation, pixel 12_5) [RMSE=0.0541; R^2=0.6813]

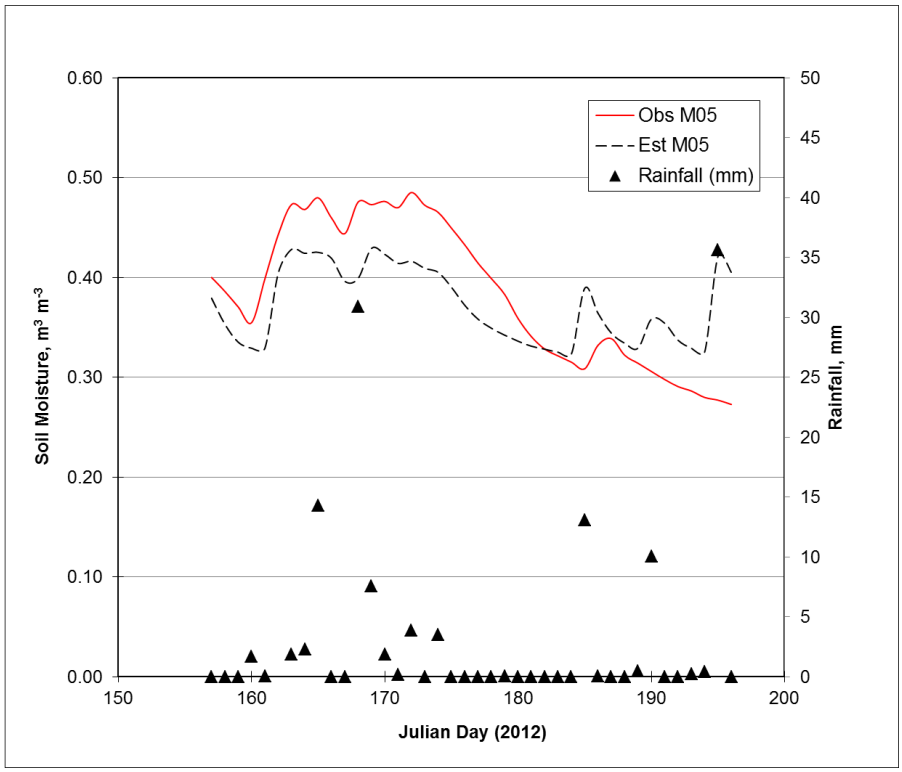

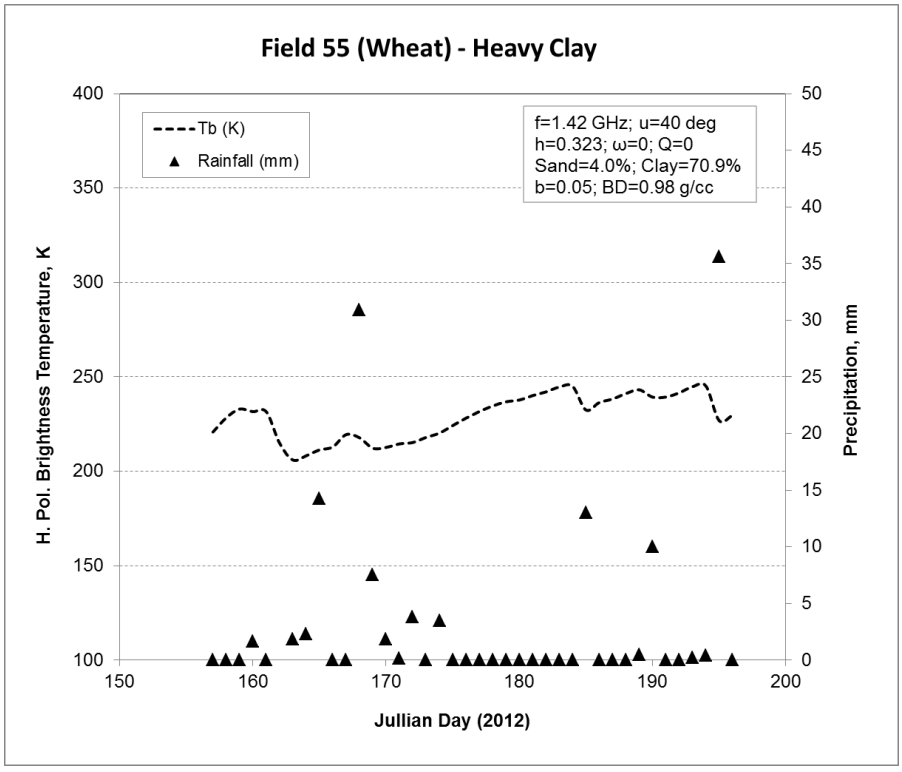

Field 61 (Canola) – Loamy Sand (using CaPA precipitation, pixel 11_5) [RMSE=0.0589; R^2=0.7147]

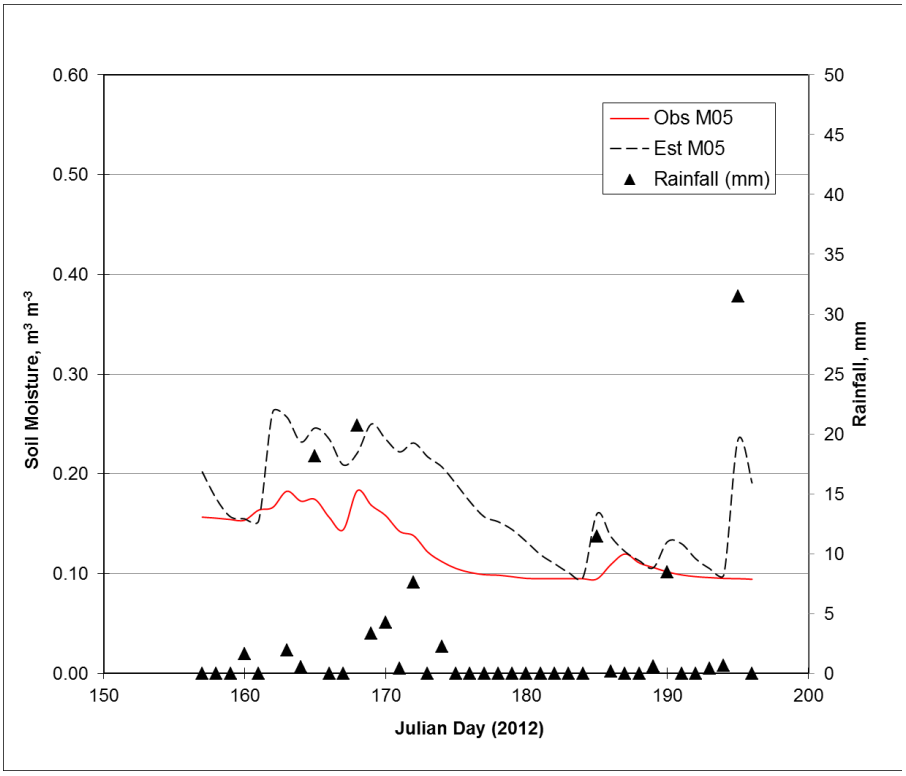

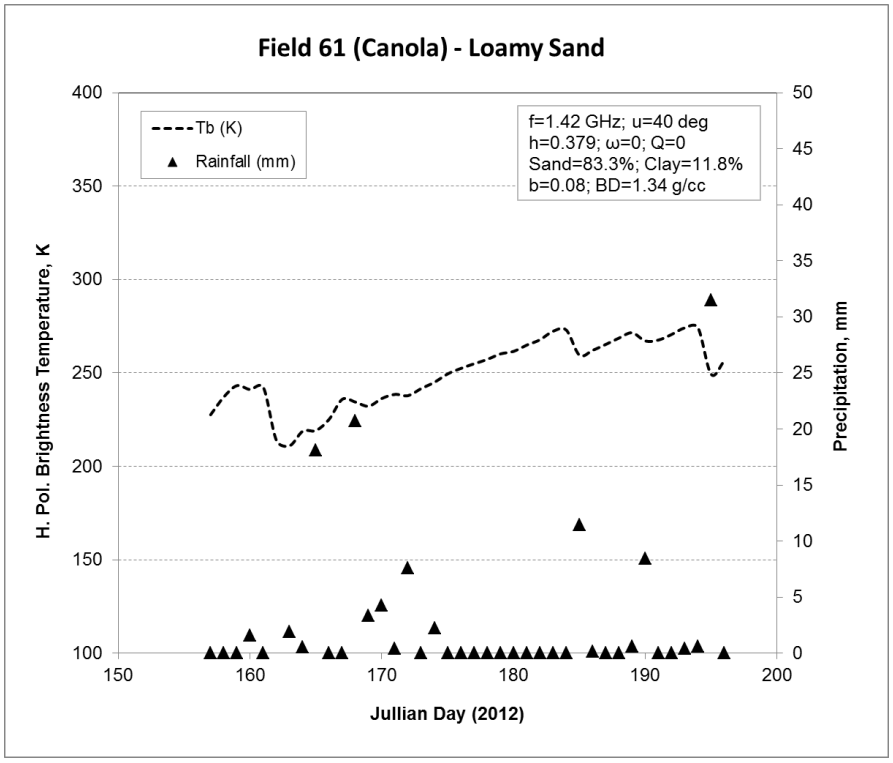

Field 62 (Corn) – Sand (using CaPA precipitation, pixel 11_5) [RMSE=0.0740; R^2=0.386]

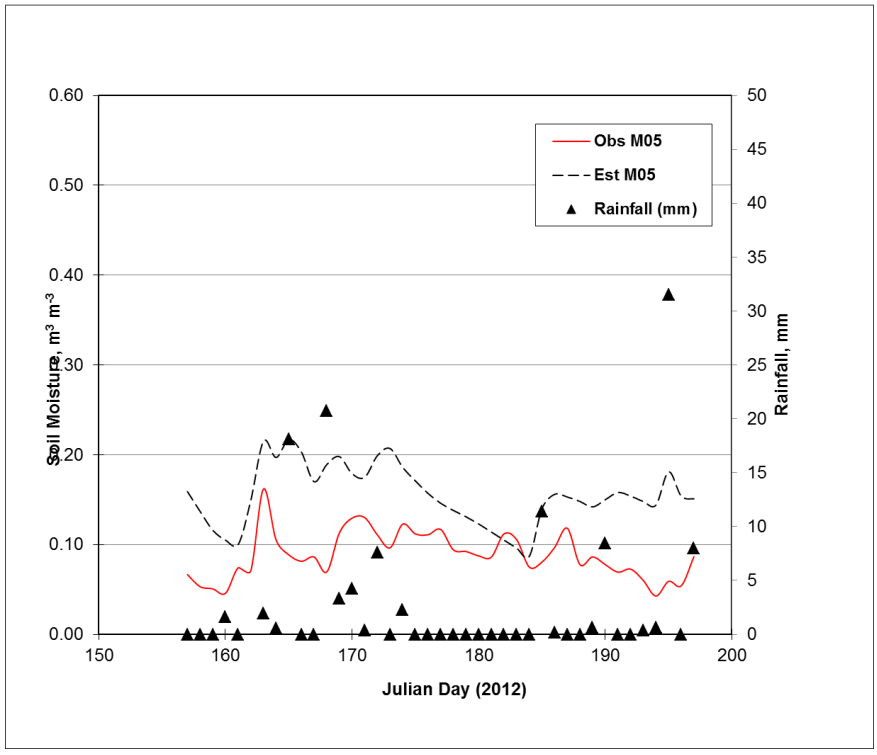

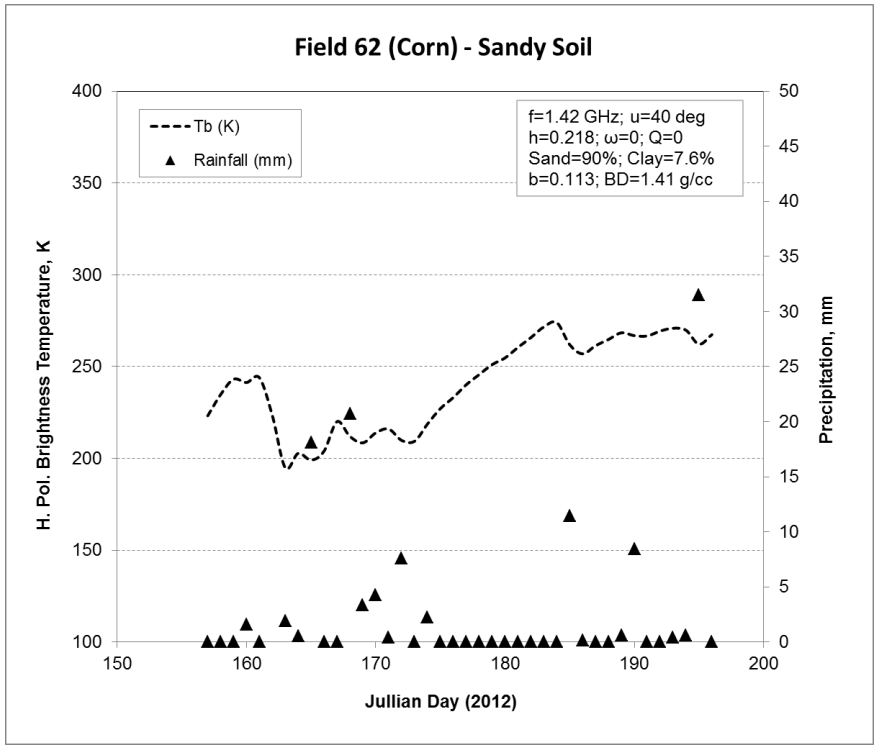

Field 63 (Soybean) – Loamy sand (using CaPA precipitation, pixel 11_5) [RMSE=0.0359; R^2=0.8021]

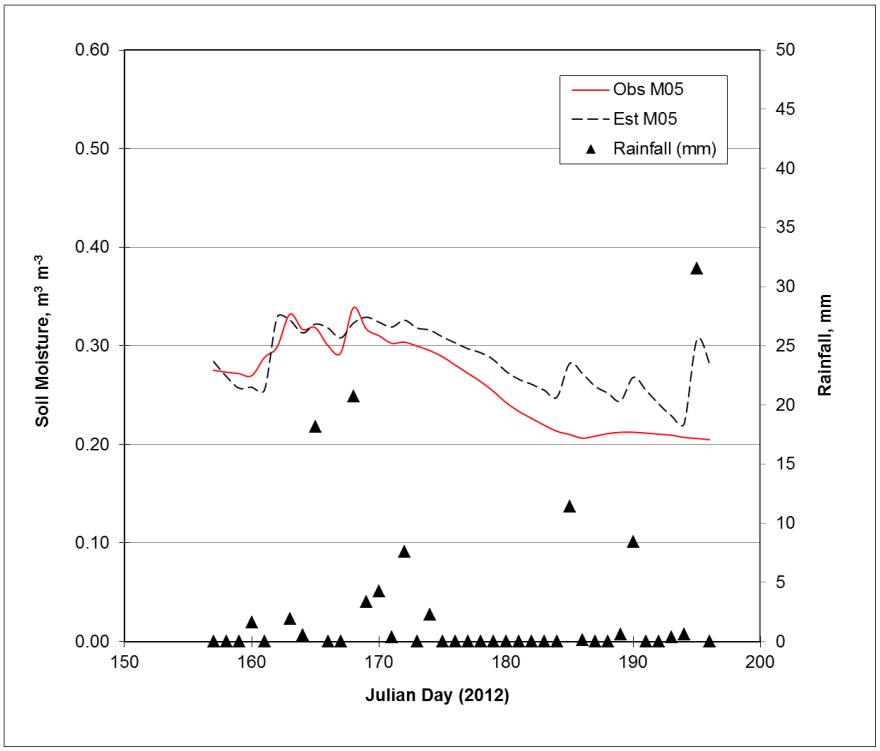

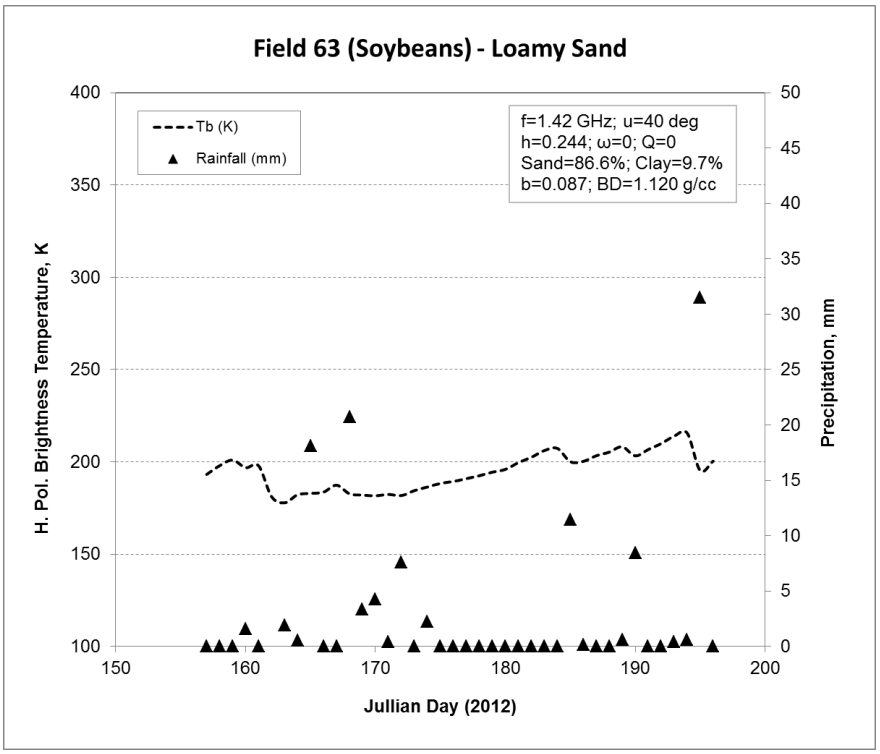

Field 64 (Soybean) –sandy clay loam (using CaPA precipitation, pixel 11_5) [RMSE=0.0242; R^2=0.7885]

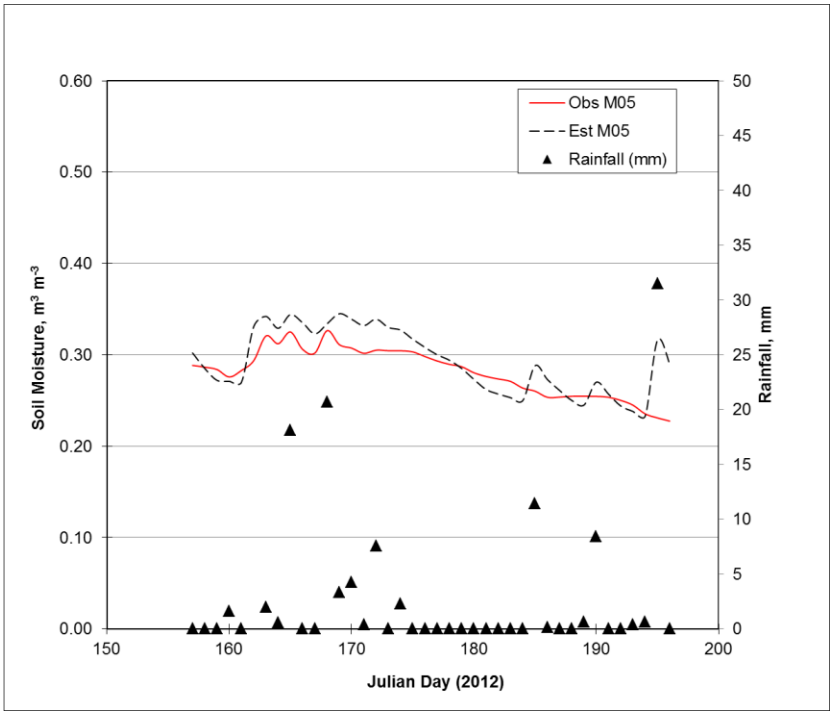

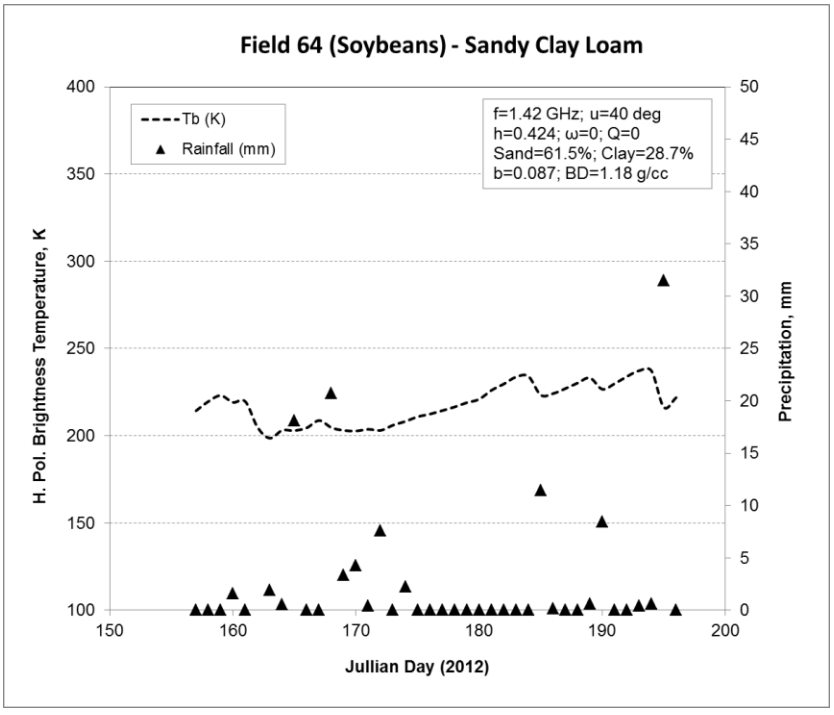

Field 71 (Corn) – Sandy (using CaPA precipitation, pixel 11_6) [RMSE=0.0480; R^2=0.4379]

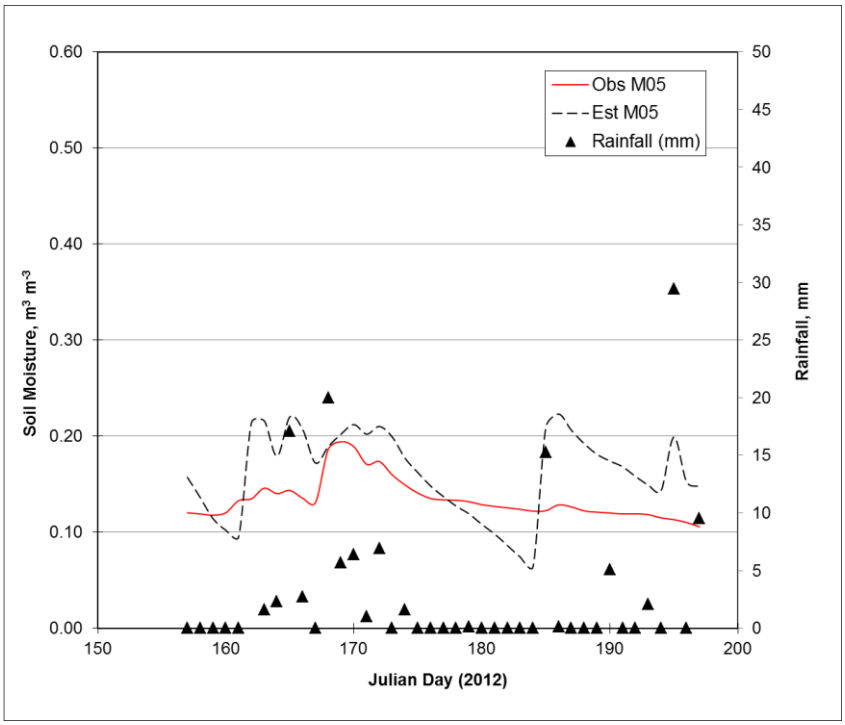

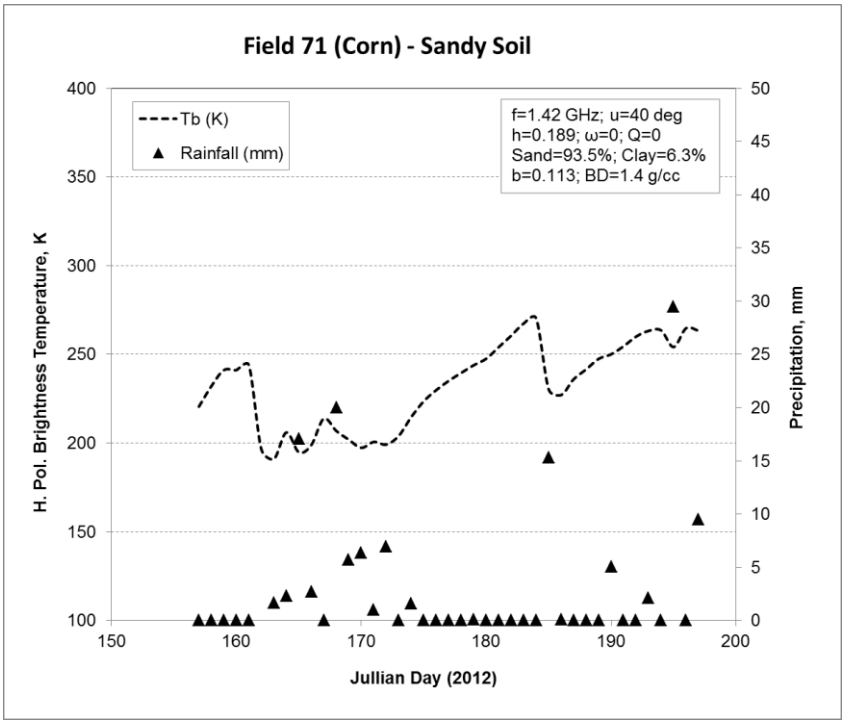

Field 72 (Corn) – Sandy (using CaPA precipitation, pixel 11_6) [RMSE=0.0434; R^2=0.6122]

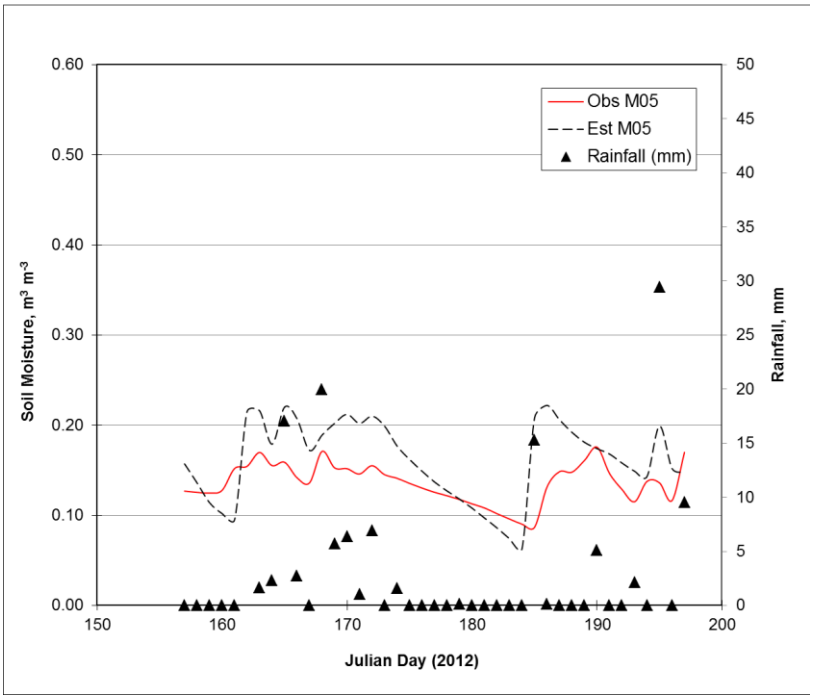

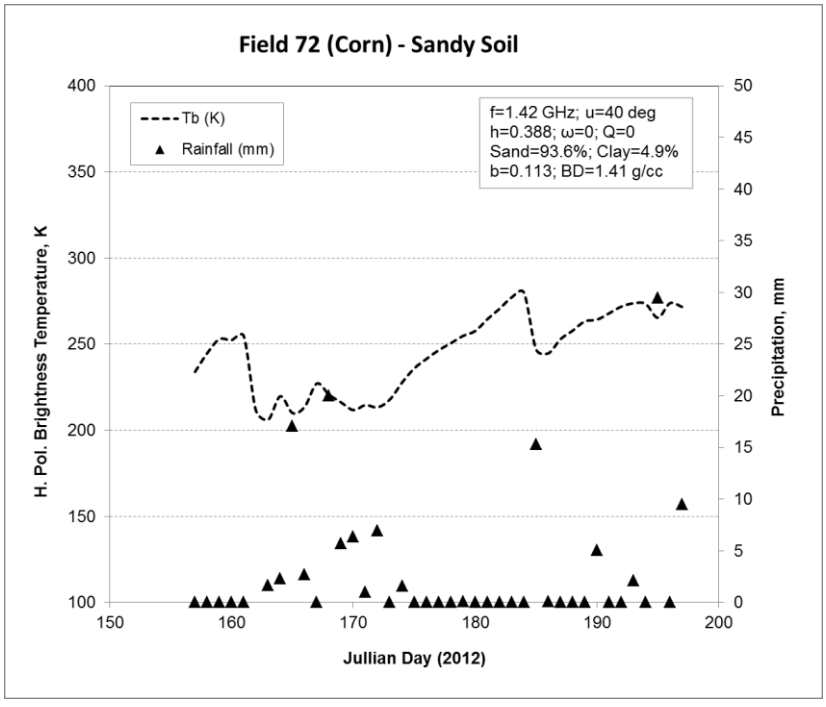

Field 74 (Wheat) – Loamy Sand (using CaPA precipitation, pixel 10_6) [RMSE=0.0686; R^2=0.6097]

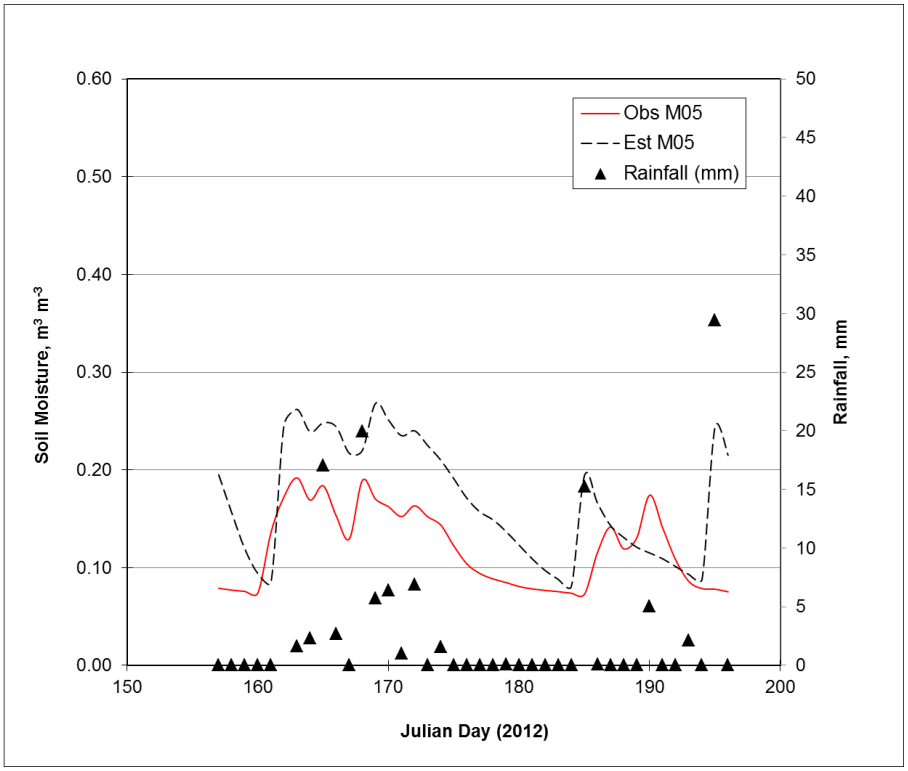

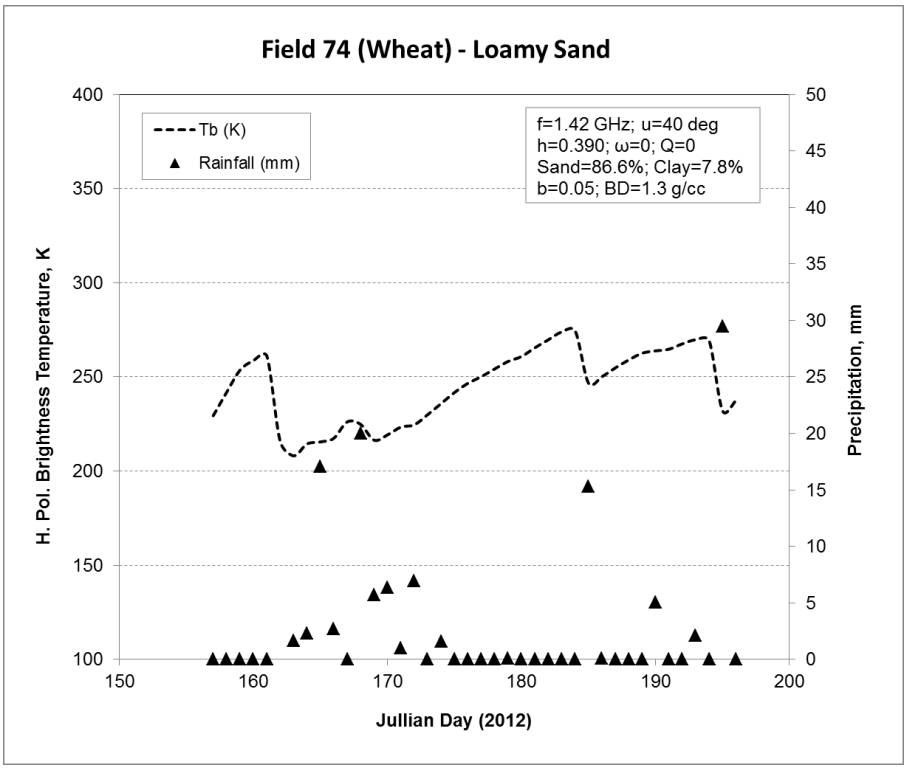

Field 81 (Wheat) – Loamy Sand (using CaPA precipitation, pixel 11_6) [RMSE=0.0603; R^2=0.6918]

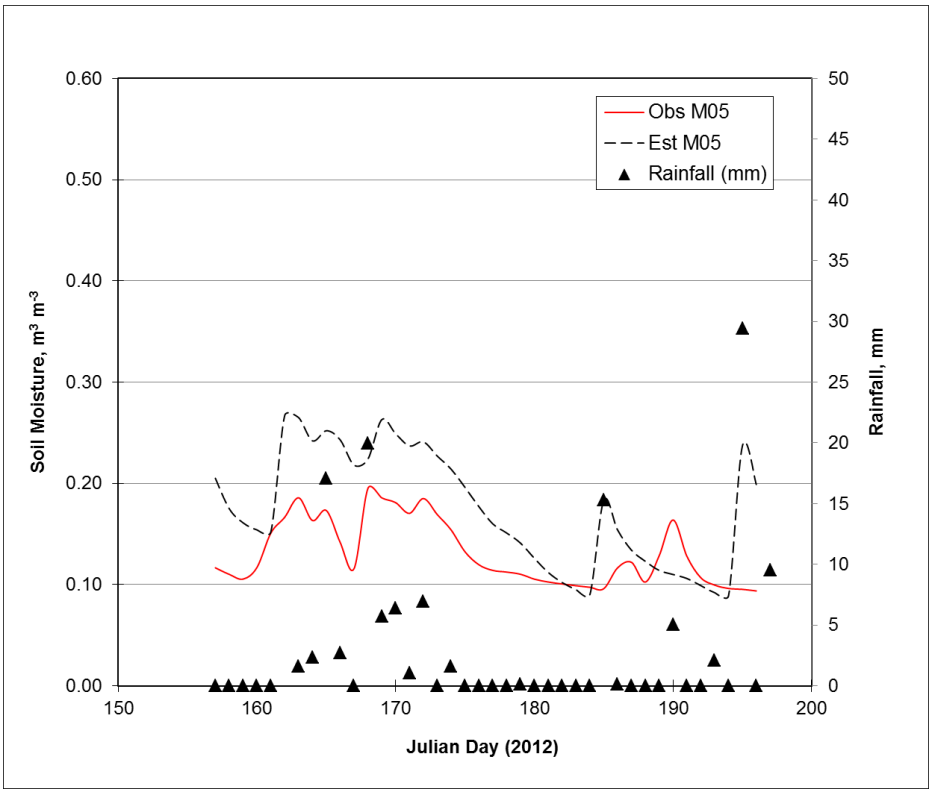

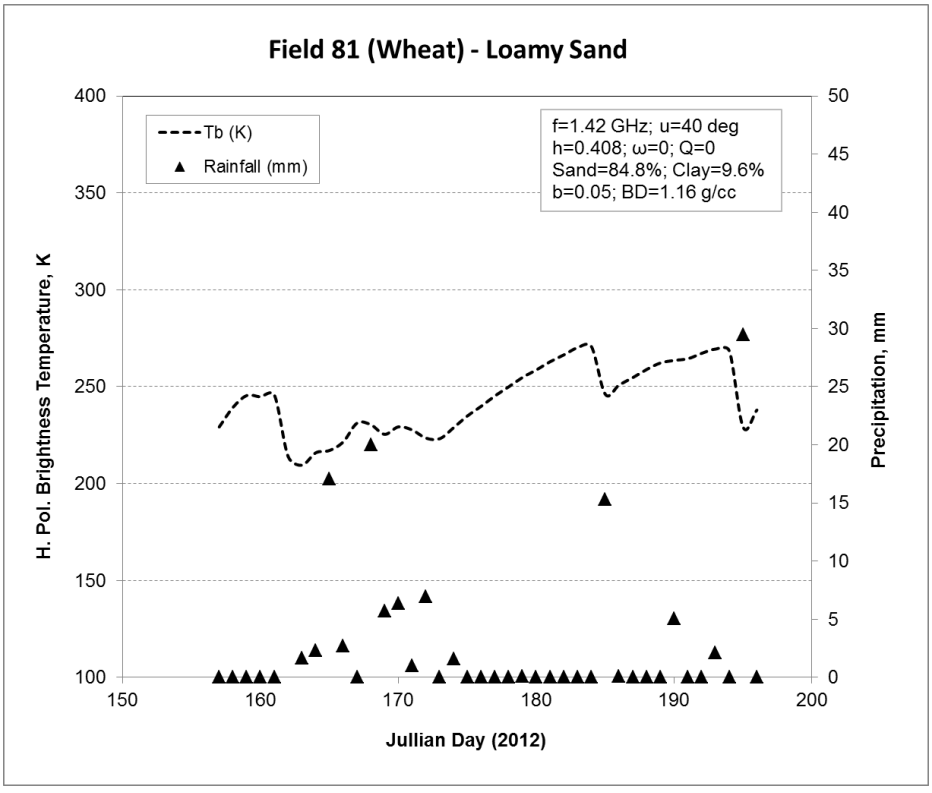

Field 82 (Soybean) – Sandy Loam (using CaPA precipitation, pixel 10_6) [RMSE=0.0403; R^2=0.6926]

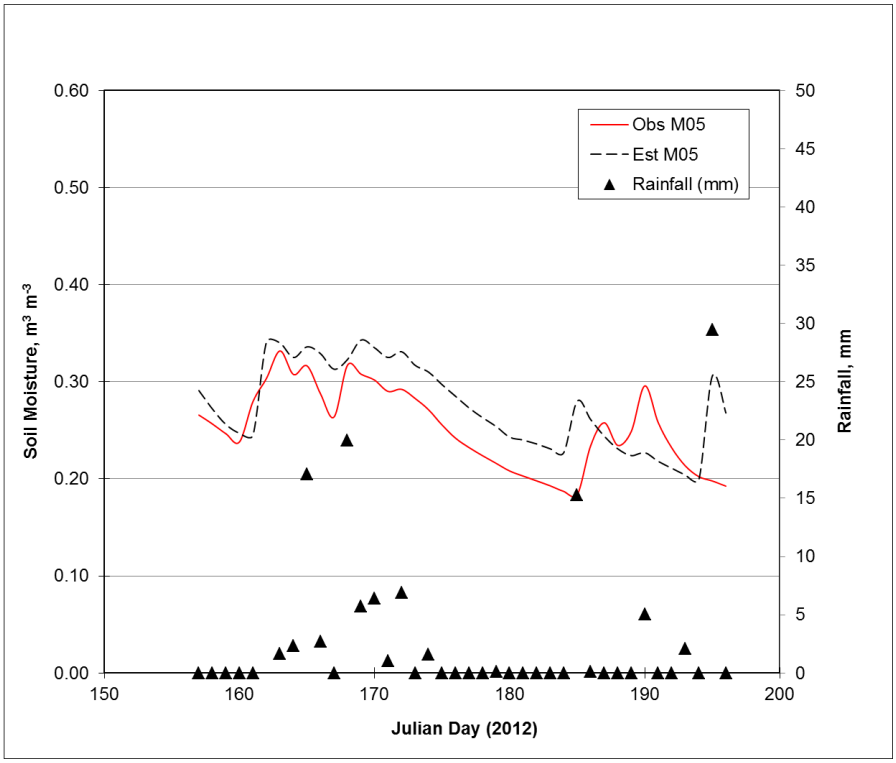

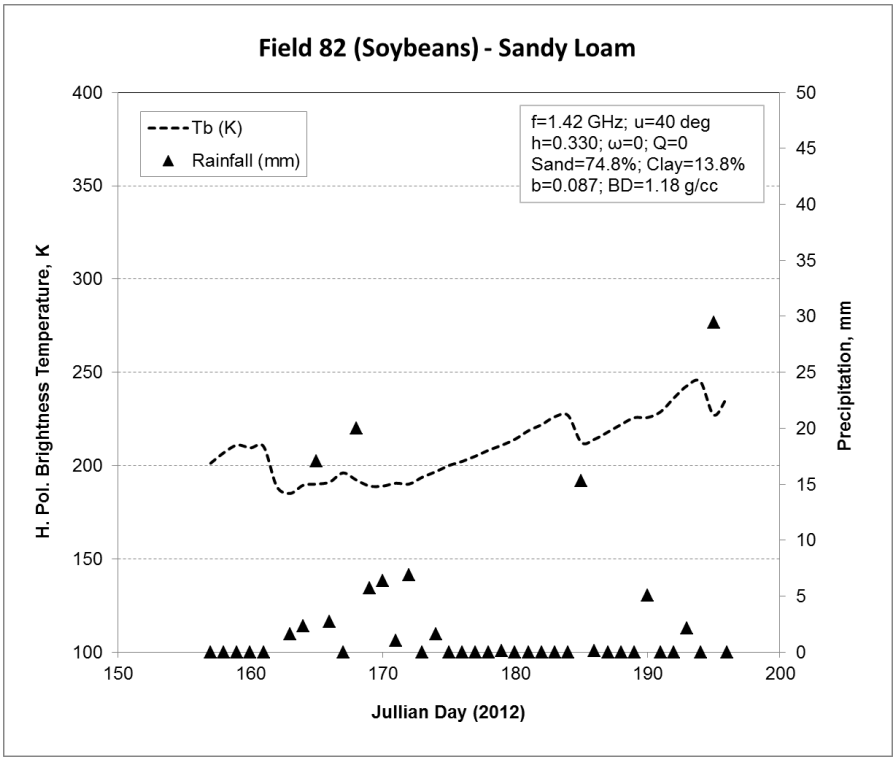

Field 84 (Canola) – Sandy Loam (using CaPA precipitation, pixel 11_6) [RMSE=0.0365; R^2=0.5863]

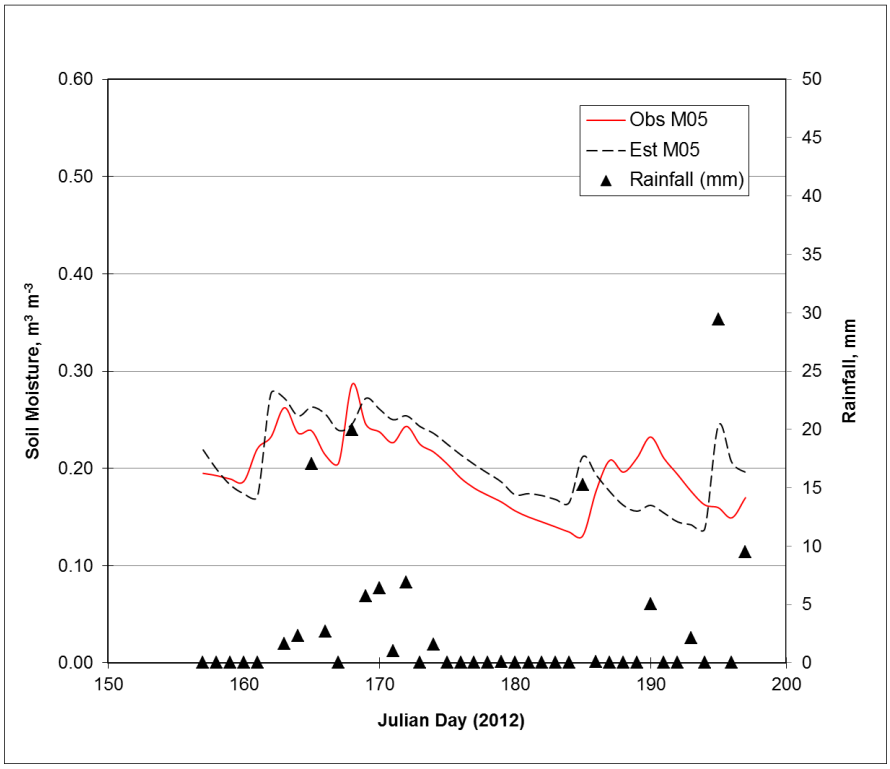

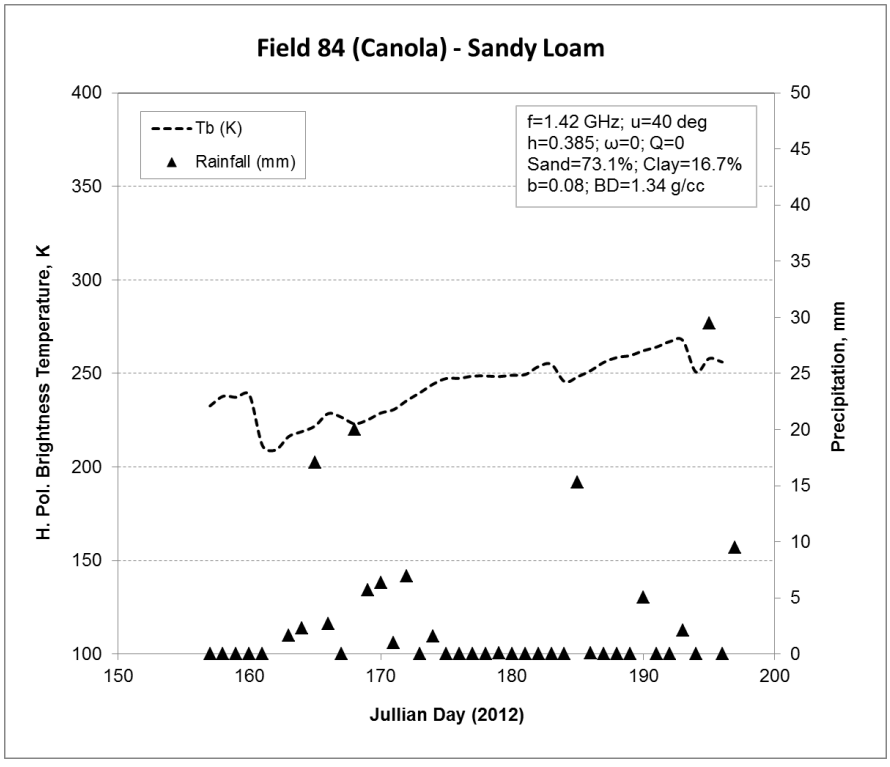

Field 85 (Wheat) – Clay (using CaPA precipitation, pixel 11_6) [RMSE=0.0362; R^2=0.7322]

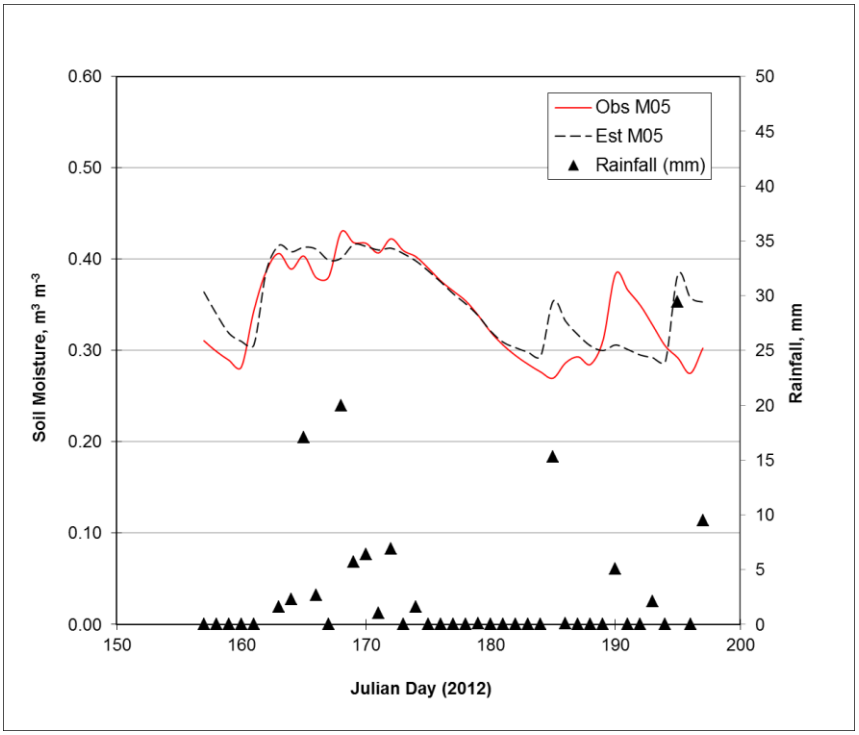

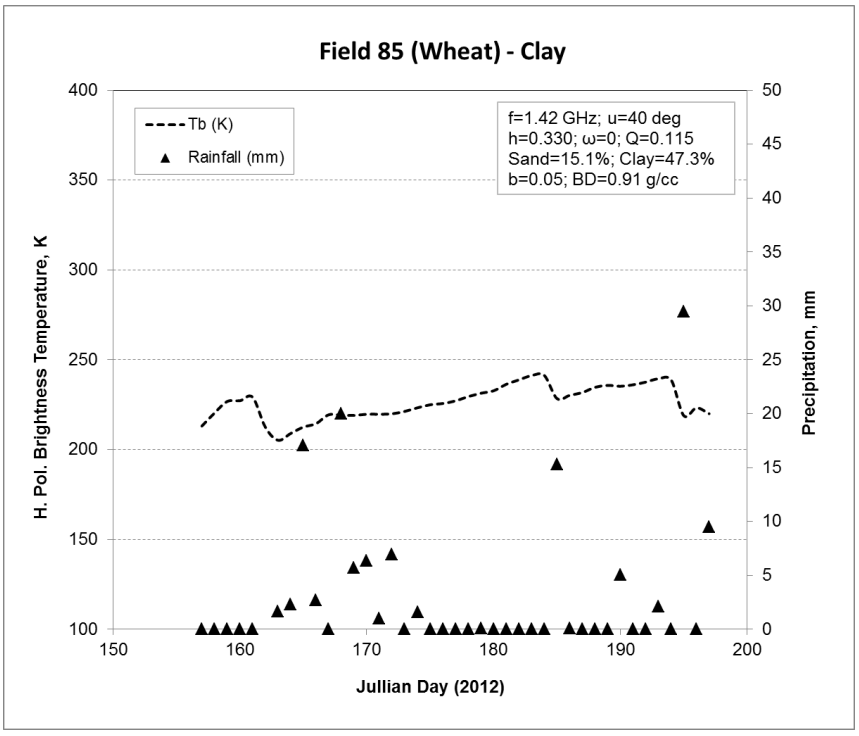

Field 91 (Wheat) – Loamy Sand (using CaPA precipitation, pixel 11_6) [RMSE=0.0627; R^2=0.6274]

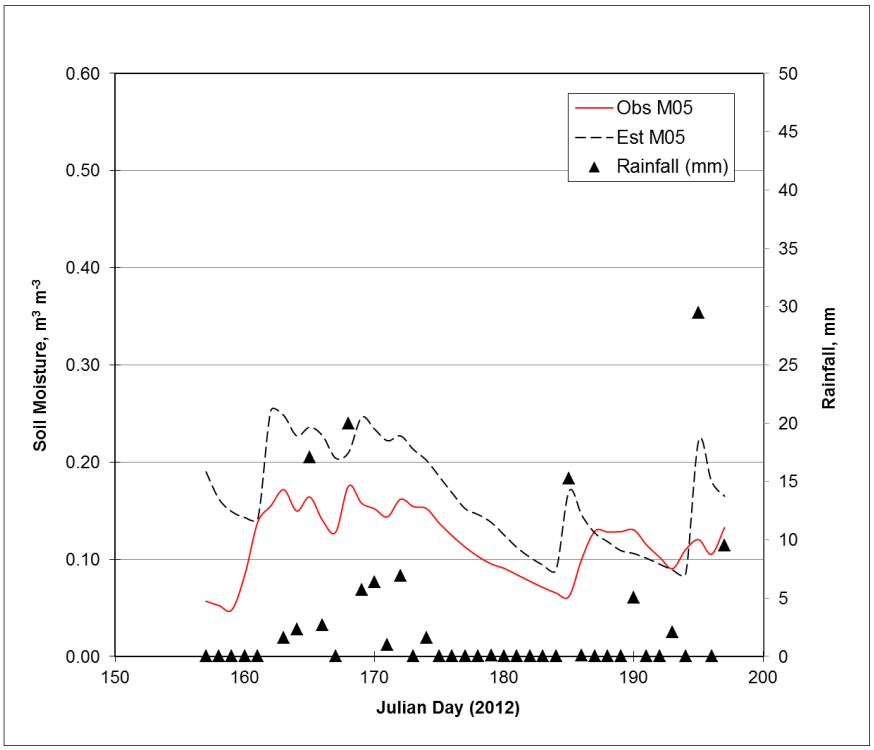

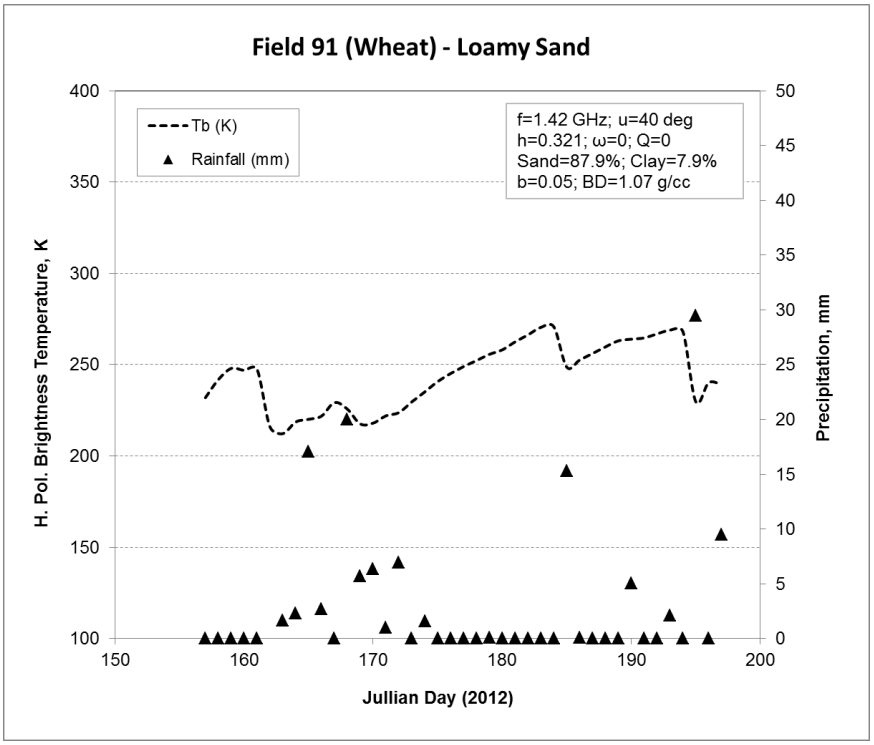

Field 94 (Corn) – Sandy Loam (using CaPA precipitation, pixel 11_6) [RMSE=0.0677; R^2=0.5254]

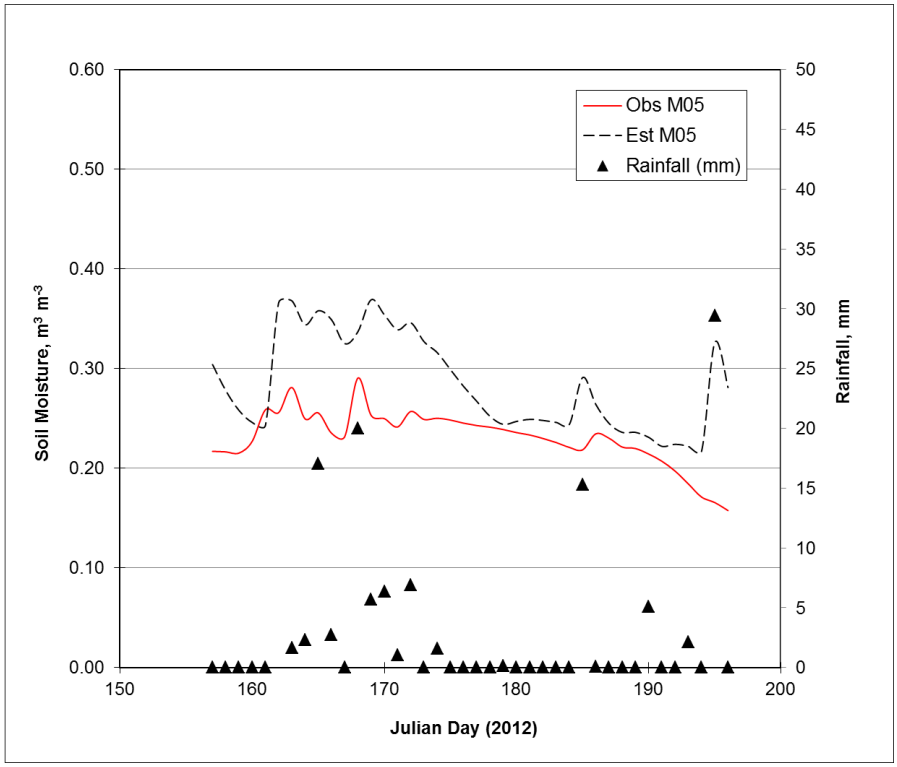

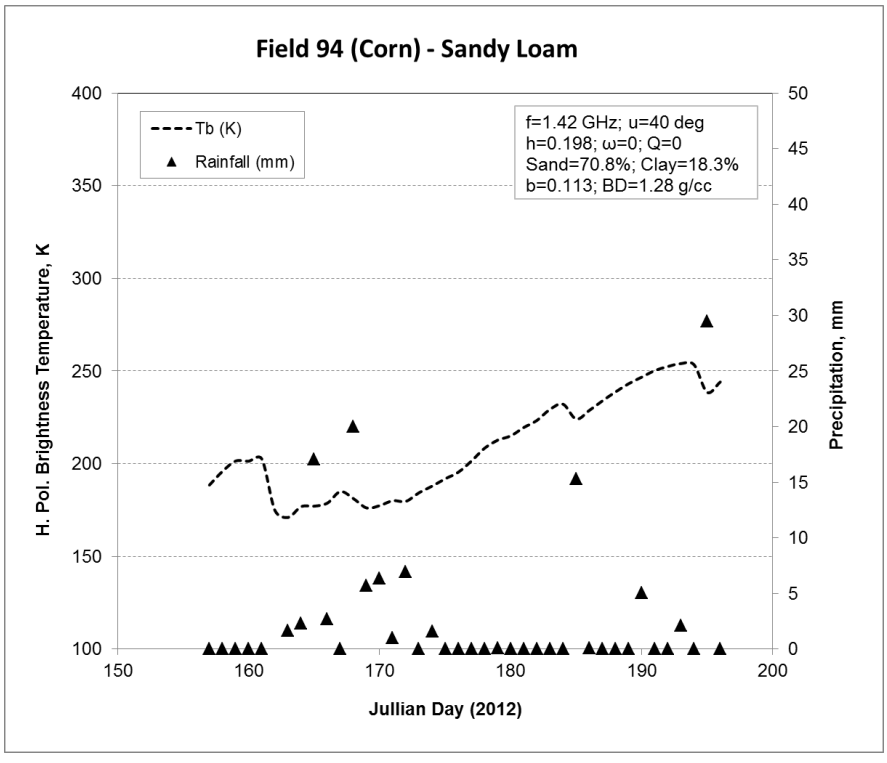

Field 104 (Wheat) – Heavy Clay (using CaPA precipitation, pixel 12_5) [RMSE=0.0695; R^2=0.8271]

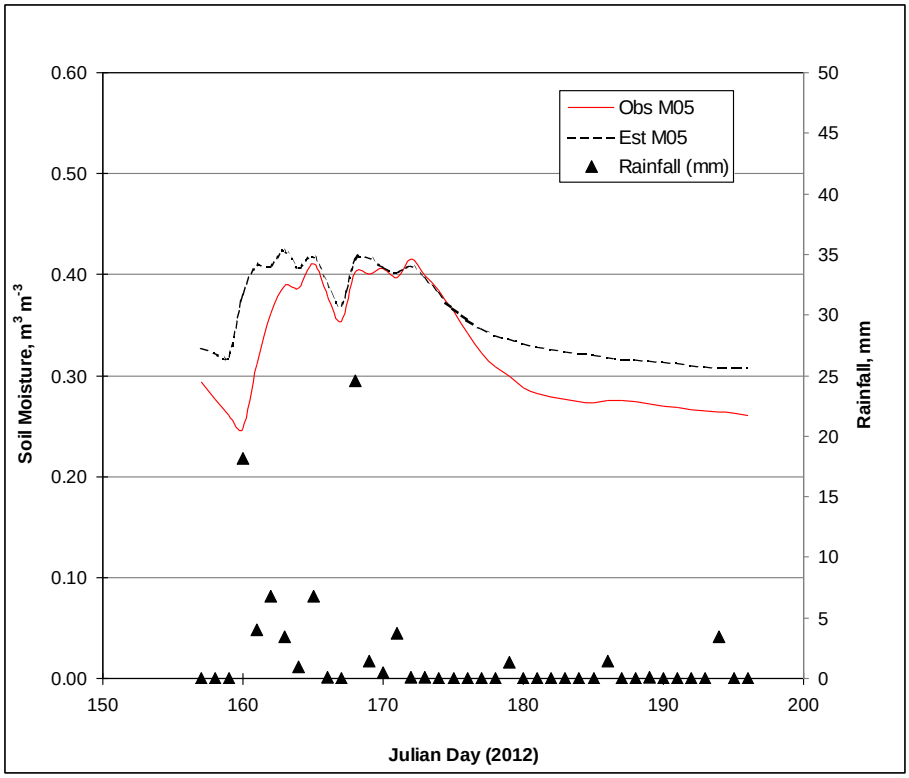

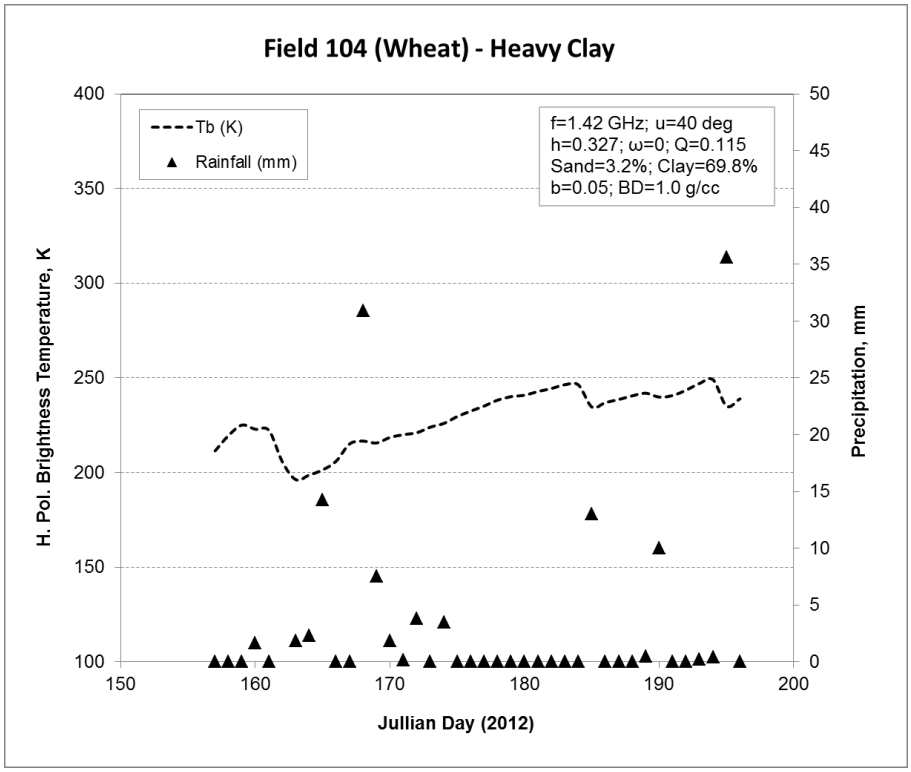

Field 112 (Soybean) – Heavy clay soil (using CaPA precipitation, pixel 12_6) [RMSE=0.0325; R^2=0.5456]

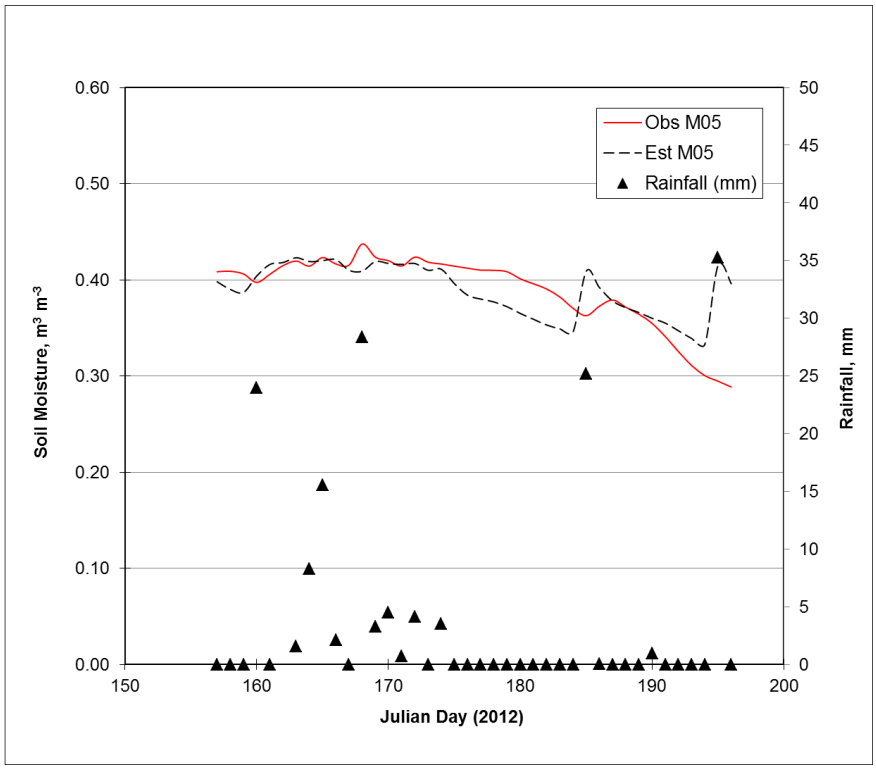

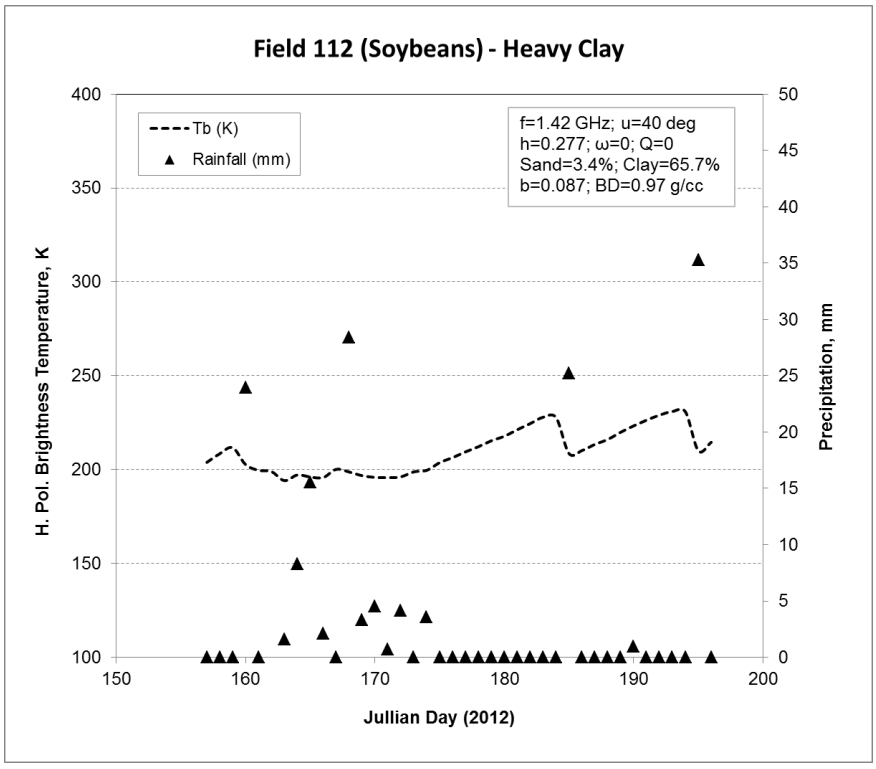

Field 113 (Soybean) – Heavy clay soil (using CaPA precipitation, pixel 12_6) [RMSE=0.0775; R^2=0.6703]

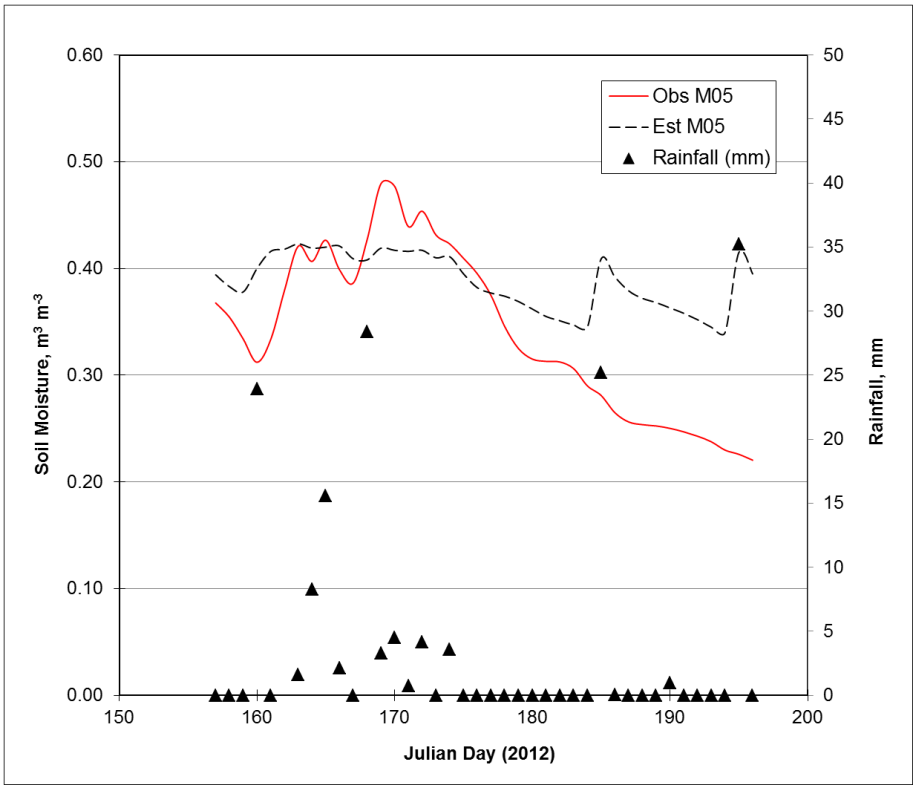

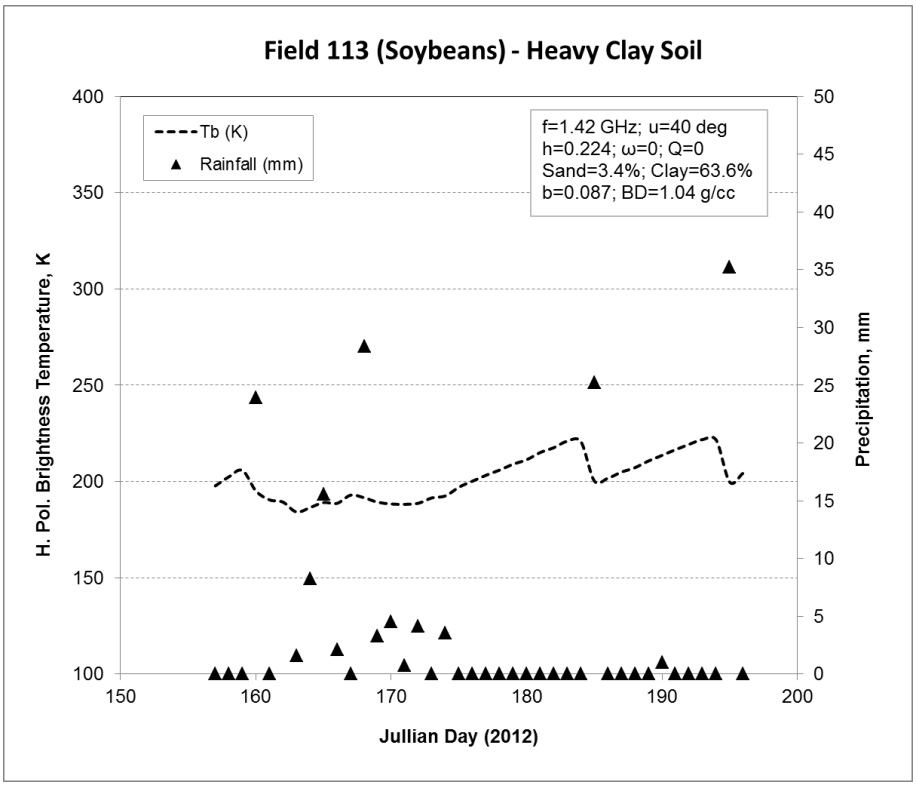

Field 114 (Soybean) –Clay soil (using CaPA precipitation, pixel 11_5) [RMSE=0.0603; R^2=0.8642]

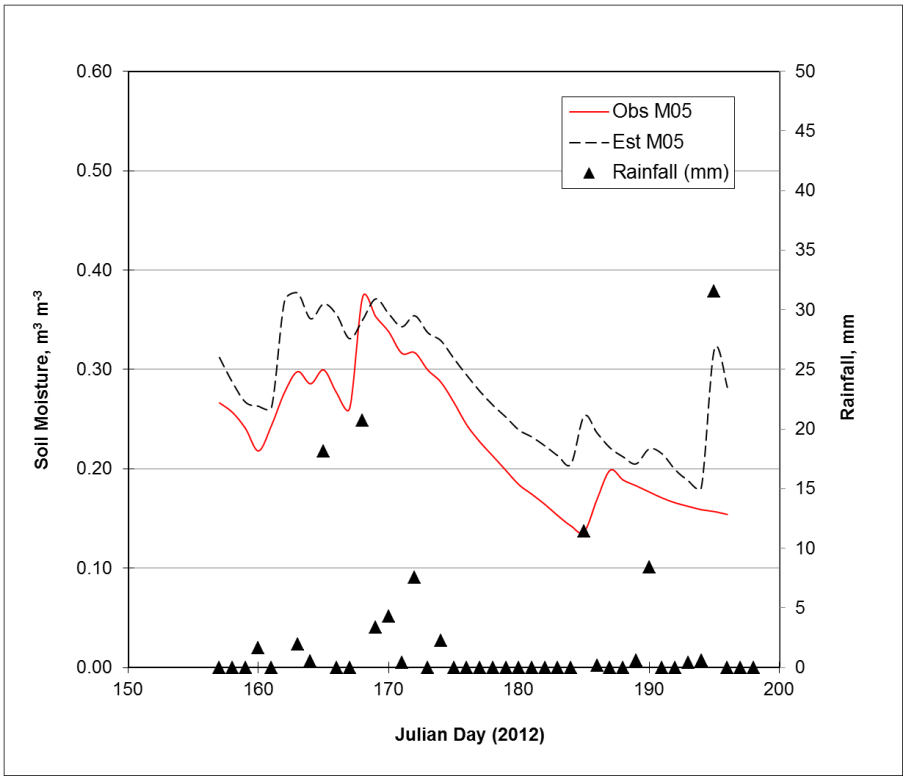

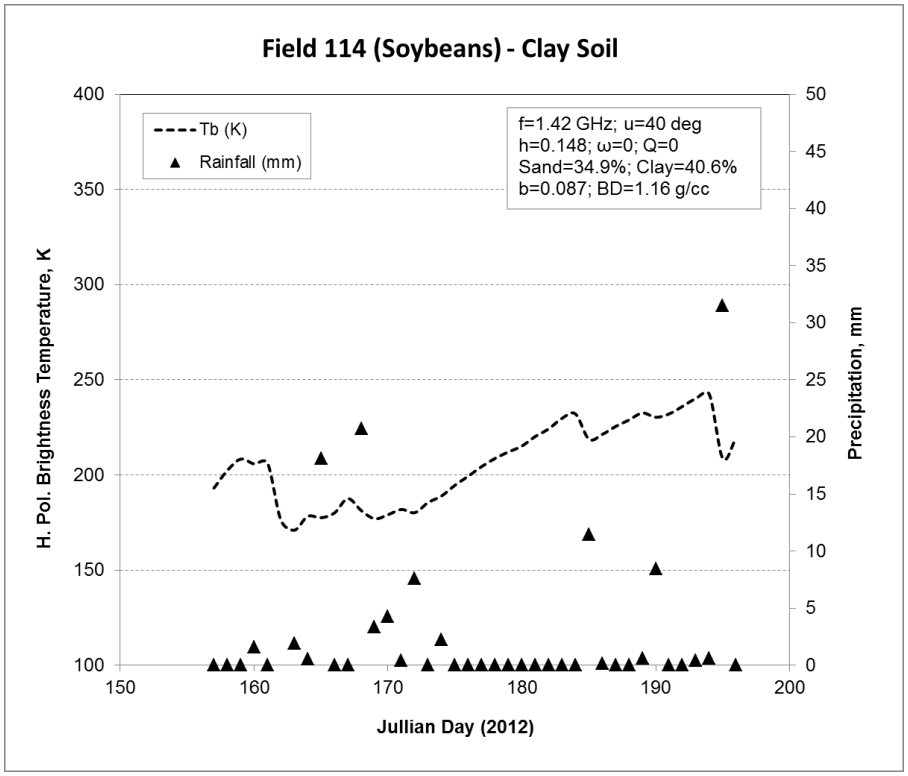

Field 123 (Soybean) – Heavy Clay soil (using CaPA precipitation, pixel 12_7) [RMSE=0.0510; R^2=0.6842]

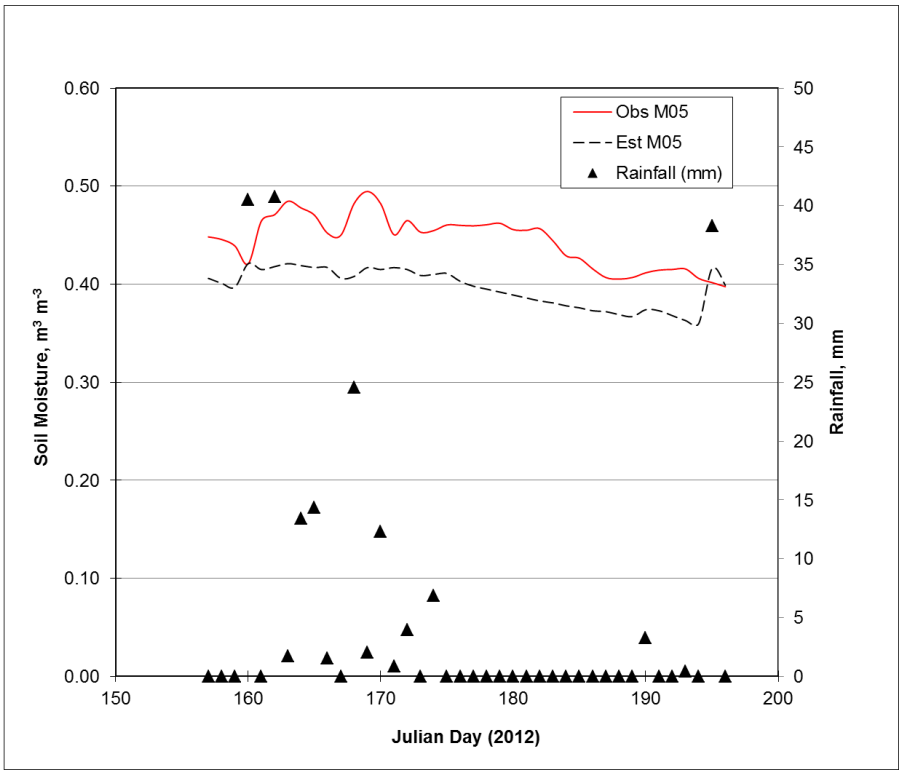

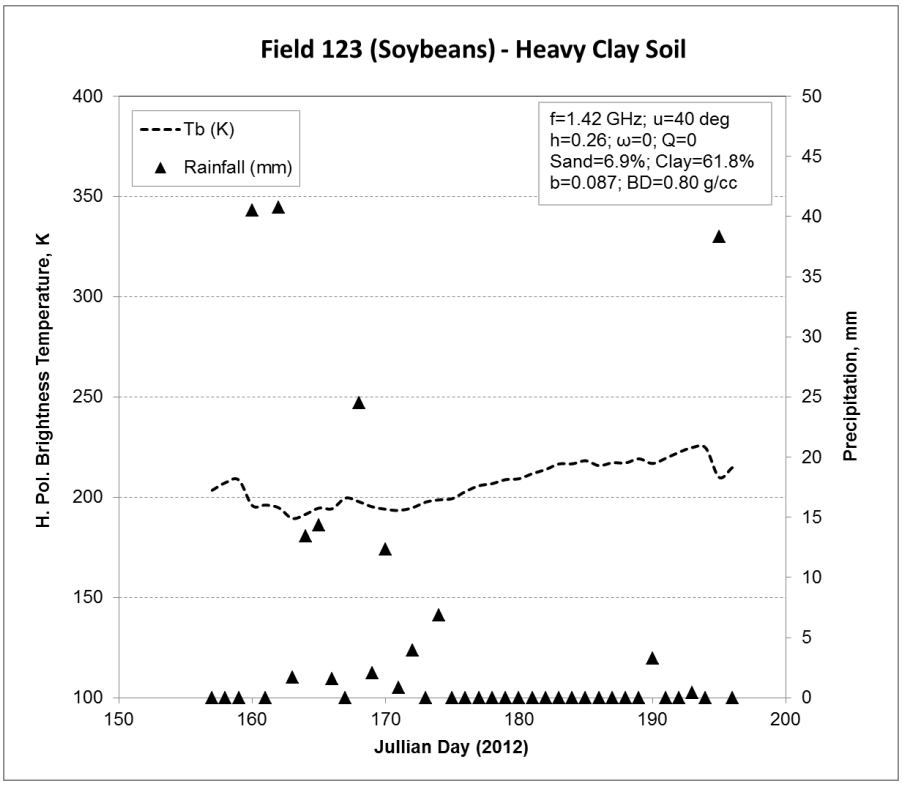

Field 124 (Canola) – Clay Loam (using CaPA precipitation, pixel 12_6) [RMSE=0.0638; R^2=0.7821]

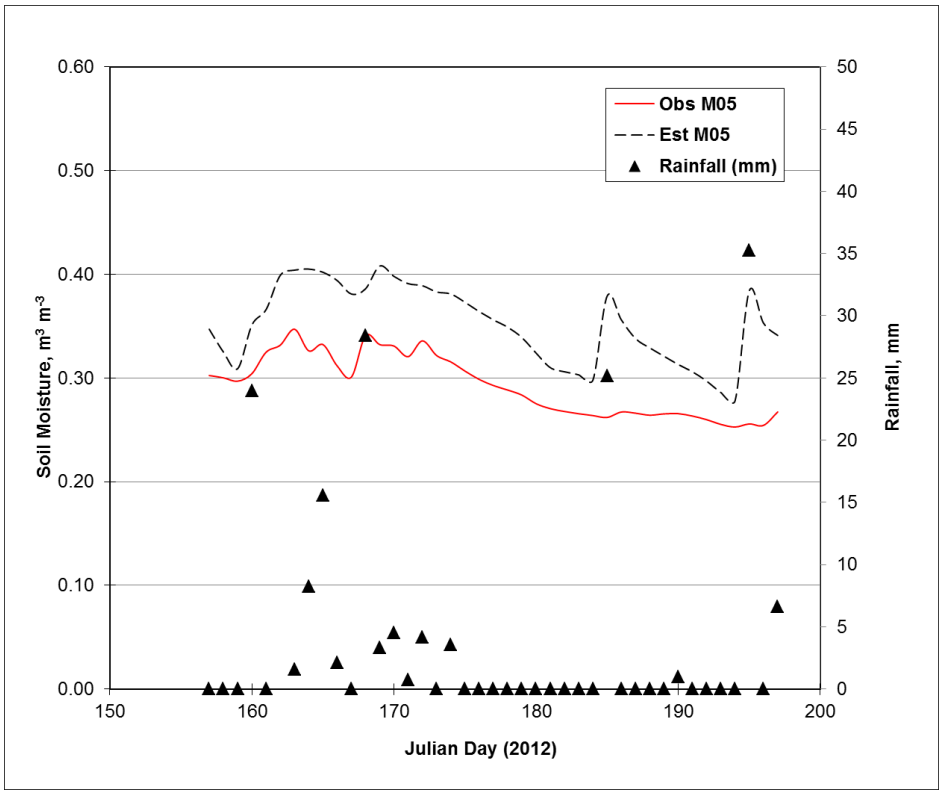

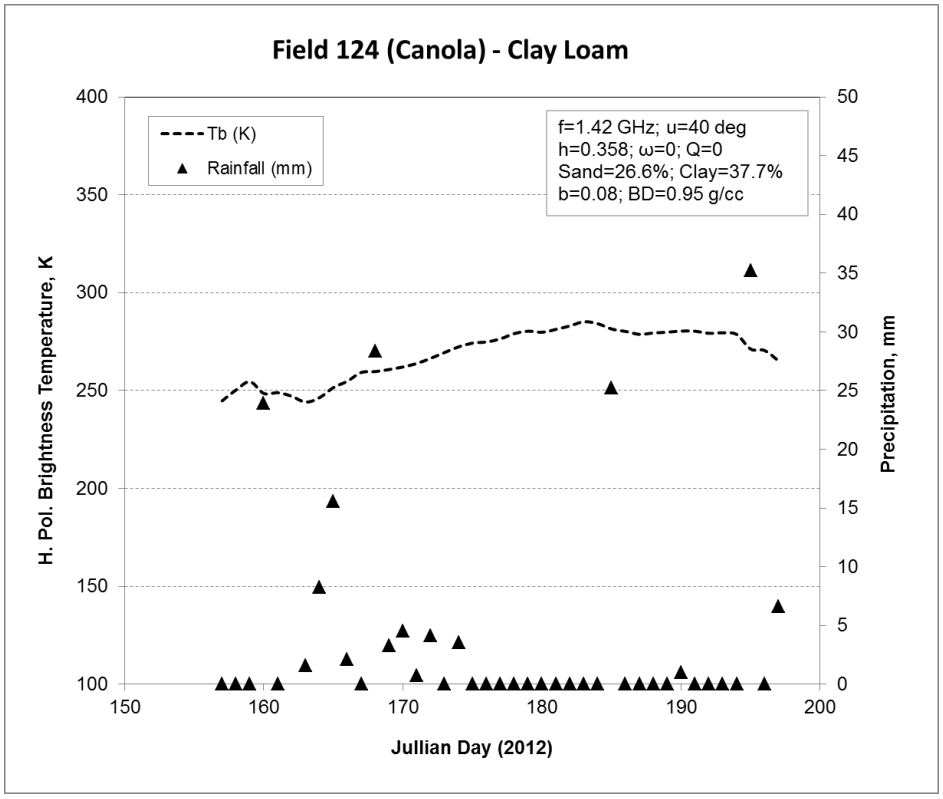

Field 125 (Canola) – Clay Loam (using CaPA precipitation, pixel 12_6) [RMSE=0.0632; R^2=0.6821]

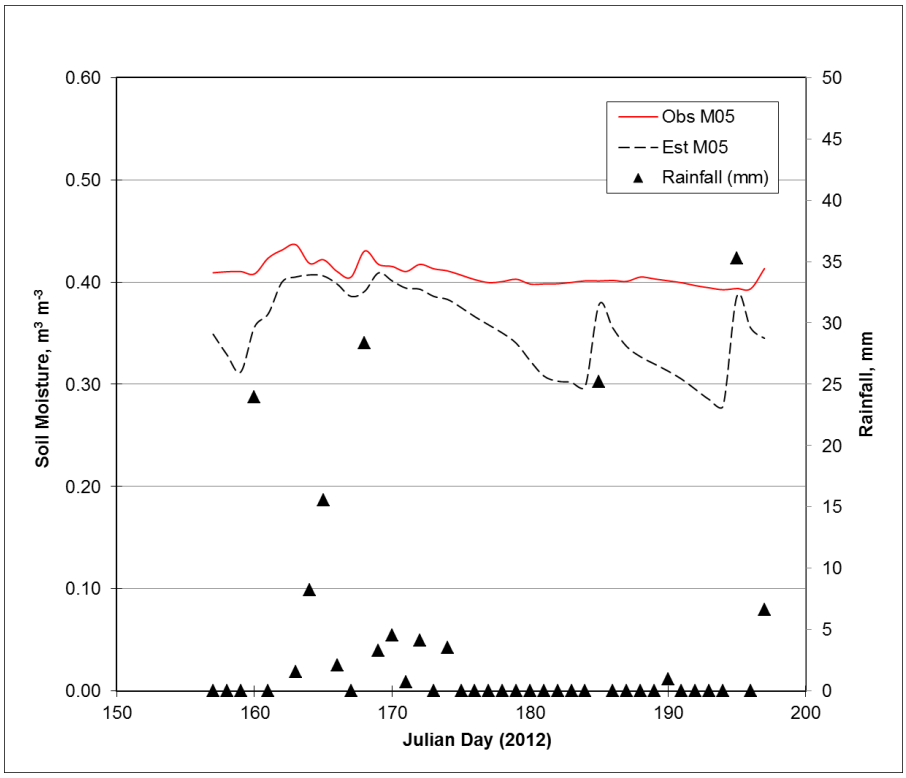

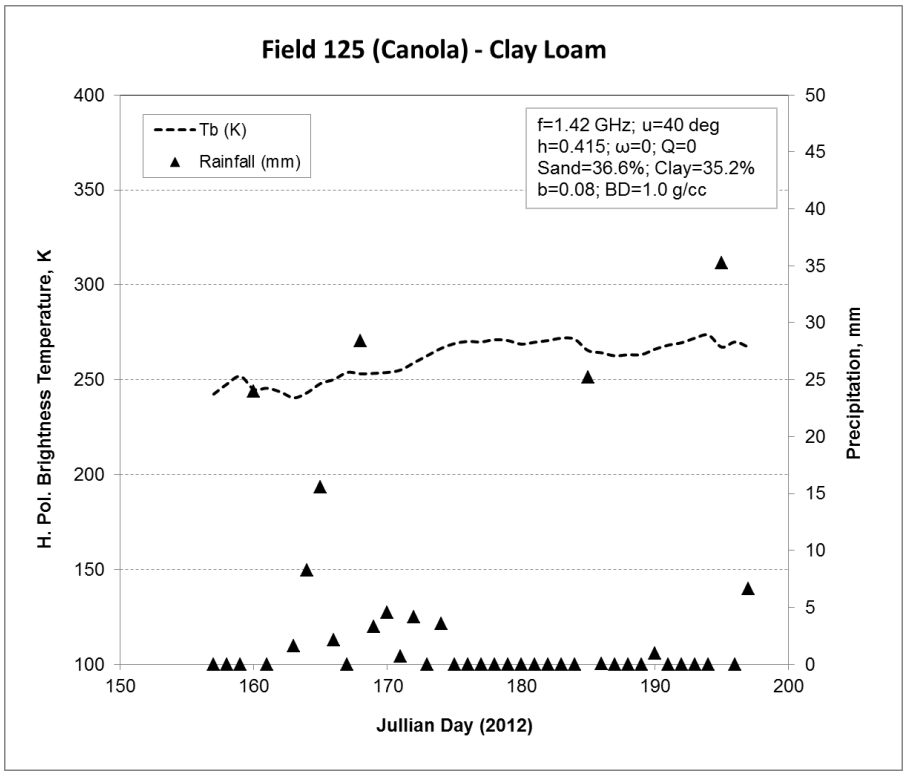

A.5a Locations of 6 SAGES sites with field ID number (solid square = *in-situ* permanent network station; dotted rectangle = CaPA forecasted precipitation pixels, 7 km x 11 km; contours = areas of different soil type).

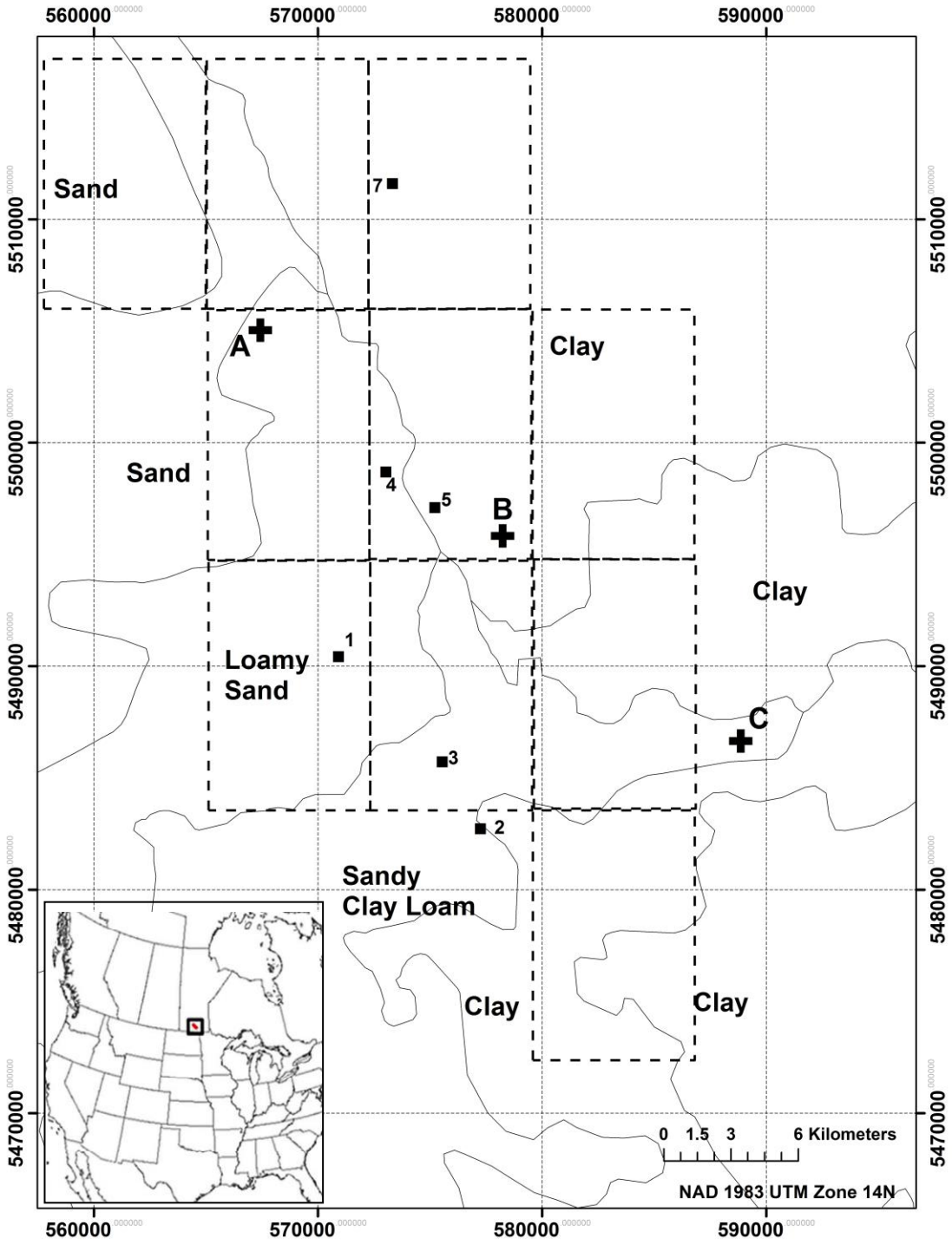

A.5b Locations of probes placement at different soil depths in permanent network station (SAGES site 4) (Walker, 2012)

A.5c Soil characteristics and crops of permanent network field sites

Table 3.2: Soil characteristics and crops of permanent network field sites

SAGES Field #	Field	X	Y	Soil Depth	Soil	Soil Texture		Bulk Density	Crop
						Sand	Clay		
		(m)	(m)	(m)		%	%	(kg m^{-3})	
SAGES-1	73	570923.80	5490433.80	0.05	Loamy fine sand	78.0	11.0	1.28	Wheat
				0.20	Loamy fine sand	80.0	11.0	1.56	
				0.50	Loamy fine sand	81.0	10.0	1.53	
				1.00	Loamy fine sand	81.0	12.0	1.57	
SAGES-2	92	577216.50	5482753.40	0.05	Sandy Clay loam	44.0	34.0	1.35	Soybean
				0.20	Loam	62.0	24.0	1.63	
				0.50	Loam	66.0	21.0	1.63	
				1.00	Loamy fine sand	75.0	10.0	1.57	
SAGES-3	93	575527.00	5485733.70	0.05	Sandy clay loam	47.0	31.0	1.46	Corn
				0.20	Clay loam	45.0	33.0	1.51	
				0.50	Clay	31.0	45.0	1.44	
				1.00	Sandy loam	70.0	12.0	1.41	
SAGES-4	24	575274.80	5497064.60	0.05	Sand	90.0	9.0	1.33	Corn
				0.20	Loamy sand	89.0	10.0	1.50	
				0.50	Loamy sand	89.0	10.0	1.59	
				1.00	Loamy sand	86.0	9.0	1.58	
SAGES-5	65	573063.10	5498662.90	0.05	Clay loam	41.0	40.0	1.46	Winter wheat
				0.20	Clay	22.0	57.0	1.41	
				0.50	Clay	4.0	68.0	1.33	
				1.00	Clay	3.0	69.0	1.32	
SAGES-7	32	573303.90	5511613.90	0.05	Sandy loam	78.0	13.0	1.40	Winter wheat
				0.20	Loamy sand	82.0	12.0	1.59	
				0.50	Sandy loam	78.0	13.0	1.57	
				1.00	Sandy loam	80.0	12.0	1.58	

Note: X and Y followed Universal Transverse Mercator coordinate system (UTM Zone 14); soil texture and bulk density recorded at probe's location

A.5d Some SHAW input files for SAGES-1 site

File: Trial.sit

```
SITE WITH CORN DURING 2012          ****** (SAGES-1)                    LINE A
 123  00  112  273  112              ****** SIMULATION PERIOD            LINE B
 49 33.72  0.01  90.0  12.5  268      ****** LOCATION                     LINE C
 1  0  0  15  0  0.01   1  0   0   0   1   0   0    ***** NODES          LINE D
 0.4  2.0  0.00                ****** WEATHER CHARACTERISTICS            LINE E
 1   -53.72  1.32   0.2          ***** PLANT GROWTH / CANOPY             LINE F
 1   1   0.23  7.0  100.  5.0  -100.   2.0E05   3.0E05  **** WHEAT       LINE F1-1
 wheat.112
 1.0  .15                            ****** SNOW                         LINE G
 1  1  0.15 0.0                        ****** SOIL                       LINE J
 0.00  5.   -0.2    4.    1280.  0.437  78.0  11.  11.  3.               LINE J-1
 0.05  5.   -0.2    4.    1280.  0.437  78.0  11.  11.  3.               LINE J-2
 0.10  6.   -0.3    3.    1560.  0.437  80.0   9.  11.  3.               LINE J-3
 0.20  6.   -0.3    3.    1560.  0.437  80.0   9.  11.  3.               LINE J-4
 0.30  6.   -0.3    3.    1560.  0.437  80.0   9.  11.  3.               LINE J-5
 0.40  8.   -0.4    2.    1530.  0.437  81.0   9.  10.  0.5              LINE J-6
 0.50  8.   -0.4    2.    1530.  0.437  81.0   9.  10.  0.5              LINE J-7
 0.60  8.   -0.4    2.    1530.  0.437  81.0   9.  10.  0.5              LINE J-8
 0.70  8.   -0.4    2.    1530.  0.437  81.0   9.  10.  0.5              LINE J-9
 0.80 11.   -0.6    1.    1570.  0.437  81.0   7.  12.  0.17             LINE J-10
 0.90 11.   -0.6    1.    1570.  0.437  81.0   7.  12.  0.17             LINE J-11
 1.00 11.   -0.6    1.    1570.  0.437  81.0   7.  12.  0.17             LINE J-12
 1.10 11.   -0.6    1.    1570.  0.437  81.0   7.  12.  0.17             LINE J-13
 1.20 11.   -0.6    1.    1570.  0.437  81.0   7.  12.  0.17             LINE J-14
 1.30 11.   -0.6    1.    1570.  0.437  81.0   7.  12.  0.17             LINE J-15
```

File: wheat.112

90	112	0	0	0	0	0	APR 01
139	112	0	0	0	0	0	MAY 18
165	112	0.38	1	0.12	1.75	0.2	JUN 13
182	112	0.78	1.5	0.19	1.0	0.6	JUN 30
191	112	0.85	1.8	0.20	1.63	0.8	JUL 09
200	112	0.84	2.2	0.24	1.7	1.2	JUL 18
272	112	0	0	0	0	0.4	SEP 28
275	112	0	0	0	0	0.3	OCT 01

A.6a Observed and simulated root zone soil moisture of individual permanent network sites

Field SAGES-1 [Field 73] (Wheat) – (using CaPA precipitation, pixel 10_6)

At 0.05 m soil depth (Loamy Fine Sand; sand=78%, clay=11%; BD=1.28 kg/cu.m) [RMSE=0.0332; R^2=0.6232]

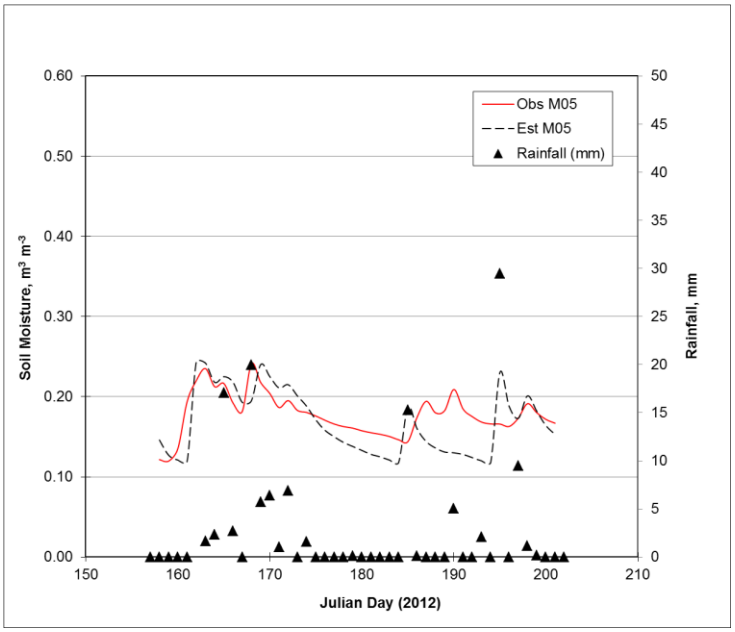

At 0.20 m soil depth (Loamy Fine Sand; sand=80%, clay=11%; BD=1.56 kg/cu.m) [RMSE=0.0290; R^2=-0.4720]

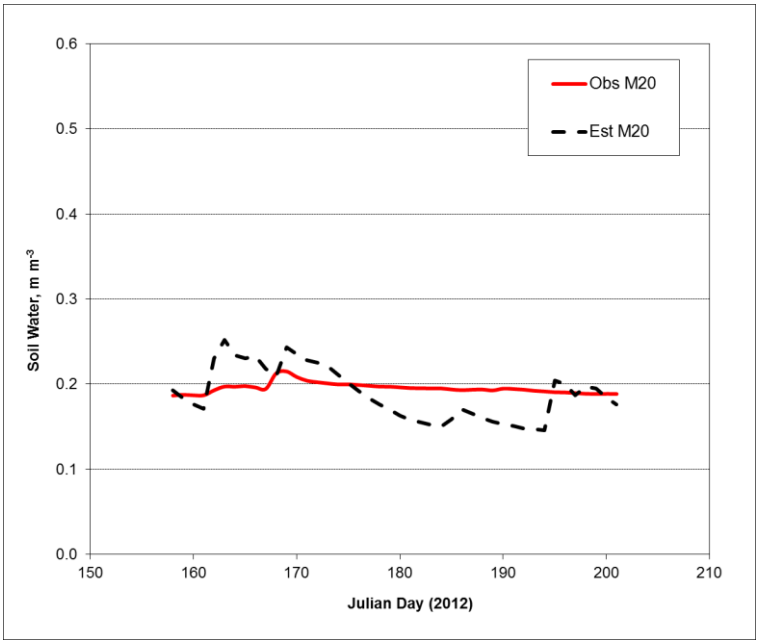

At 0.50 m soil (Loamy Fine Sand; sand=81%, clay=10%; BD=1.53 kg/cu.m) [RMSE=0.0202; R^2=0.6898]

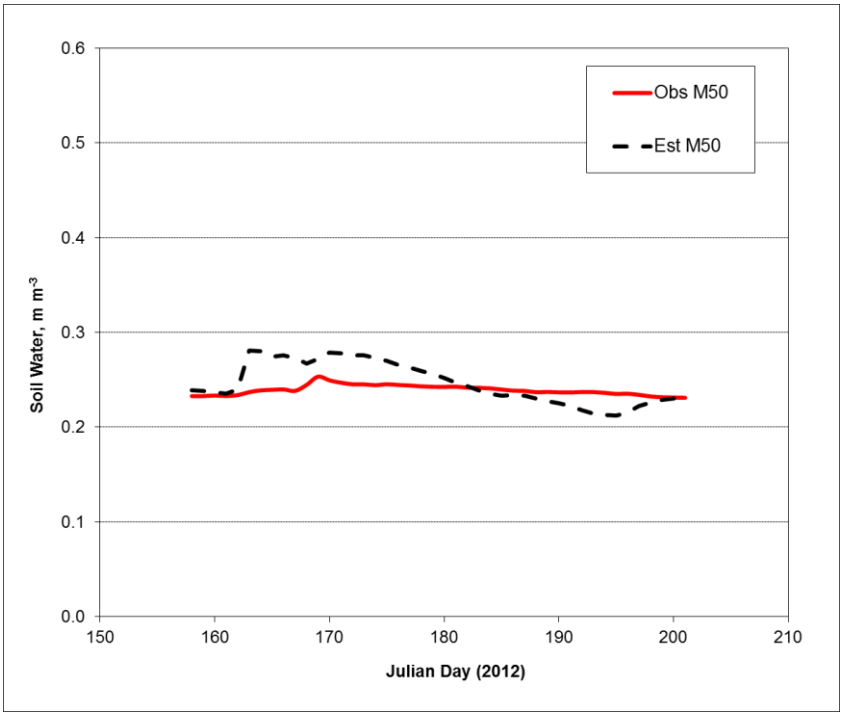

At 1.00 m soil depth (Loamy Fine Sand; sand=81%, clay=12%; BD=1.57 kg/cu.m) [RMSE=0.0209; R^2=0.7502]

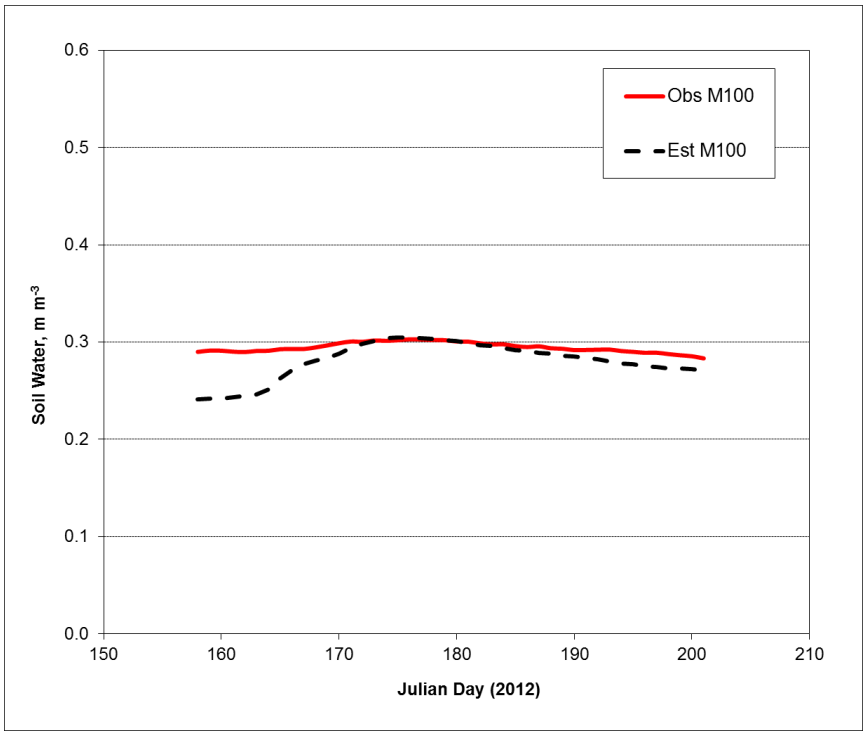

Field SAGES-2 [Field 92] (Soybean) – (using CaPA precipitation, pixel 11_6)

At 0.05 m soil depth (Sandy clay loam; sand=44%, clay=34%; BD=1.35 kg/cu.m) [RMSE=0.0277; R^2=0.5613]

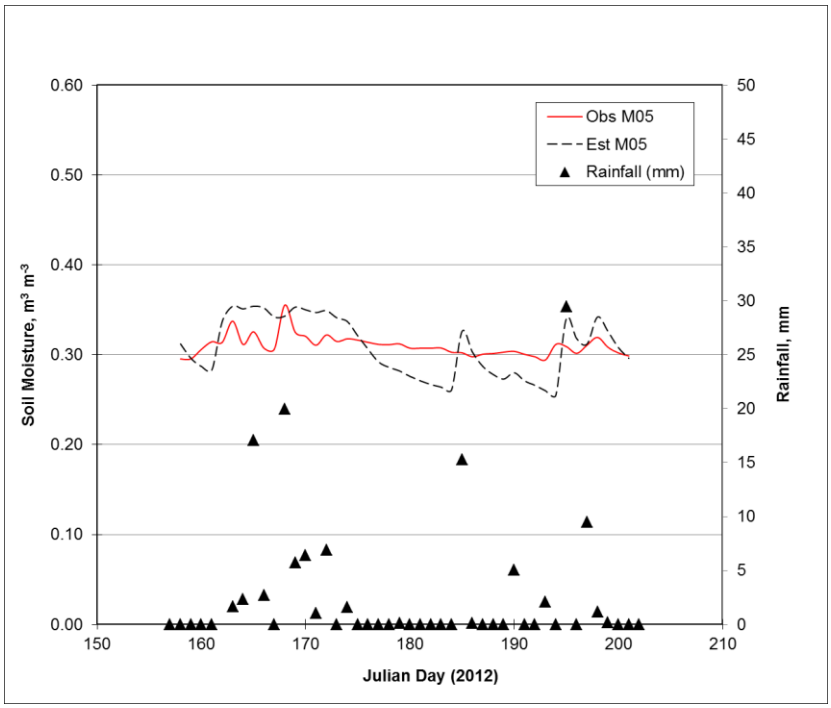

At 0.20 m soil depth (Loam; sand=62%, clay=24%; BD=1.63 kg/cu.m) [RMSE=0.0708; R^2= -0.7675]

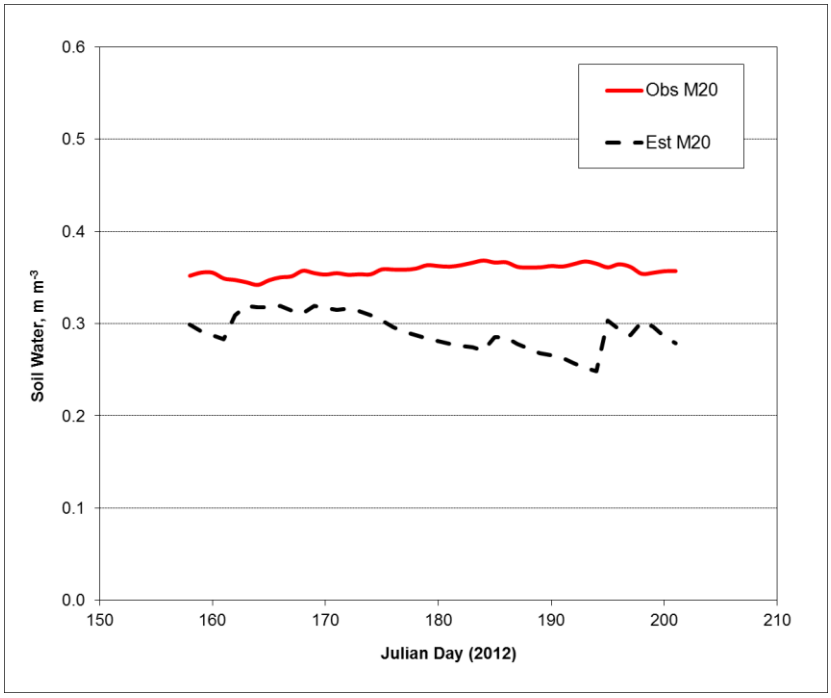

At 0.50 m soil depth (Loam; sand=66%, clay=21%; BD=1.63 kg/cu.m) [RMSE=0.0308; R^2=0.6308]

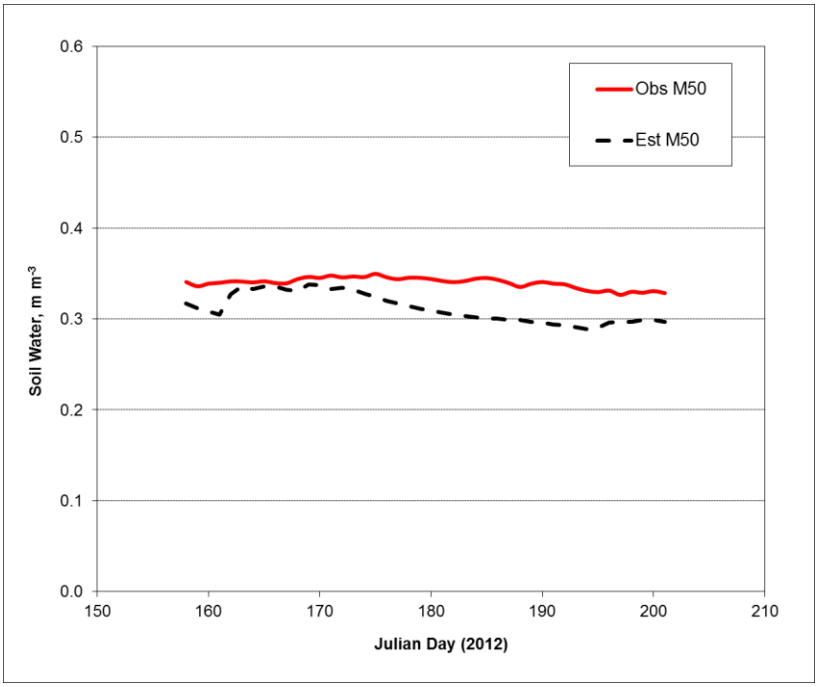

At 1.00 m soil depth (Loamy Fine Sand; sand=75%, clay=10%; BD=1.57 kg/cu.m) [RMSE=0.0123; R^2=0.3457]

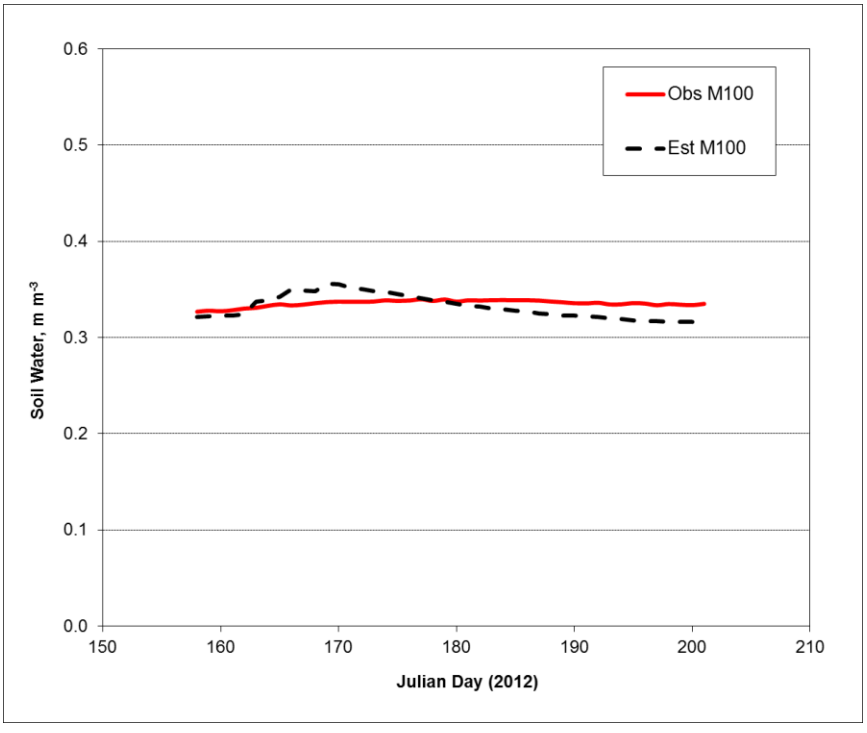

Field SAGES-3 [Field 93] (Corn) – (using CaPA precipitation, pixel 11_6)

At 0.05 m soil depth (Sandy clay loam; sand=47%, clay=31%; BD=1.46 kg/cu.m) [RMSE=0.0654; R^2=0.5768] [missing data in observation soil moisture]

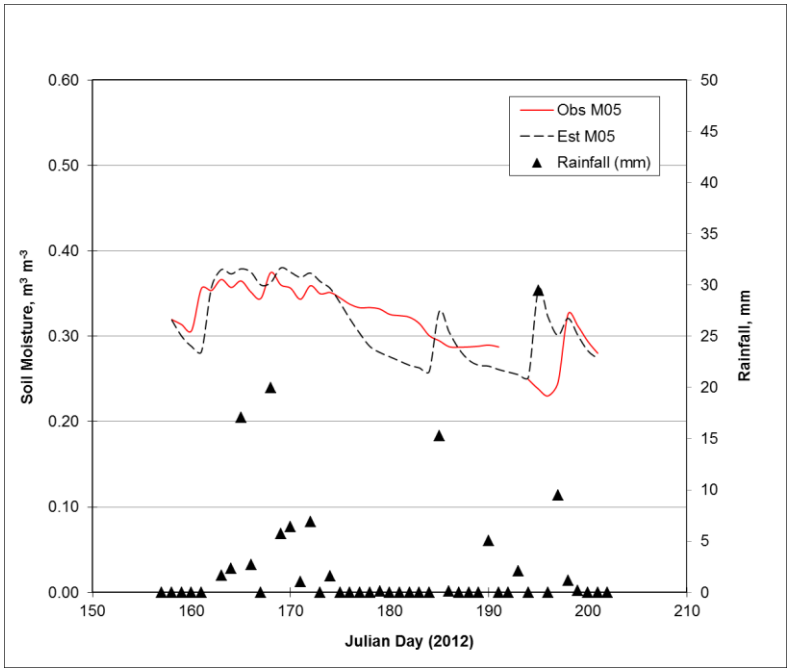

At 0.20 m soil depth (Clay loam; sand=45%, clay=33%; BD=1.51 kg/cu.m) [RMSE=0.0641; R^2=0.0744]

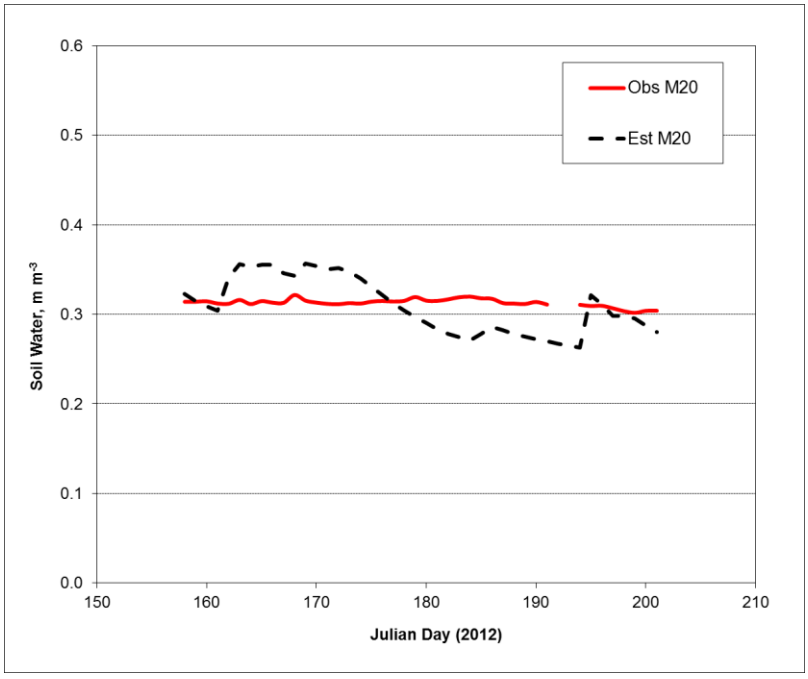

At 0.50 m soil depth (Clay; sand=31%, clay=45%; BD=1.44 kg/cu.m) [RMSE=0.0750; R^2=0.3382]

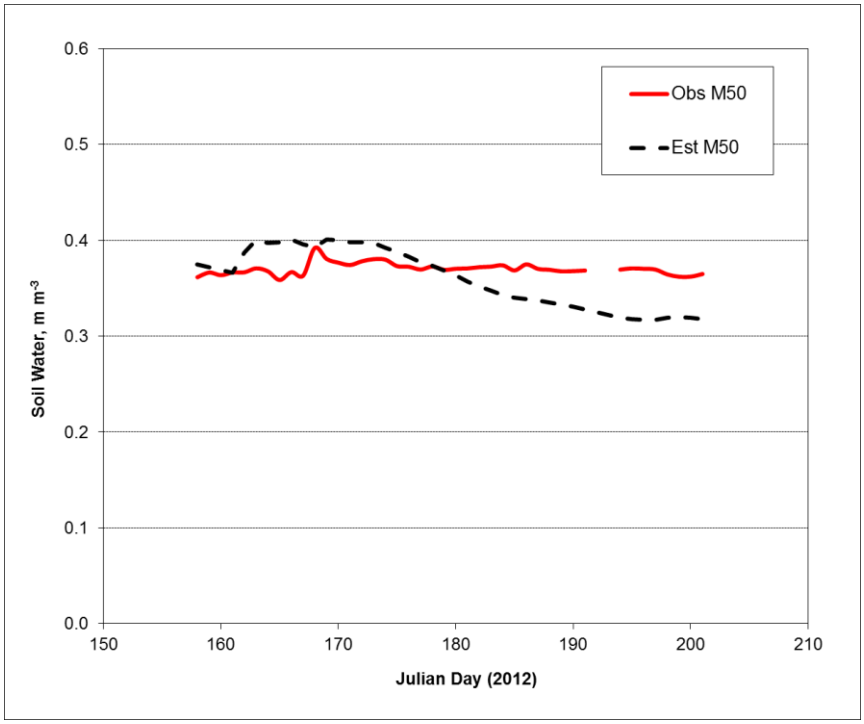

At 1.00 m soil depth (Sandy Loam; sand=70%, clay=12%; BD=1.41 kg/cu.m) [RMSE=0.0673; R^2=0.2314]

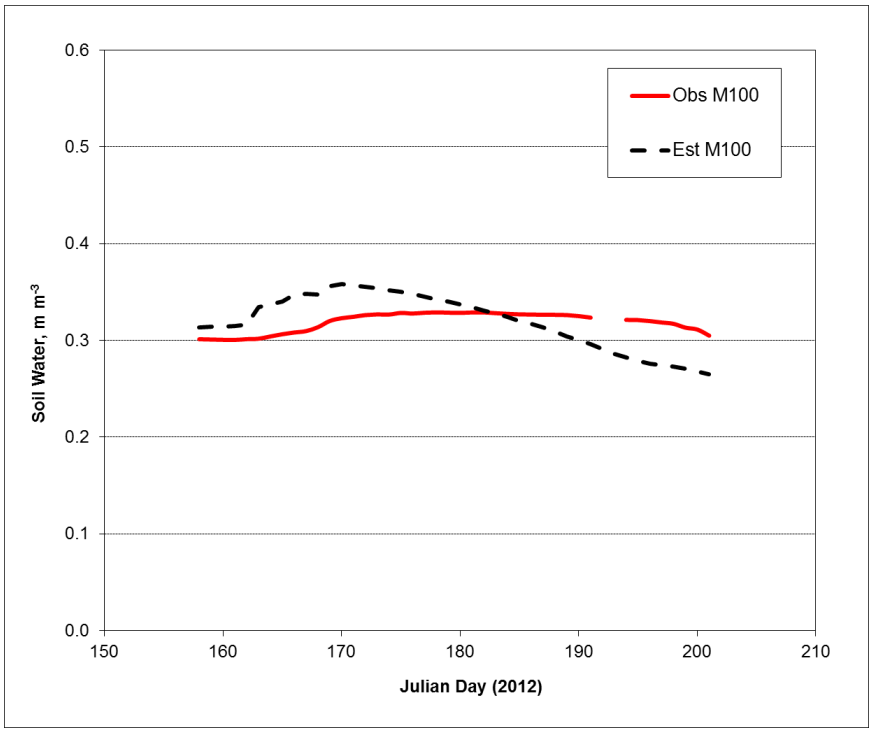

Field SAGES-4 [Field 24] (Corn) – (using CaPA precipitation, pixel 11_5)

At 0.05 m soil depth (Sand; sand=90%, clay=9%; BD=1.33 kg/cu.m) [RMSE=0.0549; R^2=0.6737]

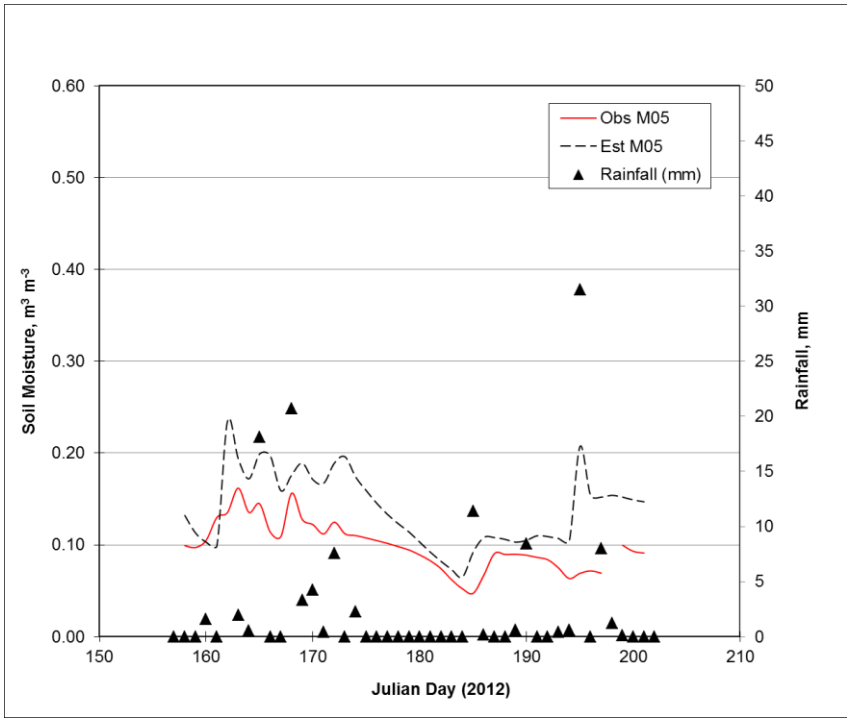

At 0.20 m soil depth (Loamy Sand; sand=89%, clay=10%; BD=1.50 kg/cu.m) [RMSE=0.0554; R^2=-0.5510]

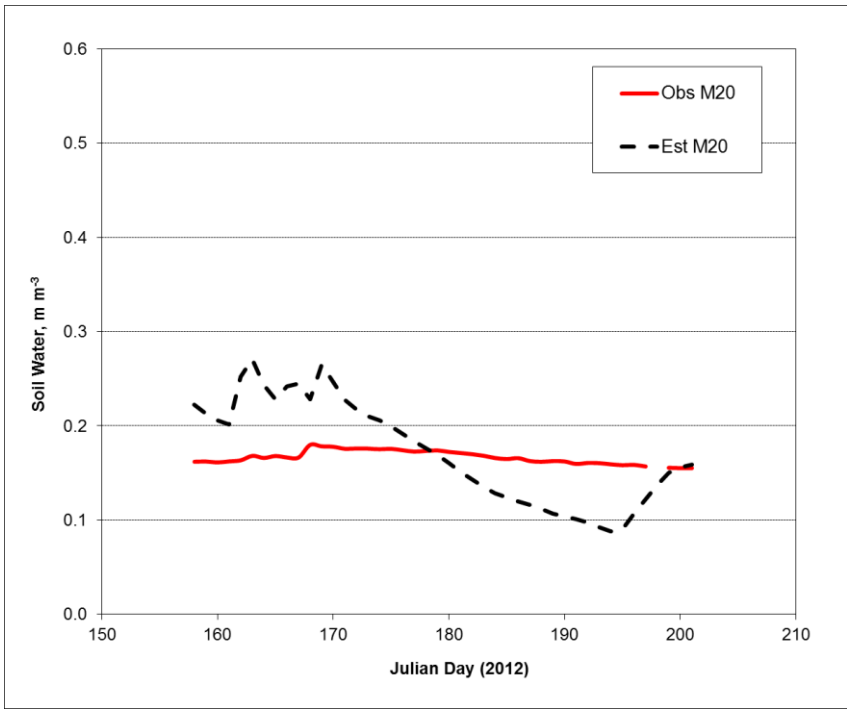

At 0.50 m soil depth (Loamy Sand; sand=89%, clay=10%; BD=1.59 kg/cu.m) [RMSE=0.0438; R^2=0.5997]

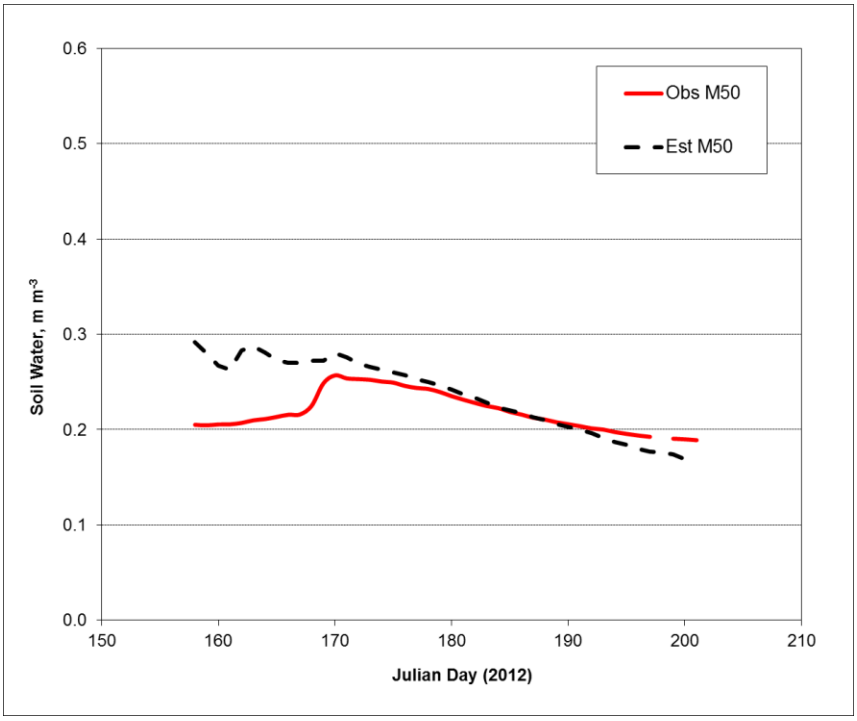

At 1.00 m soil depth (Loamy Sand; sand=86%, clay=9%; BD=1.58 kg/cu.m) [RMSE=0.0515; R^2=0.2201]

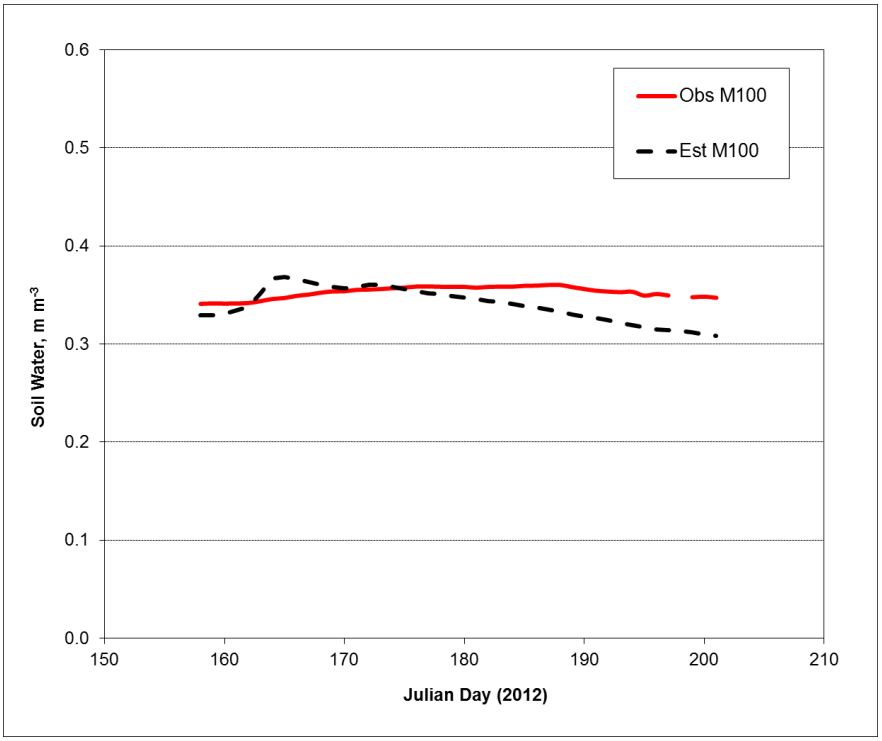

Field SAGES-5 [Field 65] (W. Wheat) – (using CaPA precipitation, pixel 11_5)

At 0.05 m soil depth (Clay Loam; sand=41%, clay=40%; BD=1.46 kg/cu.m) [RMSE=0.0509; R^2=0.3874]

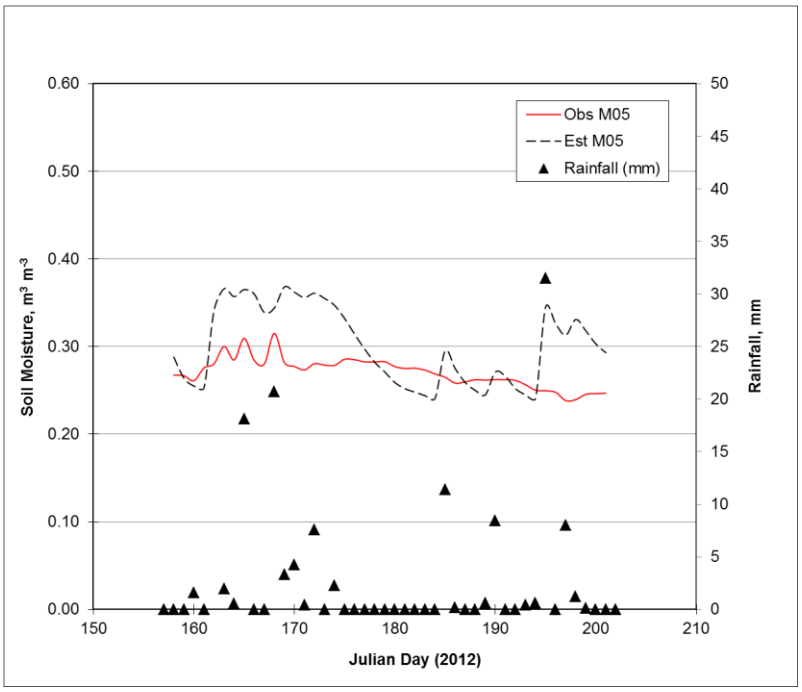

At 0.20 m soil depth (Clay; sand=22%, clay=57%; BD=1.41 kg/cu.m) [RMSE=0.0436; R^2= -0.5382]

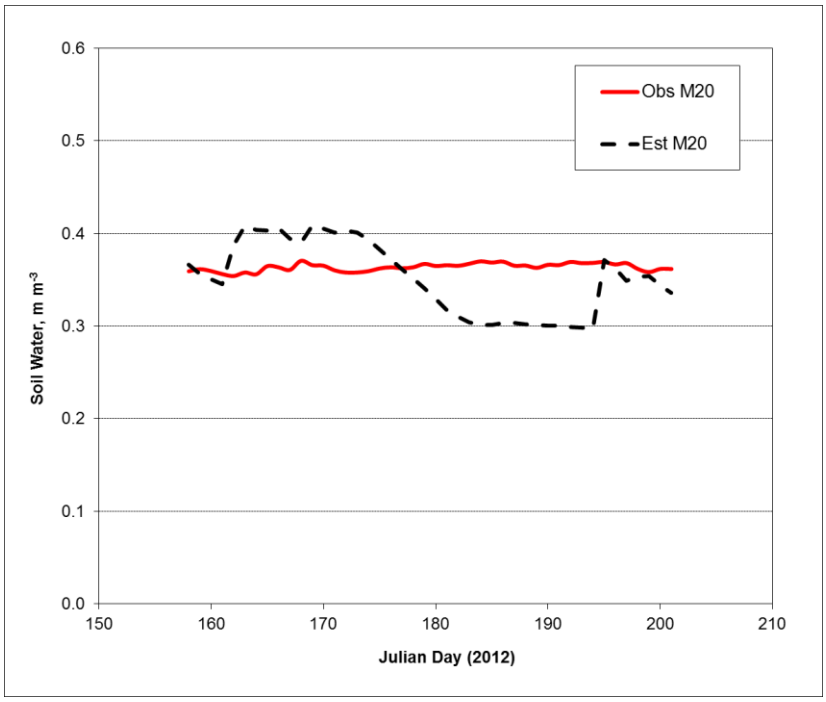

At 0.50 m soil depth (Clay; sand=4%, clay=68%; BD=1.33 kg/cu.m) [RMSE=0.0403; R^2= -0.45727]

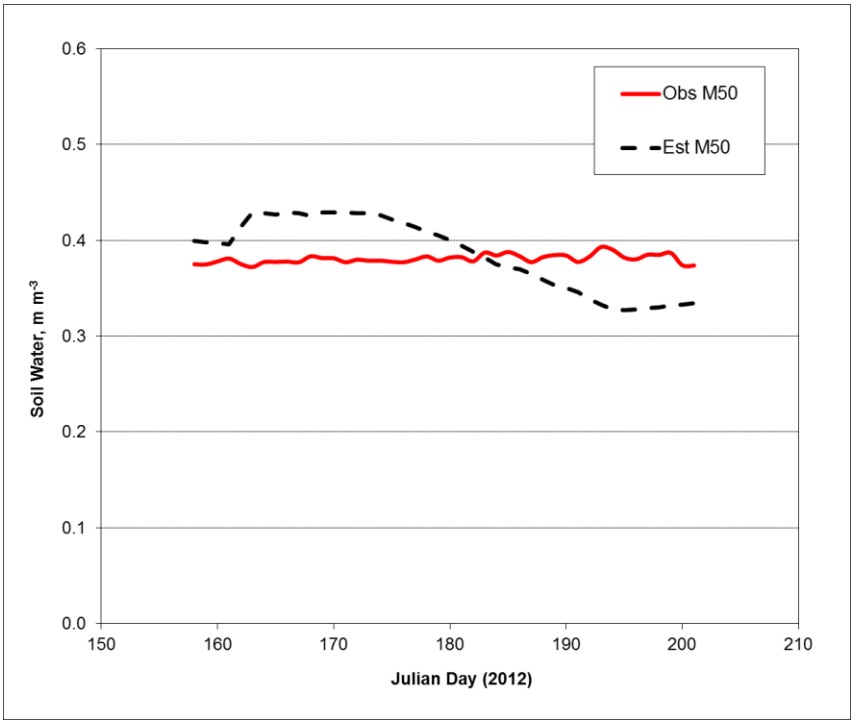

At 1.00 m soil depth (Clay; sand=3%, clay=69%; BD=1.32 kg/cu.m) [RMSE=0.0213; R^2= -0.3315]

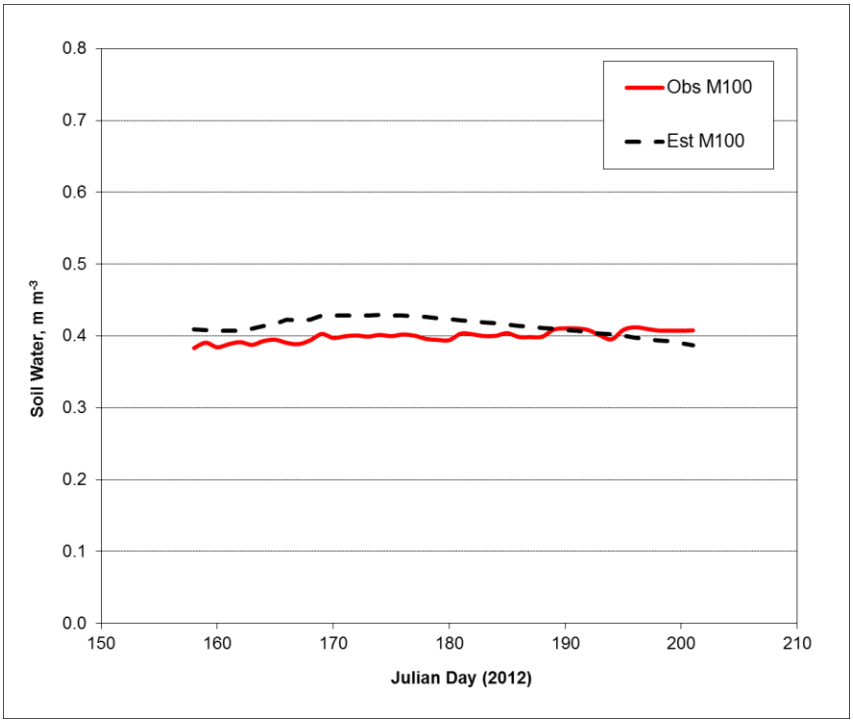

Field SAGES-7 [Field 32] (W. Wheat) – (using CaPA precipitation, pixel 11_4)

At 0.05 m soil depth (Sandy Loam; sand=78%, clay=13%; BD=1.40 kg/cu.m) [RMSE=0.0497; R^2=0.6731]

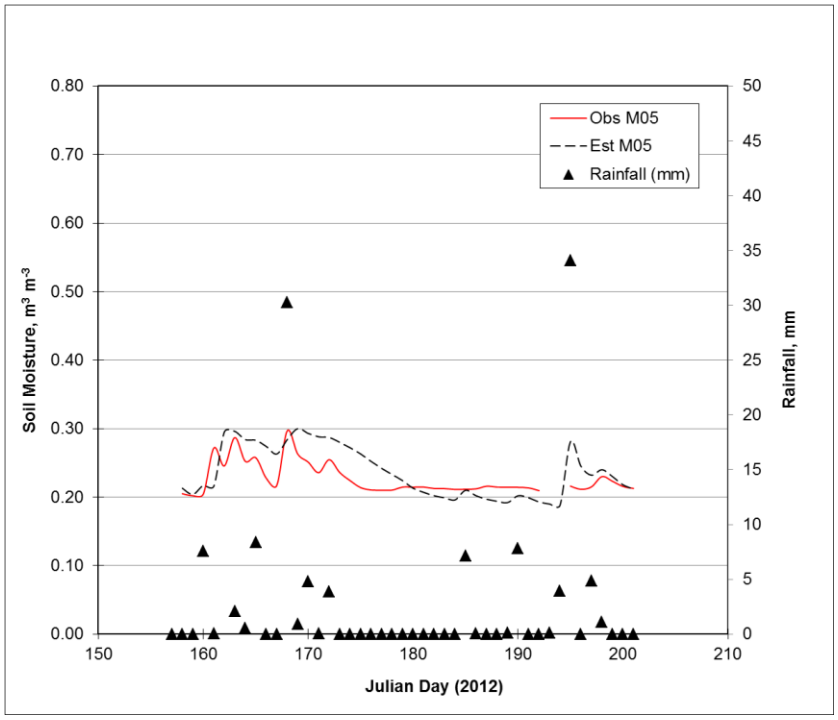

At 0.20 m soil depth (Loamy Sand; sand=82%, clay=12%; BD=1.59 kg/cu.m) [RMSE=0.0500; R^2= 0.8189]

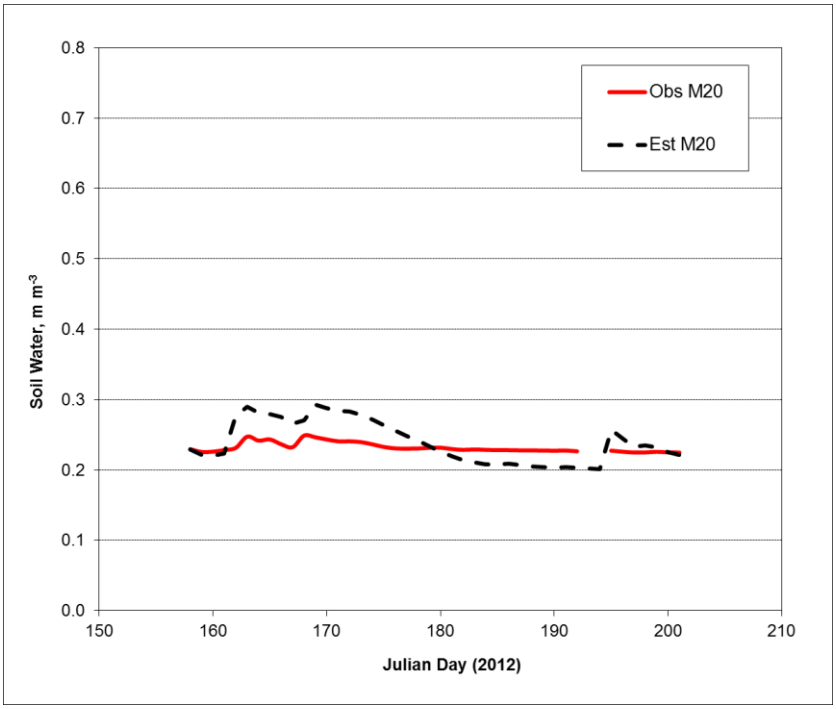

At 0.50 m soil depth (Sandy Loam; sand=78%, clay=13%; BD=1.57 kg/cu.m) [RMSE=0.0513; R^2= 0.8591]

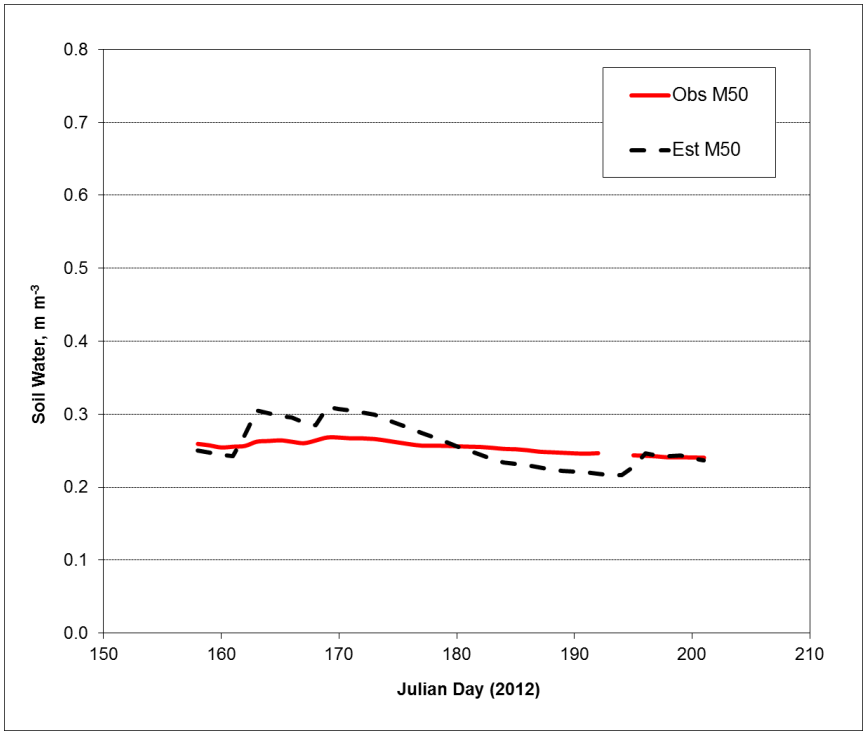

At 1.00 m soil depth (Sandy Loam; sand=80%, clay=12%; BD=1.58 kg/cu.m) [RMSE=0.0735; R^2= 0.0259]

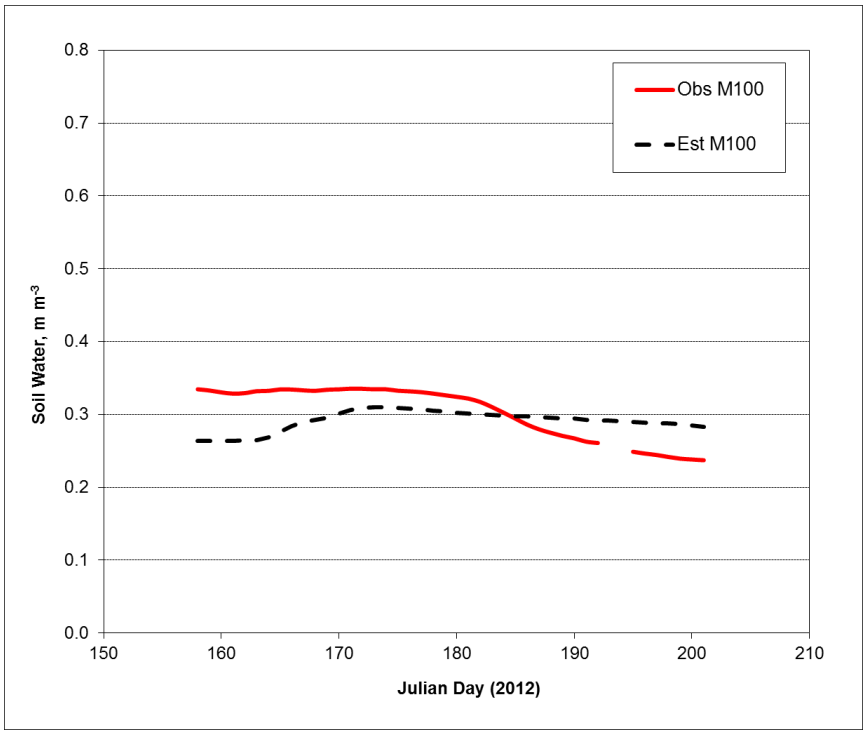

A.6b Trends of observed and simulated soil moisture of 6 agricultural fields at different soil depths for data period of 6 June – 19 July 2012served

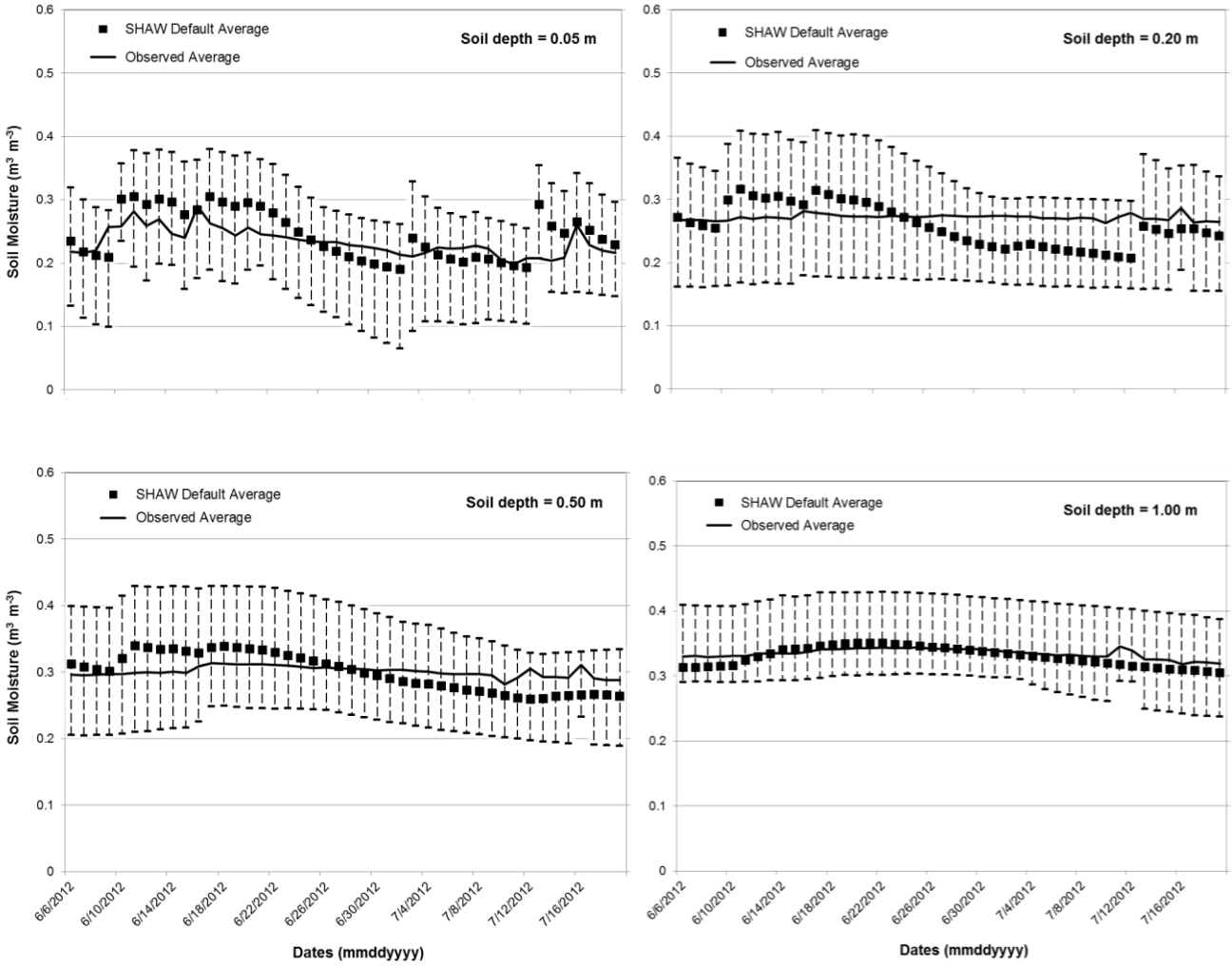

A.6c Relationship between measured and simulated soil moisture of 6 agricultural fields at different soil depths (for data period of 6 June – 19 July 2012